From the
Medizinischen Klinik und Poliklinik I Großhadern
of the Ludwig-Maximilians-Universität München
Direktor: Prof. Dr. med. Steffen Massberg

# Megakaryopoietic islands in the bone marrow balance platelet production and maintain megakaryocyte homeostasis

Dissertation
zum Erwerb des **Doctor of Philosophy (Ph.D.)**
an der Medizinischen Fakultät der
Ludwig-Maximilians-Universität München

submitted by
Wenwen Fu
from
Wuhan, China

08.08.2017

Supervisor: Prof. Dr. med. Steffen Massberg

Second evaluator: Prof. Dr. med. Christian Schulz

Dean: Prof. Dr. Reinhard Hickel

Date of oral defence: 24.11.2017

# TABLE OF CONTENTS

# LIST OF FIGURES

# 1 ABSTRACT

Megakaryocytes (MKs) are large and rare polyploidy bone marrow (BM) cells, the main function of which is producing platelets. They are predominately localized at the BM sinusoids and form cytoplasmic extensions which penetrate into the vessels and release platelets from their tips. Despite numerous studies on thrombopoiesis, little is known about megakaryopoiesis, that is how MKs are dynamically developed from hematopoietic stem and progenitor cells in vivo. Apart from the production of platelets, MKs display versatile roles as BM niche cells that regulate the quiescence as well as expansion of hematopoietic cells in steady state and under stress conditions. In pathological conditions including acute inflammation or thrombocytopenia when large numbers of platelets are rapidly consumed, the platelets in the circulation are replenished by the accelerated consumption of MKs. However, the indispensable niche functions of MKs also require a mechanism that could maintain MK homeostasis, and it still remains unclear how distinct functions of MKs are coordinated under these conditions. Here, we used whole-mount staining techniques and Two-photon Intravital Microscopy (2P-IVM) of vWF-eGFP mouse calvarian to investigate the spatial-temporal organization of MK populations in BM. Firstly, we found that mature MKs and their precursors localize in close proximity within the BM forming functional units which we termed “megakaryopoietic island” (MK island). We show that megakaryopoiesis takes place within MK islands and is tightly associated with the sinusoid throughout the entire MK development. In MK islands, megakaryopoiesis is spatial-temporally coupled to thrombopoiesis, since MK progenitors replenish vanished MKs which tightly control MK numbers within the BM. This process is augmented under hematopoietic stress when we induced the mice with immune-thrombocytopenia. The spatial-temporal maintenance of MK islands suggests signals conveyed from MKs to their precursors. Consequently, the depletion of mature MKs from the BM results in abnormal megakaryopoiesis with MKP cellular expansion but disrupted MK islands and severely ceased MKP growth. Taken together, the work of this thesis contributes to a better

understanding of megakaryopoiesis which dynamically takes place in unit of MK islands that function a balance between platelet production and the maintenance of MK homeostasis for its essential niche function. MKs as an important component of the island regulate the development of their own precursors. This work also provides clinical implications for understanding the cause of thrombocytopenia. Since a tight spatial relationship is involved among MK populations as well as the sinusoids to ensure normal megakaryopoiesis, decreased platelet number in certain patients might result from the redistribution of MK populations. Future work on deciphering the molecular signals might provide potential therapeutic targets on the treatment of these patients.

# 2 INTRODUCTION

## 2.1 Megakaryocytes in the bone marrow

### 2.1.1 Thrombopoiesis: megakaryocytes give rise to platelets

Platelets are blood anuclear cells which play an essential role in divers physiological as well as pathological processes such as hemostasis, inflammation, atherosclerosis, cancer immunity [1-4]. The main role of platelets is to sustain the integrity of vessels and prevent bleeding by forming thrombi. During this process platelets adhere to the site of injury, initiate the coagulation pathways and form aggregates that recruit more platelets. In non-hematologic disease, platelets were found as important inflammatory cells by interacting with leukocytes at site of infection [5]. Considering the huge and prompt consumption of platelets in the circulation every day, the body must have evolved a way that the number of platelets could be quickly supplemented. Nearly $10^{11}$ platelets are produced daily in adults. The origin of platelets is the cytoplasmic fragments of a large and rare bone marrow cell called megakaryocyte (MK) [6, 7]. During the maturation, MKs become highly polyploidy as the nucleus of the MKs undergo repeated endomitosis without cell division [8-11], the cell size keeps growing to as huge as 50-100 μm, meanwhile the cytoplasm is rapidly filled with proteins and organelles which are prepared for producing platelets [12]. Actually, people first observed in vitro that mature MKs give rise to platelets in a highly efficient way by forming demarcation membrane system (DMS) which are the source of proplatelets [13, 14] (Fig. 2. 1). Later on, Junt et al. directly observed in vivo by two-photon intravital imaging that MKs form cytoplasmic extensions into the sinusoid (proplatelets), and these proplatelets release platelets from their tips [15], a process which can happens as fast as only in a few minutes. It was shown that this process depends on Sphingosine 1-phosphate (S1P) [16]. Recently a new study reported a novel behavior of platelet biogenesis, that MKs rupture into small cytoplasm fragments in response to acute and rapid platelets demand, which was

regulated by the increasing level of Interleukin-1 (IL-1) [17]. This pattern of thrombopoiesis generates much more platelets at once. It was reported that one MK is able to produce thousands of platelets into the blood. That explains why such a rare population in the bone marrow (~0.01% of nucleated cells) [18] is capable of fitting the demand of billions of platelets everyday.

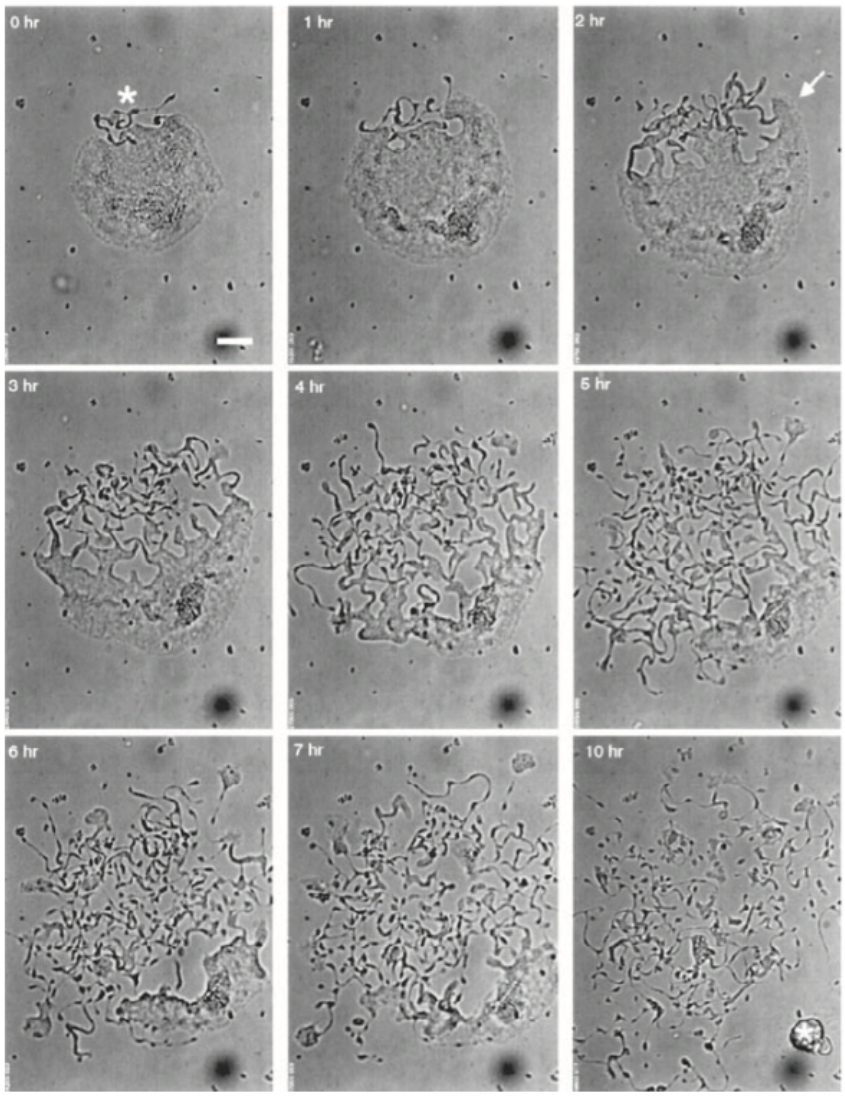


Figure 2.1 In vitro proplatelet formation of a cultured mouse megakaryocyte. Asterisk at 0 hr indicates one pole of MK where proplatelet formation initiates. Arrowhead at 2 hr indicates that the cytoplasm forms pseudopodia at the erosion site during proplatlet formation. Asterisk at 10 hr indicates a naked nuclear from

MK that has been consumed to proplatelets. Scale bar 20 μm. (from Italiano JE, et al. [14])

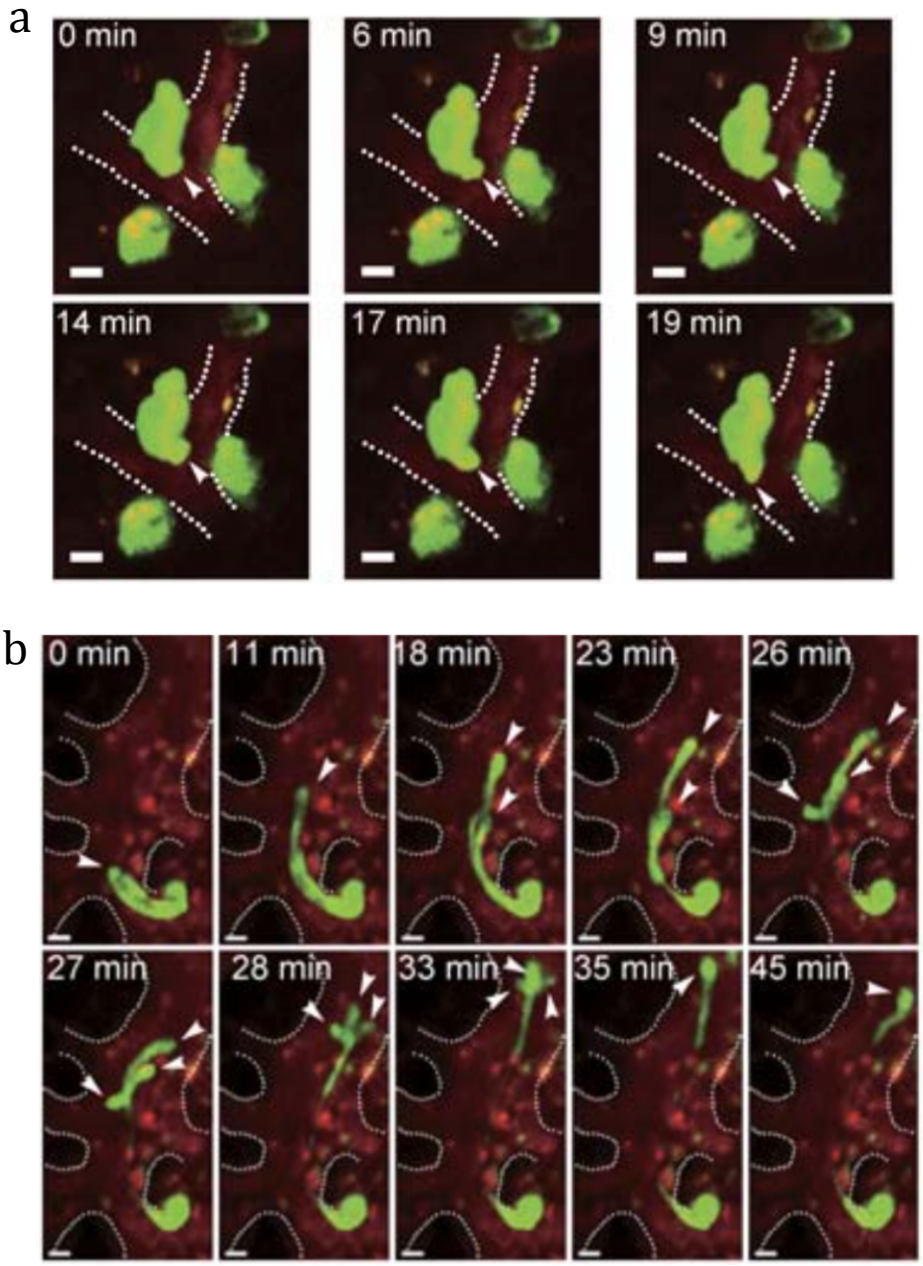


Figure 2.2 MK (green) proplatelet formation in calvarial bone marrow of a living CD41-YFP mouse. Arrowhead indicates proplatelet. (a) short proplatelet protusions. (b) long proplatelet extensions. Scale bar 20 μm. (from Zhang L, et al [16])

### 2.1.2 The positioning of megakaryocytes within the bone marrow niche

The bone marrow (BM) is a unique organ for maintaining hematopoietic stem cell (HSC) quiescence as well as for their differentiation into lineage cells that are then released into the circulation in response to demand. These lineage cells include megakaryocytes. Besides hematopoietic cells, BM is also enriched with multiple environmental cells such as endothelial cells, osteoblastic cells, stromal cells and so on. Together, they provide an ideal habitat not only by forming an anatomic structure to support the cells, but also by secreting all kinds of cytokines and chemokines as regulators and nutrients [19, 20]. The definition of stem cell “niche” has been proposed by Schofield in 1978 [21], in order to better categorize different niche cell components and to investigate their functional relevance on HSCs and lineage cell development. Currently the most well known niche cells include osteoblasts, bone marrow endothelial cells, mesenchymal stem cells (MSCs), CXCL12-abundent reticular (CAR) cells as well as the sympathetic nerve system [22-27]. Among these niches, the vascular niche is most important for the MKs. Before platelet formation, it is pivotal that MKs localize adjacent to the bone marrow sinusoidal vasculature so that the protrusions can penetrate the endothelium and reach the blood stream. MKs are shown to have very intimate relationship with the bone marrow vasculature [28-31]. MK cell surface express various receptors and adhesion molecules including Glycoprotein (GP)Ib, GPIIb, very late antigen 4 (VLA-4), lymphocyte function-associated antigen 1 (LFA-1) [30]. They bind to certain ligands like von Willebrand Factor (vWF) and vascular-cell adhesion molecule 1 (VCAM-1) on endothelium, thereby enhance the cell-cell interactions between MKs and the endothelial cells [30, 32]. The perivascular niche contains MSCs and CAR cells, both of which are main sources of stromal cell-derived factor 1 (SDF-1, also known as CXCL12) in the bone marrow, a chemokine that activates the migration of leukocytes [23, 25]. It has been observed ex vivo that MKs relocate to the bone marrow vascular niche after triggered by SDF-1 [33]. In vitro studies also showed that MKs directly migrate

towards the gradient of SDF-1 [34, 35], further highlight the motility of MKs and their interactions with the bone marrow vessels. However, very few study use in vivo live imaging to explore MK dynamics within an intact BM, therefore little is known regarding their real behavior.

## 2.2 Megakaryopoiesis: from hematopoietic stem and progenitor cells to megakaryocytes

### 2.2.1 The cellular hierarchy of megakaryopoiesis

While the process of platelet formation has been well studied, it remains poorly understood how MKs are generated from their precursor cells in vivo and which regulations are involved in this process. Briefly, MKs are derived from their progenitors which are unipotent, and these progenitors are differentiated from stem cells which have self-renewal capacity as well as the ability of differentiating into all lineage cells [36, 37]. The traditional concept of megakaryopoiesis, which dominates for decades, described this process as a long term hematopoietic stem cell (HSC) loose quiescence and becomes a short term HSC, then undergoes cell division into a multipotent progenitor (MPP) [38], then continues division to common myeloid progenitor (CMP) [39] and common lymphoid progenitor (CLP) [40]. CMPs are responsible for producing granulocytes, monocytes-macrophages, erythrocytes and platelets [39]. CMP gives rise to megakaryocytic-erythrocytic progenitor (MEP) and then finally differentiate into MK [41-44]. Cell surface markers are used to identify MKs at different stages of their maturation. CD41 is widely expressed in majority of MK populations, while CD42 is expressed at later stage and marks mature MKs [45-47]. It is widely accepted that CD41 identifies MK progenitors [45, 46]. One study also suggested that, since CD9 is a marker expressing on MK lineages but not erythrocytic lineages [48], they defined MKPs as $CD9^{+}$ $CD41^{+}$ $FcγR^{lo}$ $c\text{-}kit^{+}$ $Sca\text{-}1^{-}$ $IL7Rα^{-}$ $Thy1.1^{-}$ $Lin^{-}$ cells and proved their functions with both in vivo and in vitro studies [49]. Recently Sanjuan-Pla and colleagues has identified a distinct population of HSCs with the expression of von

Willebrand Factor (vWF), which are both in short term as well as long term capable of producing significantly more platelets than $vWF^-$ HSCs [50]. These $vWF^+$ HSCs, which they called platelet-biased stem cells, exist at the apex of the HSC hierarchy, and their potential to differentiate into the MK lineage has already initiated at the HSC stage. Despite the well-addressed MK differentiation process, these long sequential steps questioned the efficiency of megakaryopoiesis and thus thrombopoiesis especially under emergency conditions such as acute haemorrhage, inflammation or thrombocytopenia when large numbers of platelets and MKs are urgently to be supplemented quickly [1-4]. In these circumstances, additional patterns of MK differentiation should be back up which allow rapid platelet replenishment. To note, several recent studies proposed alternative differentiation programs for MK lineage. First of all, a novel study by Haas and colleagues introduced a fraction of stem cell-like MK progenitors in the bone marrow which are quiescent as the HSCs in steady state, whereas are quickly activated and develop into MKs in order to replenish the platelet source under acute inflammation [51]. Later, Notta and colleagues reported that MK progenitors actually exist within the stem cell compartment and, in hierarchy, MK lineage tightly follows the multipotent progenitors [52]. Altogether, these current studies updated our knowledge of how a HSC is becoming a MK with hierarchical perspective; meanwhile tempt us to explore the anatomic localization of MK lineage cells with different stages of maturation within the space of the bone marrow microenvironment.

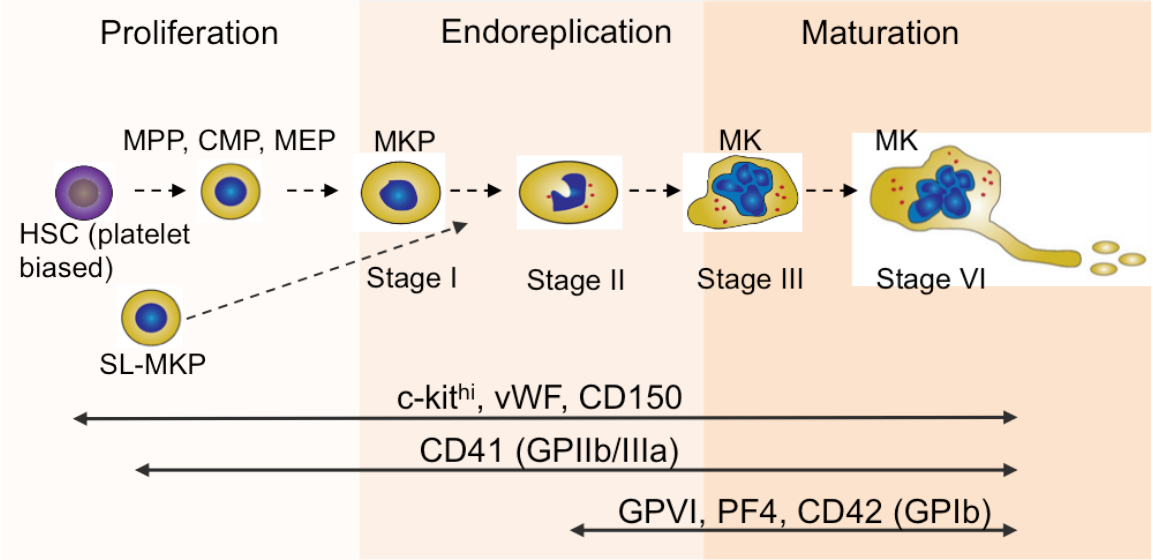


Figure 2.3 Megakaryocyte differentiation scheme and expression of related markers at different stages [49-51, 53, 54].

### 2.2.2 The spatial localization of megakaryopoiesis

As previously described, MKs locate in proximity with the bone marrow sinusoid [28, 31]. Since MKs are differentiated from HSCs, it is critical to find out the spatial distribution of HSCs within diverse certain niches. Decades ago, the endosteum, or the osteoblasts, was the first defined BM niche, as a critical trigger of marrow regeneration. The manipulation of either osteoblasts or endosteal-derived proteins altered the number of HSCs and their functions as well [55, 56]. Further studies found the transplanted lineage negative bone marrow cells preferably homing to the endosteal region, suggesting it provides a shelter to maintain the HSCs [57]. Thus, during the differentiation from HSCs towards MKs, a location shift was assumed to take place from the osteoblastic niche towards the vascular niche, an idea dominated for years. However, this idea was challenged when the SLAM markers CD150, CD244, CD48 were discovered as an effective approach to identify HSCs and progenitors, and these SLAM-HSCs were shown to occupy the sinusoidal endothelium niche [58]. Following studies demonstrated that the perivascular niche, where a lot of SCF and CXCL12 were secreted by pericytes and bone marrow stromal cells, was actually more important in maintaining the

pool of HSCs [23, 59, 60]. The depletion of CXCL12 or stem cell factor (SCF), important molecular regulators of HSCs, from the osteoblasts did not impair the function of HSCs, indicating that the endosteum was not the most critical compartment for HSC sustainment [60]. Interestingly, bone marrow arterioles as another type of vessels was recently found to regulate the quiescence of the HSCs, as the depletion of arterioles-ensheathed $NG2^+$ cells resulted in the proliferation of HSCs and thus reduced long term HSCs [61]. Taken together, the spatial localization of the HSCs is a controversial topic that has been long debated. Nowadays it has become a consensus that HSCs are preferably localized at the perivascular niche. There is little known about the spatial localization of the MK progenitors. In vitro studies showed that a low oxygen environment such as the endosteal region inhibited the maturation of MKs and the formation of proplatelet, indicating the osteoblastic niche less likely for MK progenitors to occupy [62]. Meanwhile, an ex vivo study showed the interactions between MK progenitors and the bone marrow sinusoidal endothelium, which was mediated by chemokine CXCL12 and fibroblast growth factor-4 (FGF-4) [30]. In order to decipher the spatial migration or repositioning of the MK lineage cells within megakaryopoiesis, it will be a vital task to find out more clues about the distribution of MK progenitors as well as HSCs, especially platelet-biased stem cells.

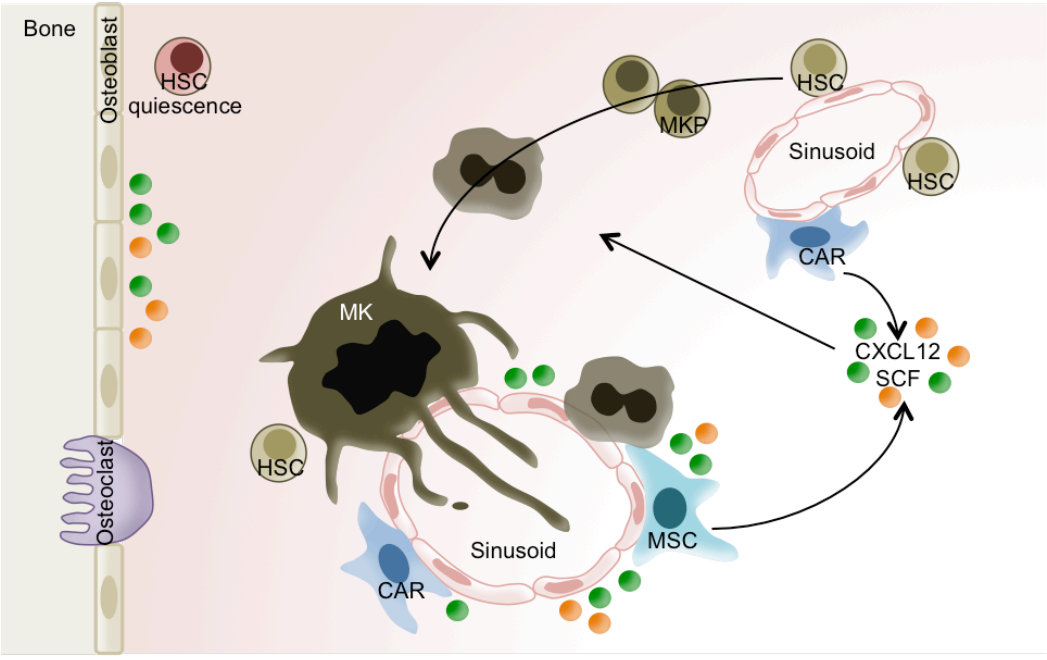

Figure 2.4 Megakaryopoiesis within the bone marrow niche. HSC, hematopoietic stem cell; MKP, MK progenitor; MK, megakaryocyte; MSC, mesenchymal stem cell; CAR, CXCL12-abundant reticular cell; SCF, stem cell factor.

## 2.3 Potential regulators in megakaryopoiesis

### 2.3.1 The role of bone marrow sinusoid in megakaryopoiesis

The sinusoid is an important compartment of the bone marrow. It is evenly distributed within the bone marrow and occupies ~30% of the total bone marrow volume [61]. This dense vascular network ensures a sufficient perfusion of oxygen, nutrients and soluble factors to supply the bone marrow [63]. It is also the place where the bone marrow frequently exchanges hematopoietic cells with the circulation [64]. According to previous studies, the majority of the MKs are sitting at the sinusoids [28-31]. It has been reported decades ago that the adhesion of MKs to endothelial cells upon inflammatory factors promotes the maturation of MKs including augmented GPIb and GPIIb/IIIa expression as well as an elevated DNA content [29]. The sinusoid and perivascular region inhabit not only endothelial cells, but also abundant MSCs and CAR cells. These cells contribute to high gradient of SDF-1 and SCF at the perivascular niche, both of which were important regulators in maintaining the HSCs [23, 59, 60]. SCF is the ligand of c-kit, a receptor mostly expressed on HSCs and progenitors [65-67]. The SCF/c-kit signaling is indispensable for hematopoiesis at both embryonic stage as well as adulthood [68-70]. Years ago, researchers already found the expression of c-kit on megakaryocytes, and the treatment of SCF/c-kit induced MK proliferation and cytokine secretion [71, 72]. More recently, it was found that a fraction of HSCs express high levels of c-kit, and these c-kit$^{hi}$ HSCs exhibit potential megakaryocytic bias [53]. These observations shed light on an important role of SCF/kit signaling in promoting megakaryopoiesis. Besides SCF/kit, Avecilla and colleagues in 2004 reported that SDF-1 and FGF-4 mediated interactions between MK progenitors and bone marrow endothelial cells, and this interaction

enhanced platelet production [30]. Later on, more studies focused on the migration of MKs towards the sinusoidal vessels after SDF-1 application [33, 34]. Altogether, these results highlight a sinusoidal vascular niche enriched with SDF-1 and SCF that supports megakaryopoiesis by guiding MKPs and MKs relocate to the vessels, inducing proliferation and providing a suitable microenvironment to maintain these cells.

### 2.3.2 The role of megakaryocytes in megakaryopoiesis: more than just a progeny?

The main function of MK is to produce platelets. Due to the huge size and distinct morphology, it is no surprise that a megakaryocyte physically contact with other cell types in the crowded bone marrow. Besides, the huge capacity of cytoplasm of a mature MK contains multiple proteins, soluble factors and chemokines, which can be secreted to the surrounding environment and might play a role in regulating megakaryopoiesis [73, 74]. This also suggests that MKs might play additional roles other than platelet formation [75]. Therefore, this question has been addressed within the last few years. It has been reported that MKs exert diverse influence on at least two types of bone marrow niche cells, the osteoblastic niche and the vascular niche [75]. There was one study using GATA-1 deficient mice to show that these mice generate increased numbers of immature MKs which support osteoblast proliferation through higher cellularity as well as increased longevity of MKs [76]. The interaction between MK and osteoblast involves integrins including very late factor-3 (VLF-3), VLF-5 as well as CD41 [77]. Furthermore, it was shown that MKs help to reconstitute bone marrow niches after radioablation, by relocalizing at the endosteal niche, promoting the expansion of osteoblastic cells and therefore enhancing HSC engraftment [78, 79]. The proliferation of osteoblasts is mediated by platelet-derived growth factor (PDGF) as well as FGF which are MK-derived factors [78, 79]. Apart from its influence on osteoblasts, researchers also showed that MK has an effect on vascular niche. In vitro culture of MKs showed that they secret vascular

endothelial growth factor (VEGF) which might promote the proliferation of endothelial cells [80]. Using thrombospondin knockout mice people also showed that restored MK and platelet numbers accelerate revascularization upon myelosupression, indicating the role of MK on vascular niche [81]. Nowadays, researchers are getting increasingly aware of the versatile role of MKs serve themselves as niche cells in regulating hematopoietic cells. There were two papers strikingly reported that MKs play a role in regulating the quiescence of HSCs by secreting platelet factor 4 (PF4, also named CXCL4) and transforming growth factor β1 (TGF-β1), while triggering HSC regeneration upon 5-FU treatment [82, 83]. For the first time people realized that highly mature hematopoietic cells can controls the fate of primitive cells. Very recently another paper showed that MKs regulate granulocytes/macrophage progenitor (GMP) cluster formation through secreting niche signals including SCF, IL-1 as well as G-CSF upon stress of bone marrow suppression [84]. Considering these versatile roles of MK, it might also play a role in regulating their own precursors. Since quiescent HSCs are lying very close to MKs, do these HSCs already obtain a bias towards MKs and platelets? On the other hand, when our body is undergoing great platelet consumption in short period of time, urgent mechanisms must be initiated in order to fill up the platelet loss and stimulate increasing MK development. How are these signals immediately conveyed to the stem cells and progenitors? One possibility could be that the precursors and their progeny already localize adjacent to each other. Therefore, in our study we would like to find out if an intimate interaction takes place between MKs and their precursors, and we hypothesize that MKs as mature cells might regulate their own precursors during megakaryopoiesis.

### 2.3.3 Thrombopoietin

Thrombopoietin (Tpo) was first purified in 1994 as a key protein that regulates MK development [85, 86]. Tpo receptor c-Mpl is mainly expressed on MKs, platelets and HSCs [87, 88]. C-Mpl is activated to form dimers after binding to Tpo, and this

leads to the activation of a series of downstream signaling pathways including JAK2/STAT, MAPK and PI3K [87, 89, 90]. The signals are then conveyed to the nucleus for related gene transcription [87]. Tpo regulates all stages of megakaryopoiesis. Its central role is to induce the expansion of MK progenitors and their differentiation towards MKs [91]. Mice treated with Tpo showed augmented MK numbers, increased MK size and polypoidization in the bone marrow and elevated platelet level [90]. In vitro culture of bone marrow cells supplied with Tpo effectively yielded higher numbers, bigger size and more mature MKs with increased expression of surface markers [92, 93]. These results confirmed that Tpo is the dominant cytokine for megakaryopoiesis. Based on the cell surface expression of c-Mpl also on HSCs and certain progenitors, people discovered the versatile effects of Tpo on hematopoiesis. Tpo itself maintains the survival of HSCs. Combined with other cytokines like IL-3 or SCF, Tpo promotes HSC differentiation and proliferation [94].

Tpo is produced mostly in the liver, a small amount in the kidney and in bone marrow stromal cells [95-97]. Tpo is degraded in the circulation by binding to c-Mpl on platelets. When under thrombocytopenia, the reduced platelets lead to increased serum Tpo level due to less degradation, and this enhances the production of platelets [98]. However, this is achieved through the Tpo stimulation on MK precursors rather than direct on MKs and platelets [99]. Notably, Tpo does not directly influence proplatelet formation and the release of platelets [87, 100]. Still, it remains unclear whether Tpo participates in spatial orientation of megakaryopoiesis such as cell migration or localization. It would be interesting to investigate in detail how Tpo dominates megakaryopoiesis in these aspects other than cell differentiation and proliferation.

## 2.4 In vivo live imaging of megakaryopoiesis

The study of megakaryopoiesis has been undergoing for many years and dramatic progress has been made. Yet hampered by technical difficulties, overwhelming majority of them were based on bone marrow histological staining

or in vitro cell culture, neither of which could mimic the real bone marrow environment. The histology displays very limited amount of bone marrow tissue, while in vitro culture altered bone marrow conditions completely. We should keep in mind that megakaryopoiesis takes place in a three-dimensional bone marrow organ with dynamic cell behavior. Therefore, the most convincing approach would be to use live imaging to visualize the cell dynamics directly within an intact bone marrow cavity. However, three main technical obstacles have to be overcome in order to achieve this ambitious goal. First of all, a novel imaging technique is required to penetrate the bone barrier and ensure high-resolution live imaging of the bone marrow. Secondly, a proper imaging model of the bone marrow is indispensable for tracking single cells stably over long period of time. Finally, a transgenic mouse model is necessary to allow the visualization of MKs and precursors during live imaging.

### 2.4.1 Two-Photon microscopy

The technique of two-photon microscopy emerged in 1990. The principle is to use high power infrared lasers to excite fluorophores with 2 photons of twice the wavelength and half the energy compared to single photon excitation [101, 102]. Compared to confocal microscopy, it has at least three advantages: increased penetration depth through the tissue, less photo-bleaching and photo-toxicity, to excite the fluorophore only on the focal plane. All these characters make two-photon microscopy an ideal approach for in vivo imaging of living tissues.

The calvarium has been shown to have comparable hematopoiesis as the other bone marrow compartments (for example the femur) regarding the HSC number, function and reconstitution [103]. The bone barrier of calvarium is relatively flat and thin compared to femur, which makes it easier for laser penetration. The live imaging of the calvarium model was pioneered by Dr. Irina Mazo. In her publication in 1998, she and colleagues for the first time applied intravital live imaging in murine bone marrow microvessels [104]. This calvarian model is

currently the only noninvasive model for the bone marrow imaging. Combined with two-photon microscopy, it allows stable high-resolution imaging of the intact bone marrow for up to 8 hours. The imaging duration is largely confined by the animal tolerance of the anesthesia, as well as the photo bleaching after continuous imaging.

### 2.4.2 Chronic live imaging of murine calvarium

The development and maturation of MKs takes days to complete [12]. Therefore, the conventional live imaging is too short to capture the whole process of megakaryopoiesis. A novel technique of long term (chronic) imaging was for the first time reported in 2009, to overcome the limitation of imaging duration in cerebral imaging [105]. By replacing a small bone flap with transparent cover glass, it became possible to image the living brain over months through this chronic cranial window while the animal was kept alive during the entire process. The surgical preparation takes ~1h and allows imaging period over months with deliberate time intervals [105]. Recently two studies reported a similar imaging technique which was applied in calvarial imaging. The first study was shown by Hawkins and colleagues who achieved repeated calvarial imaging of T-cell acute leukaemia interaction with the bone marrow niche, by using a lock-and-key imaging window to reposition to the exact previous imaging area. An intrasite gel was used to protect on the exposed skull between imaging intervals [106]. This allowed an extension of the imaging duration to ~ 1 month. Another study introduced more specifically this method with the same concept, that a cover glass was attached to the upper bone layer of the frontal calvarian to allow multiple imaging over 4 weeks [107]. In this thesis, we will adapt this technique to our calvarial model using a similar method. This novel technique would be pivotal to reveal cell dynamics during megakaryopoiesis. How is one MK precursor developing into a MK? How is one MK releasing platelets and dying? Where does this process take place? How long does it last? Are niche cells involved? What are the molecular mechanisms? All these interesting questions that have never

been directly addressed before will get an answer excitingly by chronic imaging of calvarium.

### 2.4.3 Mouse models

In this thesis, we will use different mouse models to investigate megakaryopoiesis in vivo. Three transgenic mouse models CD41-YFP, PF4 Cre × Rosa26-mT/mG and vWF-eGFP mouse in which the MKs are labeled with fluorescent proteins will be used to study MK dynamics in vivo [50, 108, 109]. Since von Willebrand Factor is also expressed on MK lineage progenitors and platelet biased stem cells, vWF-eGFP mouse allows visualization of MK precursors, which will be used to study megakaryopoiesis in vivo [50].

For a mimic of immune-thrombocytopenia, mice will be treated with platelet depletion antibody (anti-GPIb α) to achieve an efficient platelet clearance which will then trigger megakaryopoiesis [110, 111]. Tpo will be used as another approach to enhance megakaryopoiesis. In order to investigate the role of MKs in regulating their precursors, we will use PF4 Cre × Rosa26-iDTR mouse as a MK depletion model, in which the PF4 cells are depleted after diphtheria toxin (DT) inducement [112]. To be able to observe this effect in vivo, we will cross these mice with vWF-eGFP mice. PF4 Cre × Rosa26-iDTR × vWF-eGFP mice will show a depleted MK and platelet population, while MK precursors remain fluorescence labeled. It serves as a useful tool for in vivo study of MK precursor dynamics under MK loss.

## 2.5 Aims of the thesis

Despite a lot of studies on platelet production, very few study focus on the generation of megakaryocytes largely due to technical difficulties such as in vivo visualization of MK populations. It is still remained unknown how megakaryopoiesis takes place in intact bone marrow microenvironment, and what

are the cellular as well as molecular mechanisms behind. Current studies used bone marrow histology or in vitro assay to show that MKs or MKPs re-localize towards the vascular niche or migrate towards the gradient of chemokines. However, these studies raise questions that a very limited spatial horizon (such as two-dimensional histology) might generate artificial results regarding cell localization, and under simplified bone marrow conditions (such as in vitro cell culture) cells might behave differently than they are in living bone marrow environment. To overcome these problems, we eagerly ask for an approach to be able to decipher dynamics of MK populations in intact bone marrow.

In this thesis, we use two-photon intravital microscopy combined with transgenic fluorescence labeled mice to study how megakaryocytes are generated in vivo, and to further explore the functional relevance of megakaryocytes themselves in regulating this process. Our study will contribute to a better understanding of megakaryopoiesis in detail.

Aim 1: Megakaryopoiesis at steady state

Our first aim is to study megakaryopoiesis at steady state as detailed as possible. Firstly, by using whole-mount immunostaining we will check the cellularity of MKs and MKPs in the bone marrow and their distribution regarding vascular niche as well as endosteal niche. Then, we will use two-photon intravital microscopy to visualize cell motility of MK populations and their interactions in vivo. Finally and importantly, we will use chronic imaging technique to track single cell over time in order to observe cell maturation and aging kinetics, and the association of niche cells during this process. We will find out in homeostasis how one MKP is gradually developing into a mature MK and where it takes place. We will also observe how one MK is breaking up into platelets and disappearing.

Aim 2: Megakaryopoiesis under stress conditions

Our second aim is to find out how megakaryopoiesis is altered upon hematopoietic stress. By doing so we need several stress models. In platelet depletion model, we inject anti-platelet antibody to induce thrombocytopenia in mice. We will study MK and MKP response after platelet depletion in time sequence, including their bone marrow cellularity and spatial localization. We will select a time point when megakaryopoiesis is most augmented in order to study in vivo how cell dynamics is altered after stress. Then we will find out single cell kinetics through chronic imaging observation. In Tpo model, we will inject Tpo to stimulate megakaryopoiesis and analyze all information described above.

Aim 3: The role of megakaryocytes as a regulator of megakaryopoiesis

Our third aim is to investigate whether MKs themselves serve directly as niche cells to regulate megakaryopoiesis. We will look at the positioning of MK progenitors and MKs to see whether there is a close association, at steady state as well as induced megakaryopoiesis. Then we will directly visualize cell dynamics in vivo to see whether there are interactions between MKs and progenitors. By using PF4 Cre × Rosa26-iDTR mouse as a MK depletion model, we will find out the cellularity and localization of MKPs, cell motility and cell growth over time. We would like to elucidate whether MKs play a role in regulating their own lineage development.

# 3 MATERIALS & METHODS

## 3.1 Mice

C57BL/6J, PF4-Cre, Rosa26-iDTR, β-actin-CreER, vWF-Cre, Rosa26-Confetti and Rosa26-mT/mG mice were purchased from The Jackson Laboratory. PF4-Cre mouse strain expresses the Cre recombinase under the control of the promoter platelet factor 4 (PF4). Rosa26 is ubiquitously expressed on embryonic as well as adult tissues. Rosa26-iDTR mouse strain has the potential of widespread expression of iDTR (induced Diphtheria Toxin Receptor) under the control of a loxP-flanked STOP sequence [112]. To generate PF4-Cre × Rosa26-iDTR mice, PF4-Cre mice were crossed with Ros26-iDTR mice. This leads to the depletion of the STOP sequence and thus the expression of iDTR on PF4-expressing cells (mainly megakaryocytes and platelets). After intraperitoneal injection of Diphtheria Toxin, these cells are specifically depleted. vWF-Cre mouse has the Cre recombinase under the control of the promoter von Willebrand Factor (vWF). Rosa26-Confetti was described previously [113]. After cross breeding with β-actin-CreER mouse, the β-actin-expressing cells express one out of four fluorescent proteins GFP, YFP, RFP and CFP stochastically once Cre is activated upon intragastric giving of Tamoxifen (40µg/g body weight for consecutive 5 days). Rosa26-mT/mG mice express cell membrane-localized red fluorescence on all the cells and tissues, and start to express cell membrane-localized green fluorescence on Cre-activated cells. After cross breeding of Rosa26-mT/mG and PF4-Cre, the offspring express green fluorescence mainly on megakaryocytes and platelets, while the rest of the tissues remain red fluorescence. CD41-YFP$^{ki/+}$ mice were described previously [108] and were provided by Prof. Dr. Thomas Graf (Center of Genomic Regulation, Barcelona, Spain). vWF-eGFP mice were described previously [50] and provided by Dr. Claus Nerlov and Dr. Sten Eirik W. Jacobsen (MRC Molecular Haematology Unit, Weatherall Institute of Molecular Medicine, University of Oxford, UK). To generate PF4-Cre × Rosa26-iDTR × vWF-eGFP mice,

vWF-eGFP mice were cross breed with PF4-Cre × Rosa26-iDTR mice, in order to obtain a depletion of PF4-expressing cells in vWF-eGFP mice. All the animals were maintained and bred in the animal facility of Walter-Brendel Zentrum and Zentrum für Neuropathologie und Prionforschung (ZNP) in Munich, Germany. Female and male mice of age >8weeks were used in these studies. All the animal experimental protocols were based on the German legislation on the protection of animals and were approved by the Government of Bavaria in Germany.

## 3.2 Chimeras

To create β-actin-CreER ×Rosa26-Confetti hematopoietic stem cell chimeras, approximately 7.3 × $10^4$ $Lin^-$ $Sca\text{-}1^+$ $c\text{-}kit^+$ (LSK) cells isolated and sorted from β-actin-CreER × Rosa26-Confetti mice were intravenous injected into lethally irradiated C57BL/6J female mice (two dose of 6.5Gy with a time interval of 8 hours) which were pre-treated with Tamoxifen intragastrically for consecutive 5 days (Fig. 3. 1). The bone marrow of chimeras was analyzed 8 weeks after the transplantation.

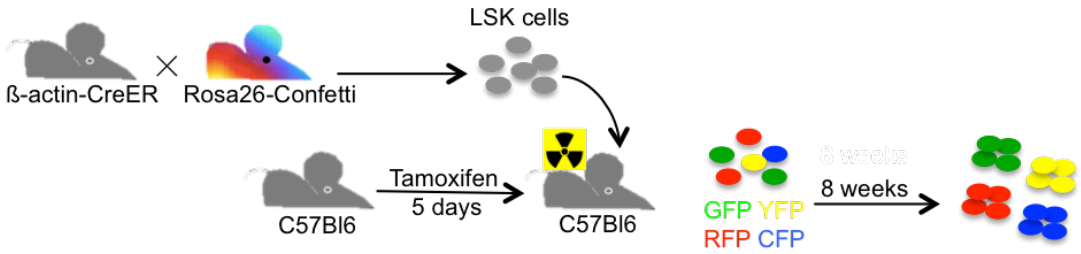


Figure 3.1 Bone marrow transplantation scheme for Confetti chimeras.

## 3.3 Reagents and antibodies

Diphtheria Toxin (DT) was purchased from Sigma-Aldrich (Saint Louis, MO, USA) and was dissolved in 500µl deionized water to reach a stock solution of 2µg/µl. In order to activate the Cre-iDTR depletion, DT was further diluted with saline and injected intraperitoneally into mice with a dose of 250ng/day for consecutive 7

days. Tamoxifen was purchased from Sigma-Aldrich (Saint Louis, MO, USA). To activate CreER mice, 80mg Tamoxifen was dissolved in 1ml Ethanol and 9ml corn oil and was mix up thoroughly. The solution was intragastric applied to mice with a dose of 40μg/g body weight for consecutive 5 days. Click-it® EdU Cell Proliferation Assay Kit, Qtracker® 705 Vascular Labels and Propidium Iodide (PI) were purchased from Thermo Fisher Scientific (Massachusetts, USA) and used according to the manufacturer's protocol. Mouse Lineage Cell Depletion Kit was purchased from Miltenyl Bioec GmbH (Bergisch Gladbach, Germany) and used according to the manufacturer's protocol. The following antibodies were used in these studies: CD41-fluorescein isothiocyanate (FITC), CD41-eFluor 450, Streptavidin-eFluor 450, CD41-biotin, Lineage-biotin (Ter-119, CD3e, CD45R, CD11b, Ly-6G, 1:200 dilution), VE-Cadherin (CD144) purified, CD150 purified, Streptavidin-phycoerythrin (PE), CD42-PE (1:100 dilution), CD45-PE, all purchased from eBioscience (San Diego, USA). CD42 purified, goat anti-rat Alexa Fluor 594, goat anti-hamster Alexa Fluor 647 (1:100 dilution), CD41-allophycocyanin (APC), CD45-APC, Lin-Pacific Blue (Ter-119, CD3, CD8a, CD45R, CD11b, Ly-6G), Sca-1-PE-Cy7, c-kit-APC, all purchased from Biolegend (San Diego, USA). Mouse CD16/CD32 (Fc block) was purchased from BD Pharmingen (New Jersey, USA). Mouse platelet depletion antibodies (anti-GPIbα) were purchased from Emfret (Eibelstadt, Germany) and used according to the manufacturer's protocol.

### 3.4 Platelet and other blood cell measurement

Mice were caged in a container with the tail exposed outside. 100ul 1:7-anticoagulant citrate dextrose solution whole blood was collected from the tail vein. Platelet and other blood cells were measured by a cell counting machine ABX Micros ES 60 (HORIBA, Kyoto, Japan).

### 3.5 Whole-mount immunofluorescence staining and imaging

Mice were anesthetized and sacrificed with Isofluran (cp-pharma, Burgdorf, Germany). The chest cavity was exposed and the right ventricle was cut open. Then the mice were perfused via left ventricle 3ml Phosphate buffer saline (PBS) followed by 3ml 4% Paraformaldehyde (PFA). Sternum, femur and tibiae were harvested and post-fixed in 4% PFA for 30min in room temperature (RT), and incubated in 15% Sucrose for 2 hours in 4℃ and then 30% Sucrose for overnight in 4℃.The next day the bones were embedded in Tissue-Tek® O.C.T. Compound (Staufen, Germany) and frozen with liquid nitrogen and 2-Methylbutane (Isopentane, Sigma-Alrich, Saint Louis, MO, USA). The frozen bones were cut on Histo Serve NX70 cryostat (Celle, Germany) until the exposure of the bone marrow cavity reached maximum. The sternum was cut as sagittal section. The femurs and tibiae were cut as coronal section or cross section, according to purpose. Then bones were carefully took out from the O.C.T. and gently washed in 1×PBS. For whole-mount staining, the cut bones were first incubated in 10% Normal Goat Serum (NGS, Thermo Fisher Scientific, Massachusetts, USA) and 0.5% Triton X-100 (Sigma-Alrich, Saint Louis, MO, USA) for at least 45min RT for blocking/permeabilization. Then bones were incubated in primary antibodies for overnight RT and secondary antibodies for 2 hours RT according to the purpose of the staining. The bones were then washed gently with 1× PBS between every step. For the staining of MKs and MKPs, CD41-FITC (1:200 dilution), purified CD42d (1:100 dilution) combined with goat anti-hamster Alexa Fluor 647 secondary antibody (1:100 dilution) were used. For the staining of bone marrow vessels, purified VE-Cadherin (1:100 dilution) combined with goat anti-rat Alexa Fluor 594 secondary antibody (1:100 dilution) was used. For the staining of platelet-biased stem cells, purified CD150 (1:100 dilution) combined with goat anti-rat Alexa Fluor 594 secondary antibody (1:100 dilution), CD41-eFluor450 (1:200 dilution) were used. For the staining of lineage cells, CD3e, CD45R, CD11b, Ly-6G, Ter-119, all labeled with Biotin (1:200 dilution), combined with Streptavidin-eFluor 450 (1:200 dilution), were used. After staining, bone samples were imaged using a multiphoton LaVision Biotech (Bielefeld, Germany) TrimScope II system connected to an upright Olympus microscope, equipped with

a Ti;Sa Chameleon Ultra II laser (Conherent) tunable in the range of 680 to 1080 nm and additionally an optical parametric oscillator (OPO) compact to support the range of 1000 to 1600 nm and a 16 × water immersion objective (numerical aperture 0.8, Nikon). Single images were acquired in 50-80μm depth, with z-interval of 2μm. The signal was detected by Photomultipliers (PMTs) (G6780-20, Hamamatsu Photonics, Hamamatsu, Japan). ImSpector Pro (LaVision) was used as acquisition software. For bones from C57Bl/6J mice, 800nm was used as an excitation wavelength. Photomultiplier values are listed: Red 65, Blue 70, Green 58, Near Infrared (NIR) 65. For bones from vWF-eGFP mice, 870 nm or 900nm wavelength was used. PMT Green 68. For EdU-labeled bones, images were acquired first by using wavelength 800nm for the blue signal, followed by using wavelength 900nm for the GFP signal, for the same position. The mosaic function of the software was used to obtain large images, usually whole sternum images.

### 3.6 Three-dimensional (3D) analysis of whole-mount bone marrow images

3D scan images were used to quantify the number and size of MKs and MKPs within the BM. The thickness of the images were ~50μm. The Imaris software (Bitplane, Zurich, Switzerland) was used in all of our further analysis. The numbers of MKs and MKPs were quantified in six individual 3D scan images from femur as well as sternum of 3 mice. The size of MKs and MKPs was quantified by manually measuring the diameters laterally as well as longitudinally and the mean value was taken. All other whole-mount quantifications were performed in whole sternum mosaic images that were stitched from single 3D images by using XuvTools software [114]. The number of MKs and MKPs were quantified in the whole mosaic image and was normalized by the volume of the BM in the image. The number of MK proplatelets, as well as the number of MKPs which attached to MKs, were measured by counting directly. We also quantified the distance from cells to certain niches (vascular niche, osteoblastic niche and MKs). The distance measurement was done semi-automatically as well as manually using Imaris software. For semi-automatic measuring, first of all, all the MKs and MKPs in the

image were rendered as spots. Then, the vessel as well as bone structure in every stack were manually contoured (Fig. 3. 1 a-b). Based on these contours we performed 3D reconstruction for the vessels and bone structure in the whole mosaic image. Then we run distance transformation (Matlab, Mathworks, Massachusetts, USA) function for the reconstructed volume, to create a distance map (Fig. 3. 1 c-d). The Imaris software then automatically calculated the shortest distance value from each spot surface to certain niches. For manually measuring, the distance was measured in 3D volume by finding out the shortest distance between a cell and certain niches.

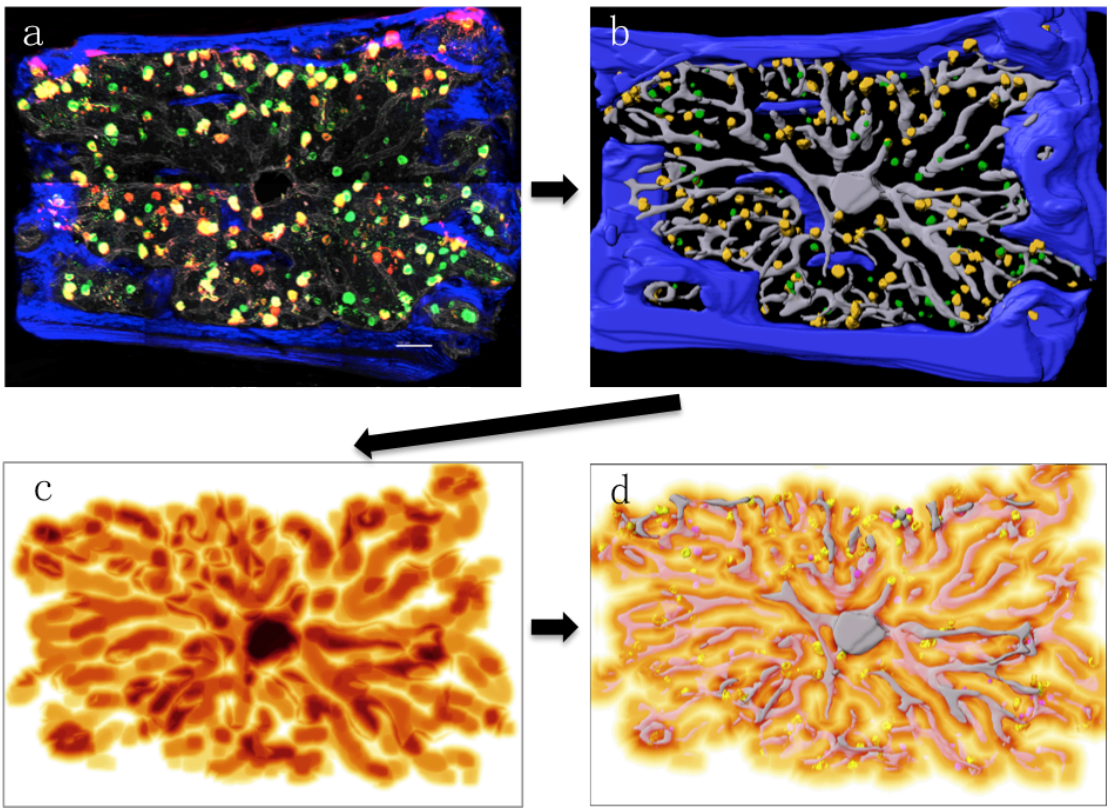


Figure 3.2 Scheme of semi-automatic distance measurement using Imaris software.

3.7 Two-Photon microscopy intravital imaging of the calvarium bone marrow

The calvarium has been shown to have comparable hematopoiesis as the other bone marrow compartments (for example the femur) regarding the HSC number, function and reconstitution [103]. The live imaging of the calvarium model is currently the only noninvasive model for the bone marrow imaging which was pioneered by Dr. Mazo, as described previously [104]. Briefly, mice were anesthetized with 5.0 Vol. % Isofluran (cp-pharma, Burgdorf, Germany) and 0.25 l/l oxygen. Then mice were injected intraperitoneally one dose of solution containing 25µl Fentanyl (0.05mg/kg body weight, Albrecht GmbH, Aulendorf, Germany), 30µl Midazolam (5mg/kg body weight, B.Braun, Melsungen, Hessen, Germany) and 15µl Medetomidine (0.5mg/kg body weight, Zoetis, Germany). When the mice were under narcosis, they were placed on a metal stage with warming pad and the hair over the skull was removed by hair removal cream (Asid-med, Asid Bonz, Herrenberg, Germany). Then the skin on the skull was cut in the midline and the frontal bone was exposed. The membrane between the skin and the bone was carefully removed and then a custom-build metal ring was glued on the center of the skull by using glue (Permabond 910, Eastleigh, Great Britain). The mouse's head was immobilized by fixing the ring on a stereotactic metal stage. Then the mice were placed and imaged using a multiphoton LaVision Biotech (Bielefeld, Germany) TrimScope II system connected to an upright Olympus microscope, equipped with a Ti;Sa Chameleon Ultra II laser (Conherent) tunable in the range of 680 to 1080 nm and additionally an optical parametric oscillator (OPO) compact to support the range of 1000 to 1600 nm and a 16 × water immersion objective (numerical aperture 0.8, Nikon). Live images were acquired from 30µm to 40µm depth, with z-interval of 2 or 3µm. 870nm or 900nm was used as an excitation wavelength, with 1030 × 1030 pixels. The signal was detected by Photomultipliers (G6780-20, Hamamatsu Photonics, Hamamatsu, Japan). ImSpector Pro (LaVision) was used as acquisition software. A customized chamber was made to cover the imaging stage, to maintain a stable 37℃ warm environment. For the vascular labeling, Dextran Tetramethylrhodamine (TRITC-Dextran, 100µg in 100µl solution, Invitrogen, Massachusetts, USA) or Qtracker® 705 (20µl in 200µl saline, Thermo Fisher Scientific, Massachusetts,

USA) was injected intravenously before imaging, according to the purpose of the imaging. For vWF-eGFP and PF4-Cre × Rosa26-mT/mG mice, we used laserpower 12.5%, wavelength 870 nm and PMT green 68 to generate proper GFP signal. For CD41-YFP mice and LSK Confetti chimeras, the images were acquired by firstly using laserpower 13%, wavelength 900nm, then the vascular signal at the same volume was acquired immediately at wavelength 800nm (for TRITC) or 870nm (for Qtracker 705).

### 3.8 Cell dynamics analysis of the intravital imaging of the calvarian bone marrow

The cell dynamics analysis was done in 3D live imaging movies by using Imaris software (Bitplane, Zurich, Switzerland). The total number of cells was counted in one microscope field (558µm × 558µm × 30µm). The cell size was quantified by manually measuring the diameters laterally as well as longitudinally and the mean value was divided. The shortest distance from cells to the vessels and the MKs was measured manually, at the beginning as well as the end of the movie. The cell migration was tracked in 3D volume at every time point of the movie. The cell speed was calculated by dividing the track length with the track duration. The cell velocity was calculated by dividing the track displacement with the track duration.

### 3.9 Two-Photon microscopy chronic (long-term) imaging of the calvarian bone marrow

In order to visualize the entire process of megakaryopoiesis, we developed a novel chronic imaging technique which allows us to extend the imaging period to 2-3 days. The chronic imaging included repeated imaging of the same BM area, with 10-14 hours time intervals. Each imaging lasted approximately 15min. For the preparation of the chronic imaging window, first of all, the mice were anesthetized with 5.0 Vol. % Isofluran (cp-pharma, Burgdorf, Germany) and 0.25 l/l oxygen. Then mice were injected intraperitoneally one dose of solution containing 25µl Fentanyl (0.05mg/kg body weight), 30µl Midazolam (5mg/kg body

weight, B.Braun, Melsungen, Hessen, Germany) and 15µl Medetomidine (0.5mg/kg body weight, Zoetis, Germany), and half dose was applied for every 45 min during the following surgery, to ensure a stable anesthesia status. Mice were subcutaneously injected 100-150µl Cefotaxim-Natrium solution (0.25mg/g body weight, Fresenius Kabi, Bad Homburg, Germany), to prevent the infection of the wound. When mice were under narcosis, the mouse head was immobilized on a customized stereotactic metal stage on a warming pad. The hair over the skull was removed by hair removal cream (Asid-med, Asid Bonz, Herrenberg, Germany) (Fig. 3. 3 a). Povidon-Iod solution (Braunol, B.Braun, Melsungen, Hessen, Germany) was embrocated on the skin for disinfection (Fig. 3. 3 b). After Povidon-Iod dried out, the skin was carefully incised and cut off with sterile instruments and the skull was exposed (Fig. 3. 3 c-e). The membrane over the skull was gently detached and removed (Fig. 3. 3 f-g). Saline was applied over the exposed skull to maintain moisture. A piece of thin and round glass of diameter 6mm was put on the center of the frontal bone with saline in between glass and the bone surface (Fig. 3. 3 h). The surrounding area of the glass was carefully dried with sterile cotton swab, while the tissue under the glass remained covered with saline. Then, a glue of mixed powder and liquid (Hager & Werken GmbH, Duisburg, Germany) was applied on the surrounding area of the glass to fully cover the exposed tissue (Fig. 3. 3 i). Before the glue got dried, a custom plastic ring with inner diameter 8mm was carefully pasted on the center of the frontal bone, with the glass exactly in the middle of the ring (Fig. 3. 3 j). The ring was further immobilized by applying the glue in the gap between the outer edge of the glass and the inner edge of the ring, as well as the gap between the outer edge of the ring and the tissue. After waiting for at least 30min, the glue got completely dried. 100µl of Buprenorphin (Bayer AG, Leverkusen, Germany) was subcutaneously injected 30min before the awake. Then mice were waked up by subcutaneously injected one dose of 272µl Antagonisierung containing Naloxonhydrochlorid (1.2 mg/kg body weight), Flumazenil (0.5 mg/kg body weight) and Atipamezol (2.5 mg/kg body weight). After surgery, the mice were gently placed in the cage with food and water. Buprenorphin was injected every 12h for

additional 2 times. The supervision and evaluation of the mice was done three times/day for the first two days, and then once a day on the following days. For every imaging, Isofuran was used for the anesthesia. Briefly, mice were anesthetized with Isofluran and the ring was immobilized on a customized stereotactic metal stage. A customized chamber was made to cover the imaging stage, to maintain a stable 37℃ warm environment. Then the mice were placed into the chamber and imaged using a multiphoton LaVision Biotech (Bielefeld, Germany) TrimScope II system connected to an upright Olympus microscope, equipped with a Ti;Sa Chameleon Ultra II laser (Conherent) tunable in the range of 680 to 1080 nm and additionally an optical parametric oscillator (OPO) compact to support the range of 1000 to 1600 nm and a 16 × water immersion objective (numerical aperture 0.8, Nikon). Live images were acquired from 30μm to 40μm depth, with z-interval of 2 or 3μm. 870nm or 900nm was used as an excitation wavelength, with 1030 × 1030 pixels. The signal was detected by Photomultipliers (G6780-20, Hamamatsu Photonics, Hamamatsu, Japan). ImSpector Pro (LaVision) was used as acquisition software. For the vascular labeling, TRITC-Dextran (100μg in 100μl solution, Invitrogen, Massachusetts, USA) was injected intravenously before imaging. For every imaging, we tried to follow the same position in the bone marrow based on the vessel and bone structure. Then 3D time-lapse movies were recorded for 15min with stack depth 2μm and time interval 1min. 3D static images were recorded with stack depth 2μm. During the imaging, the mouse breathing was frequently checked to ensure a stable anesthesia status. After imaging, mice were gently put back in cage and were closely supervised and evaluated with a score sheet.

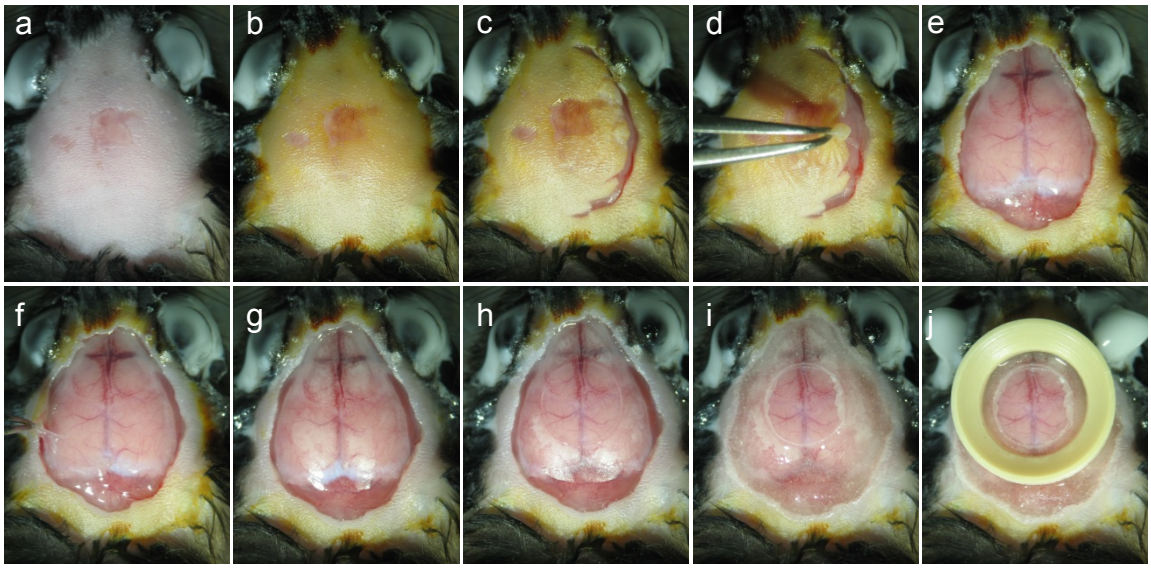


Figure 3.3 a-j Surgical preparation of mouse chronic imaging window.

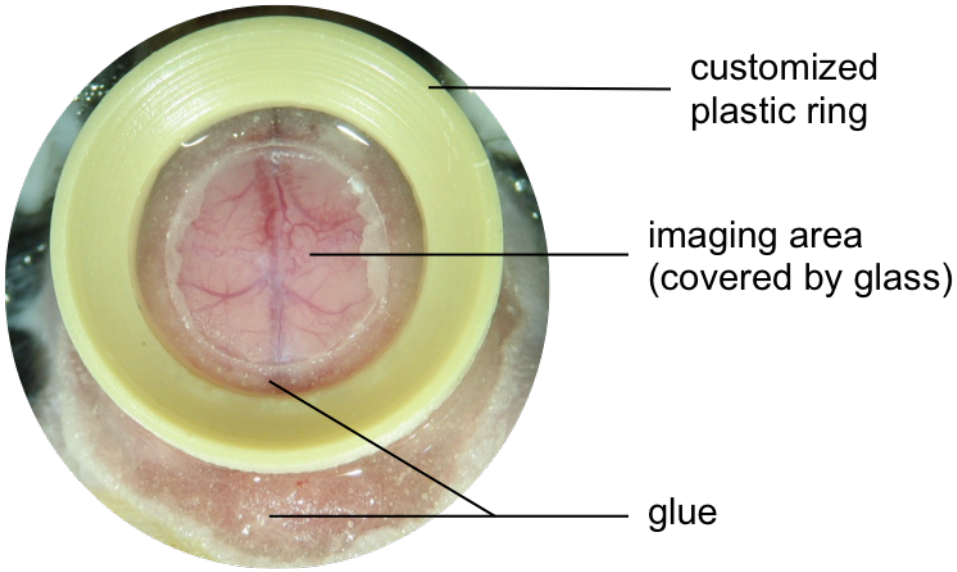


Figure 3.4 Sample picture of a chronic calvarial window on a living mouse skull. Ring inner diameter 8mm, glass diameter 6mm.

## 3.10 Cell dynamics analysis of the chronic imaging of the calvarial bone marrow

From 3D time-lapse movies which we generated from every imaging of the same position, we selected one frame with the best quality. Then we picked up one

stack from each 3D volume, which has exactly the same depth in every imaging, based on the vessel branches as well as the bone structure. The single stacks were then imported and formed a movie in time sequence, by using ImageJ (https://imagej.nih.gov/ij/index.html, an open source image analyzing software by National Institute of Health, USA). Then we used a plugin Stackreg to align all the frames, and this can be repeated several times until the frames were completed aligned. Then the cells were rendered as areas and those trash signals were removed by using brush function. The total number of cells was counted manually. Then we tracked the areas of single cells over time points. For 3D static images, Imaris software (Bitplane, Zurich, Switzerland) was used in the analysis. The static cell was counted as those without any spatial shift at every time point. The migrating cell was counted as those have spatial movement at any of the time points. The cell diameter was quantified by manually measuring the diameters laterally as well as longitudinally and the mean value was taken. The cell distance to vessels was measured manually in Slice mode. Cell and vessel surfaces were created by Imaris Surface function. Cell volume was measured by the software automatically.

### 3.11 Bone marrow cells isolation and megakaryocyte culture

Mice were anesthetized with Isofluran and sacrificed by cervical dislocation. The long bones (femurs, tibiae, humerus) were harvested immediately and put in ice-cold sterile PBS. The bones were then moved into sterile bench. The two sides of the bones were cut open with blade (Feather, Osaka, Japan). The bone marrow was flushed with PBS + 2% fetal calf serum (FCS) through a 26-Gauge needle, until the bones turned white. The bone marrow cells were further flushed through a 20-Gauge needle to achieve single cell suspension. Then the cells were filtered with a 70μm cell strainer (Miltenyl Bioec GmbH, Bergisch Gladbach, Germany) and centrifuged 4℃ 300g for 5min. The supernatant was discarded and the cells were resuspended and incubated in 3ml Erythrocytes lysis buffer for 5min. The lysis was terminated by adding 30ml PBS + 2mM

Ethylenediaminetetraacetic acid (EDTA, Sigma-Aldrich, Saint Louis, MO, USA) and followed by centrifugation 4℃ 300g for 5min. The supernatant was discarded and the cell pellet was resuspended with PBS + 0.5% bovine serum albumin (BSA, Sigma-Aldrich, Saint Louis, MO, USA). The cell number was counted with Neubauer counting chamber. For further purification of the MKs, the bone marrow cells were resuspended with PBS + 0.5% BSA to a concentration of $10^7$ cells/40µl. Then 10µl/$10^7$ cells Mouse Lineage Cell Depletion antibody cocktail (Miltenyl Bioec GmbH, Bergisch Gladbach, Germany) was added in cell suspension and incubated 4℃ for 10min, followed by 20µl/$10^7$ cells Microbeads and incubated 4℃ for 15min. After incubation, cells were centrifuged and resuspended in 2ml PBS + 2mM EDTA + 0.5% FCS. The cell suspension was placed in a FACs tube and put in EasySep™ Magnet (Stemcell Technologies, Vancouver, Canada) for 10min. The lineage cells were labeled with microbeads and attached on the tube wall. The cell suspension was slowly removed into another new tube with a movement and no shaking. Then 30ml PBS + 2mM EDTA + 0.5% FCS was added for washing. The cells were resuspended with 2ml DMEM + 10% FCS and counted. For MK culture, $1\times10^6$ lineage-depleted bone marrow cells were planted in 35mm dish or one well of the 6-well plate (Corning Costar, Sigma-Aldrich, Saint Louis, MO, USA) supplied with DMEM + 10% FCS and 100ng/ml recombinant mouse Thrombopoietin (rm Tpo, ImmunoTools, Friesoythe, Germany). Then cells were placed in an incubator with humidified 5% $CO_2$ and 95% air 37℃ and cultured for 3-6 days.

### 3.12 Fetal liver cells isolation and megakaryocyte culture

E12.5-14.5 pregnant female mice were anesthetized with Isofluran and sacrificed by cervical dislocation. The embryos were taken out and the fetal livers were isolated and put in ice-cold PBS, then moved into sterile bench. The fetal livers were separated into small pieces and gone through a 20-Gauge needle to achieve single cell suspension. Then the cells were filtered with a 70µm cell strainer (Miltenyl Bioec GmbH, Bergisch Gladbach, Germany) and centrifuged 4℃

300g for 5min. The supernatant was discarded and the cells were resuspended and incubated in 3ml Erythrocytes lysis buffer for 5min. The lysis was terminated by adding 30ml PBS + 2mM Ethylenediaminetetraacetic acid (EDTA, Sigma-Aldrich, Saint Louis, MO, USA) and followed by centrifugation 4℃ 300g for 5min. The supernatant was discarded and the cell pellet was resuspended with Dulbecco's Modified Eagle's Medium (DMEM, Sigma-Aldrich, Saint Louis, MO, USA) with 10% FCS. The cell number was counted by Neubauer counting chamber. For MK culture, $1\times10^7$ fetal liver cells were planted in 35mm dish or one well of the 6-well plate (Corning Costar, Sigma-Aldrich, Saint Louis, MO, USA) supplied with DMEM + 10% FCS and 50ng/ml recombinant mouse Thrombopoietin (rm Tpo, ImmunoTools, Friesoythe, Germany). Then cells were placed in an incubator with humidified 5% $CO_2$ and 95% air 37℃ and cultured for 4-5 days.

### 3.13 Megakaryocyte purification

The cultured cells were harvested and centrifuged. The cell pellet was resuspended with 1ml DMEM. Mature MKs were purified by BSA gradient, as described previously [115]. Briefly, 1.5 ml PBS + 3% BSA was placed at the bottom of a 15ml falcon (Corning, New York, USA). 1.5ml PBS + 1.5% BSA was gently placed on top of the 3% BSA. Then cells were gently loaded on top of 1.5% BSA. For fetal liver-derived MKs, the falcon was placed RT for 15-25min. For BM-derived MKs, the falcon was placed RT for 45min. The mature MKs were slowly fell down and enriched at the bottom due to gravity. Then the upper 2ml medium was discarded and the bottom 2ml was collected for the MKs.

### 3.14 Megakaryocyte colony forming unit (CFU-MK) assay

After whole bone marrow cell isolation, $10^5$/well cells were planted in MegaCult®-C Medium (Stemcell Technologies, Vancouver, Canada) with collagen and cytokines (rm TPO 50ng/ml, rm Interleukin-3 10ng/ml) and gently

mixed well. Then 1.5ml cell suspension was slowly loaded to 35mm culture dish or 6-well plate and put in incubator for culture. After 6 days, we scored CFU-MKs according to the manufacturer's protocol.

### 3.15 Flow cytometry

For measuring the fraction and mean fluorescence intensity of MK and MKP population in the BM, whole BM cells were stained with CD41-FITC and CD42-APC for 30min on ice. The cells were resuspended in 10μg/ml Propidium Iodide (PI) for the live/dead cell gating. MK population was defined as $PI^-$ $CD41^+$ $CD42^+$ large cells. MKP was defined as $PI^-$ $CD41^+$ $CD42^-$ cells.

### 3.16 Fluorescence-activated cell sorting (FACS)

For generating Confetti chimeras, we sorted $Lin^-$ $Sca\text{-}1^+$ $c\text{-}Kit^+$ (LSK) cells from β-actin-CreER × Rosa26-Confetti mice. Briefly, we isolated bone marrow cells and did lineage depletion, followed by incubating the cells with the following antibodies: Pacific Blue-conjugated anti-mouse lineage antibodies (Ter-119, CD3, CD8a, CD45R, CD11b, Ly-6G), PE-Cy7 anti-mouse Sca-1, APC anti-mouse c-Kit. Before sorting, the cells were resuspended in 10μg/ml Propidium Iodide (PI) for the live/dead cell gating. The LSK cells were identified as $PI^-$ $Lin^-$ $Sca\text{-}1^+$ $c\text{-}Kit^+$ and sorted by MoFlo Astrios cell sorter (Beckman Coulter, Indianapolis, USA).

### 3.17 EdU proliferation assay

Click-it® EdU Cell Proliferation Assay Kit (Thermo Fisher Scientific, Massachusetts, USA) was used in this assay. In vivo labeling of BM cells with 5-ethynyl-2'-deoxyuridine (EdU) was described previously [116]. Briefly, vWF-eGFP mice were intraperitoneally injected 0.5mg EdU in DMSO. After 4h, the mice were anesthetized with Isofluran and sacrificed by cervical dislocation. The long bones (femurs and tibiae) were harvested for FACs analysis, while the

sternum was harvested for EdU whole-mount staining. The samples were prepared as described above. The detection of EdU was performed according to the manufacturer's protocol. Briefly, for FACs analysis, cells were stained with surface marker antibodies for 30min RT in dark, followed by fixation 15min (100µl 4% PFA, provided in the kit) and permeabilization 15min (100µl saponin-based permeabilization and wash reagent, provided in the kit). The samples were washed with 1% BSA between each step. Then samples were incubated for 30min RT in dark in EdU reaction cocktail containing PBS, Copper protectant, Pacific Blue picolyl azide and reaction buffer additive, according to the manufacturer's protocol. After samples were washed and resuspended with saponin-based permeabilization and wash reagent, they were tested for flow cytometry by using LSRFortessa cell analyzer (BD Biosciences, New Jersy, USA). We gated $vWF^+$ $CD41^+$ $CD42^-$ cells and measured the $EdU^+$ cells within this population using Flowjo software (Ashland, USA). For whole-mount staining, EdU-labeled sternums were cut, blocked/permeabilized for 20min RT with 10% NGS and 0.5% Triton X-100, stained with cell surface antibodies RT overnight. Then samples were incubated for 30min RT in dark in EdU reaction cocktail containing 1× reaction buffer, Copper protectant, Pacific Blue picolyl azide and reaction buffer additive, according to the manufacturer's protocol. The bones were gently washed with 1× PBS between each step. Then the bones were imaged with Two-photon microscopy.

### 3.18 Serum Thrombopoietin measurement

1ml anti-coagulated blood was collected from the heart and kept overnight at 4℃. The next day, the blood was centrifuged with 2000g for 20min. The supernatant (serum) was collected for TPO measurement. We used Quantikine Mouse Thrombopoietin ELISA Kit (R&D Systems, Minneapolis, USA) to measure serum TPO levels, according to manufacturer's protocol.

### 3.19 Statistical analysis

GraphPad Prism software (San Diego, USA) was used for all the statistical analysis. All data were assumed to have Gaussian distribution, unless specified. Before doing statistic analysis, the data were confirmed to have equal variance using F test, and Student's unpaired t-test was used for the comparison of two groups; otherwise unpaired t-test with Welch's correction was used when variences are significantly different. For compairson of multiple groups, one-way ANOVA was used. Error bar indicates standard error of the mean (SEM). P value less than 0.05 was considered significant.

# 4 RESULTS

## Part I: Spatio-temporal organization of megakaryopoiesis at steady state

### 4.1 Criteria for distinguishing megakaryocytes and progenitors

CD41 and CD42 are markers which are widely used to identify MKs. CD41 was shown to be an early stage marker of MKs [45-47], while CD42 is a later stage marker for mature MKs. Immunostaining of CD41 combined with CD42 distinguished the MK progenitors as small, roundish, and $CD41^{+}$ $CD42^{-}$ cells (Fig. 4. 1). Importantly, MKPs and MKs express heterogeneous levels of CD41 (Fig. 4. 2-3), confirmed in immunostaining as well as flow cytometry, which would be another criteria for distinguishing these two populations.

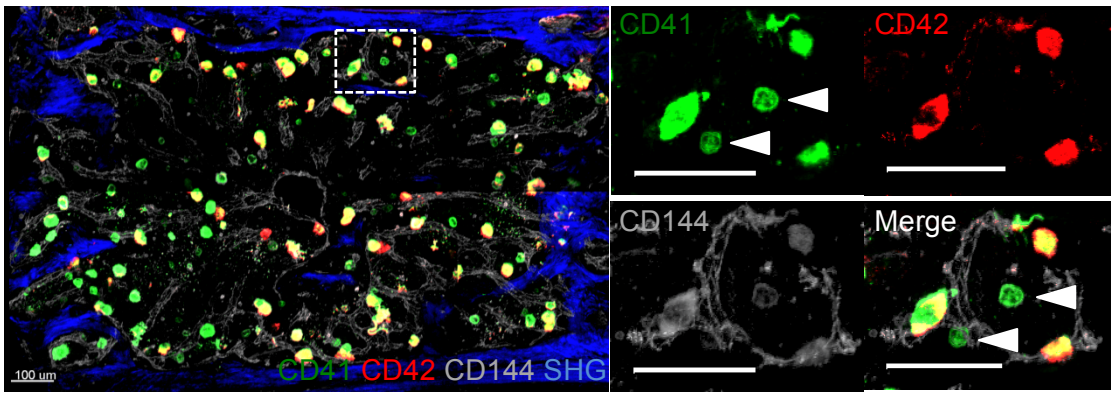


Figure 4.1 Representative whole-mount immunostaining of megakaryocyte progenitors and mature megakaryocytes in murine sternum bone. CD41 labeled early and late stage of MKs. CD42 labeled mature MKs. CD144 labeled endothelial cells. The blue signal indicated the bone structure from the SHG. Arrowhead indicated MK progenitors. Scale bar= 100μm.

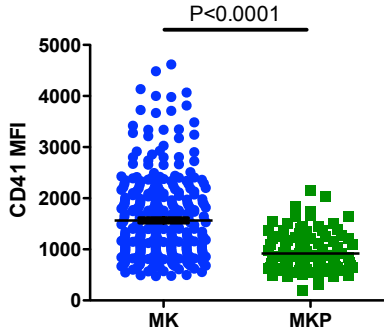


Figure 4.2 Mean Fluorescent intensity of CD41 expressed on MKs and MKPs in WT mice, tested in whole-mount staining. MK: n=328 cells from 3 mice; MKP: n=108 cells from 3 mice. Unpaired t-test with Welch's correction; P<0.0001; error bar=SEM.

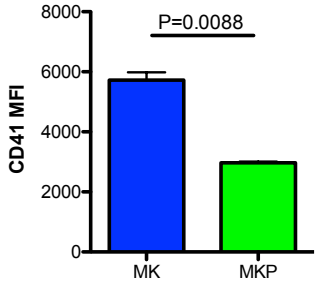


Figure 4.3 Mean Fluorescent intensity of CD41 expressed on MKs and MKPs in WT mice, tested in flow cytometry. n=3 mice in each group. Unpaired t-test with Welch's correction; P=0.0088; error bar=SEM.

## 4.2 Distribution of megakaryocytes within the bone marrow niche

First we would like to find out the spatial localization of megakaryocytes among bone marrow niche cells. We used the whole-mount staining of sternum. Compared to the tissue slice staining, the advantage of the whole-mount staining is to obtain a volume of the bone marrow to a depth of ~70 μm. This will minimize the mistakes of distance measurements. We stained MKs as $CD42^+$ cells, $CD144^+$ as bone marrow endothelial cells, and bone structure as blue signal (second harmonic generation) under two-photon microscopy. We used the CD42

antibody to label the later stage or mature MKs. The vasculature was stained with VE-Cadherin (CD144) antibody, while the osteoblastic niche generates blue signal from the second harmonic generation (SHG) of the two-photon microscopy [117]. Then we measured the distance from MKs to different niche cells. Our whole-mount staining showed that MKs are siting very close to the vascular niche (Fig. 4. 4), with 81.47 ± 3.52 % (n=3) of the MKs located within 5μm to the vessels (Fig. 4. 5). However, their distribution towards the osteoblastic niche was more even without a preference (Fig. 4. 6). Compared with the MKs which were close to the bone (≤20μm), there were much more MKs which were close to the vessels (≤5μm) (Fig. 4. 7). This data indicates that MKs are predominately located at the vascular niche.

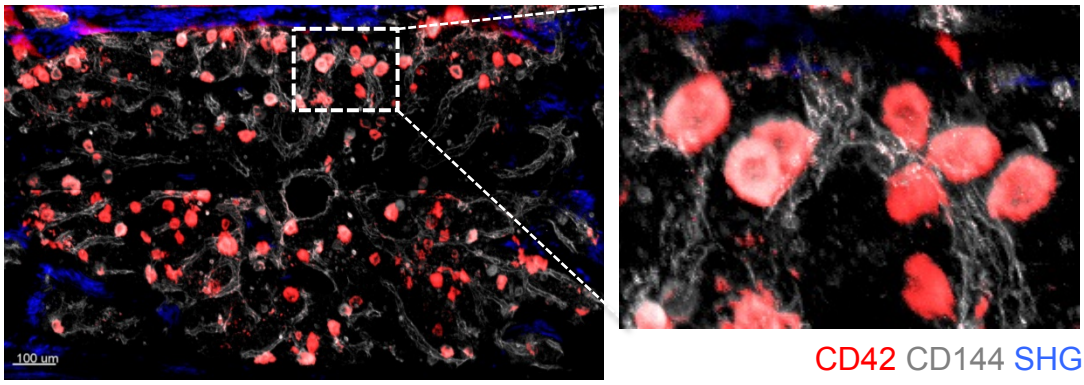


Figure 4.4 Representative whole-mount immunostaining of mature megakaryocytes in murine sternum bone. CD42 labeled mature MKs. CD144 labeled endothelial cells. The blue signal indicates the bone structure from the SHG. Scale bar= 100μm.

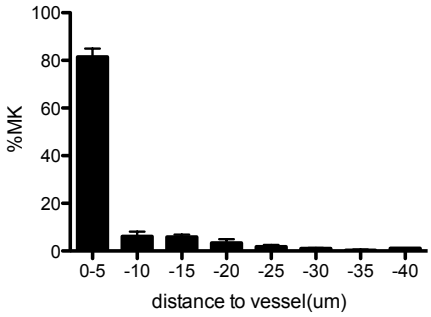


Figure 4.5 Distance between MKs and the vessels, and the percentages of MKs.

The distances were binned into 5-μm intervals. Data are pooled from 3 mice. Error bar=SEM.

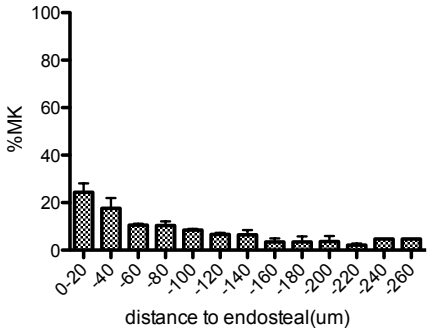


Figure 4.6 Distance between MKs and the bone, and the percentages of MKs. The distances were binned into 20-μm intervals. Data are pooled from 3 mice. Error bar=SEM.

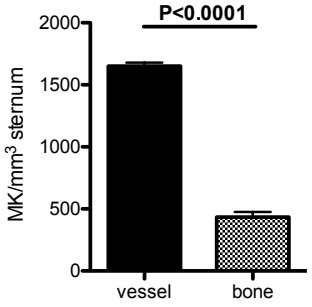


Figure 4.7 Numbers of MKs per 1 $mm^3$ sternum marrow, which are close to the vessels and bones, respectively. Data are pooled from 3 mice. Unpaired t-test; P<0.0001; error bar=SEM.

## 4.3 Distribution of megakaryocyte progenitors within the bone marrow niche

Since MKs are located adjacent to the vessels, next we would like to investigate the positioning of the MK progenitors within the sternum bone marrow niche. As previously described, MKPs are defined as $CD41^+$ $CD42^-$ small cells with low CD41 intensity (Fig. 4. 1). We found 69.63 ± 4.35 % (n=3) of the MKPs are close

(≤5μm) to the vascular niche (Fig. 4. 8), while only a fraction of 14.57 ± 4.49 % (n=3) was found close to the endosteum (Fig. 4. 9). Compared with the MKPs which were close to the bone (≤20μm), there were much more MKPs which were close to the vessels (≤5μm) (Fig. 4. 10). This indicates that the MKPs are generally located close to the vascular niche. They occupy the same niche as their progeny MKs.

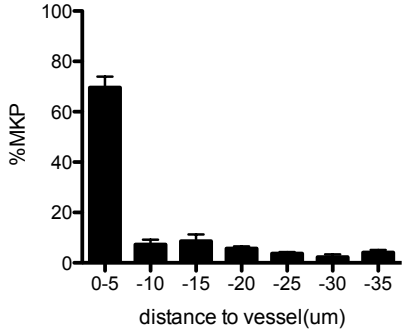


Figure 4.8 Distance between MKPs and the vessels, and the percentages of MKPs. The distances were binned into 5-μm intervals. Data are pooled from 3 mice. Error bar=SEM.

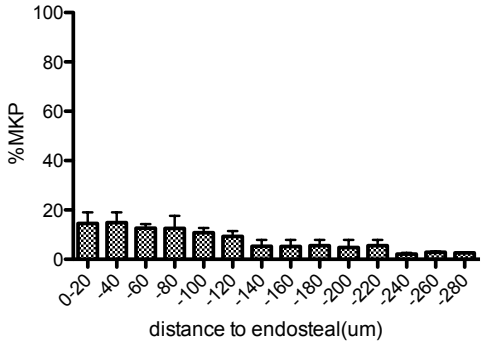


Figure 4.9 Distance between MKPs and the bone, and the percentages of MKPs. The distances were binned into 20-μm intervals. Data are pooled from 3 mice. Error bar=SEM.

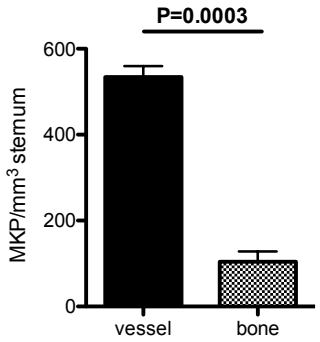


Figure 4.10 Numbers of MKPs which are close to the vessels and bones, respectively. Data are pooled from 3 mice. Unpaired t-test; P=0.0003; Error bar=SEM.

## 4.4 vWF-eGFP mouse model

vWF, also known as von Willebrand Factor, is an important glycoprotein involved in platelet aggregation [118]. It is highly expressed in endothelial cells, platelets and MKs and is responsible for the adhesion of platelets to the endothelium in case of bleeding [118]. The vWF-eGFP mouse was for the first time generated by Dr. Claus Nerlov and Dr. Sten Eirik W. Jacobsen in the University of Oxford and described previously [50]. It was reported that GFP is expressed on the whole MK lineage including platelet-biased stem cells, MK progenitors, MKs as well as platelets. Therefore, it provides a nice tool to visualize MK populations in vivo. We tested this mouse and detected uniform strong GFP signal expressed in platelets, MKs as well as MK precursors. Unexpectedly, GFP barely express on bone marrow endothelium, perhaps due to vWF heterogeneity on different types of vessels in various organs [119]. In order to see whether vWF-eGFP mice have normal expression of MK markers, we performed immuostaining of the MKs in the bone marrow of vWF-eGFP mice, and saw a high correlation of CD42 and GFP which indicated the mature MKs (Fig. 4. 11). The small $GFP^+$ $CD42^-$ cells indicated MK progenitors (Fig. 4. 11). The strong GFP expression also ensures that we can detect the signal in live imaging. We performed a staining of CD41 and found again the high correlation of CD41 and GFP (Fig. 4. 12). The high

overlap of vWF-eGFP with CD41 and CD42 also suggests that these markers are ideal tools to identify MKs and MKPs. Compared with the WT mice, the vWF-eGFP mice have normal numbers of platelets, and also normal numbers as well as size of the MKs and MKPs (Fig. 4. 13-15). This indicates that vWF-eGFP mice have normal expression of MK markers and normal megakaryopoiesis. Next, in order to test whether the GFP signal is specifically expressed on MK lineage, we co-stained the bones from vWF-eGFP mice with different lineage markers, and did not find the overlap of GFP expression on lineage cells including neutrophils, monocytes, lymphocytes and erythrocytes (Fig. 4. 16). This indicates that the GFP signal in vWF-eGFP mice specifically labels the MK lineage cells. Therefore, the vWF-eGFP mouse is an ideal mouse model for studying the MK lineage cells.

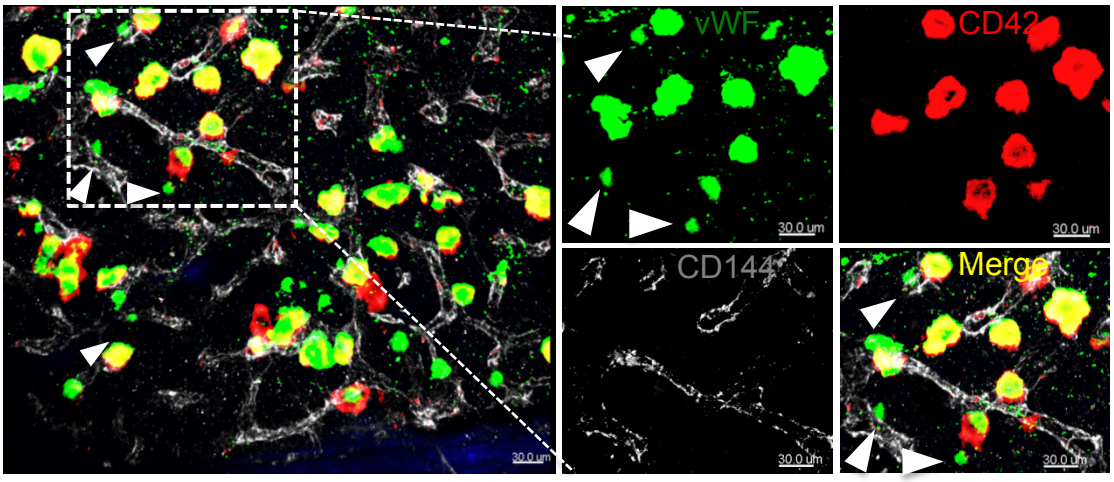


Figure 4.11 Representative whole-mount immunostaining of megakaryocytes in femur of vWF-eGFP mouse. CD42 labeled mature MKs. CD144 labeled the endothelial cells. Arrowhead indicated MK progenitors. Scale bar=30µm.

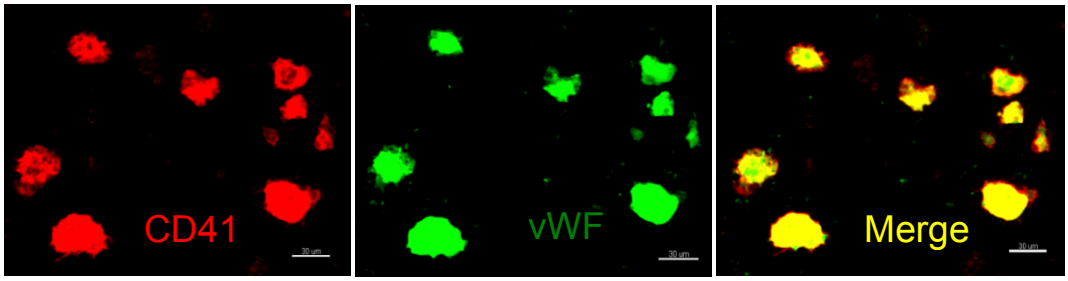


Figure 4.12 Representative whole-mount immunostaining of megakaryocytes in femur of vWF-eGFP mouse. CD41 labeled mature and immature MKs. Scale bar 30μm.

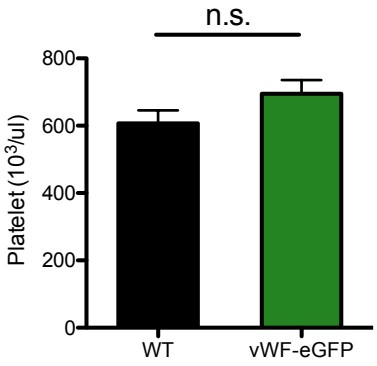


Figure 4.13 Platelet numbers in peripheral blood from wide type mice (WT) and vWF-eGFP mice. WT group n=14, vWF-eGFP group n=7. Unpaired t-test; error bar= SEM. n. s.= no significance (P=0.17).

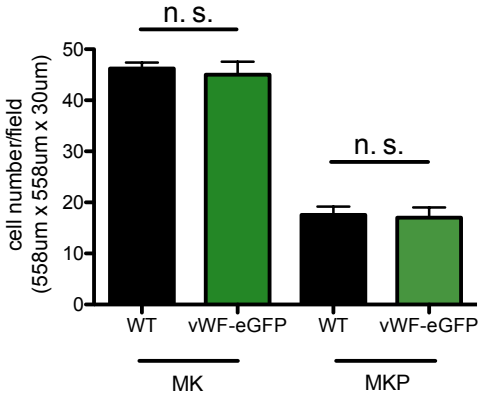


Figure 4.14 MK and MKP numbers in the bone marrow of wide type mice (WT) and vWF-eGFP mice respectively. n=3 in each group. Unpaired t-test; error

bar=SEM. n. s.= no significance (P=0.68 for MK comparison; P=0.84 for MKP comparison).

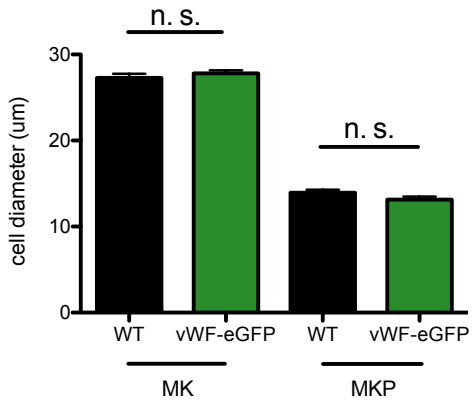


Figure 4.15 MK and MKP diameters in the bone marrow of wide type mice (WT) and vWF-eGFP mice respectively. For MK comparison, WT group: n=83 cells from 3 mice; vWF-eGFP group: n=68 cells from 3 mice; upaired t-test with Welch's correction. For MKP comparison, WT group: n= 62 cells from 3 mice; vWF-eGFP group: n=56 cells from 3 mice; unpaired t-test. Error bar=SEM. n. s. = no significance (P=0.38 for MK comparison; P=0.10 for MKP comparison).

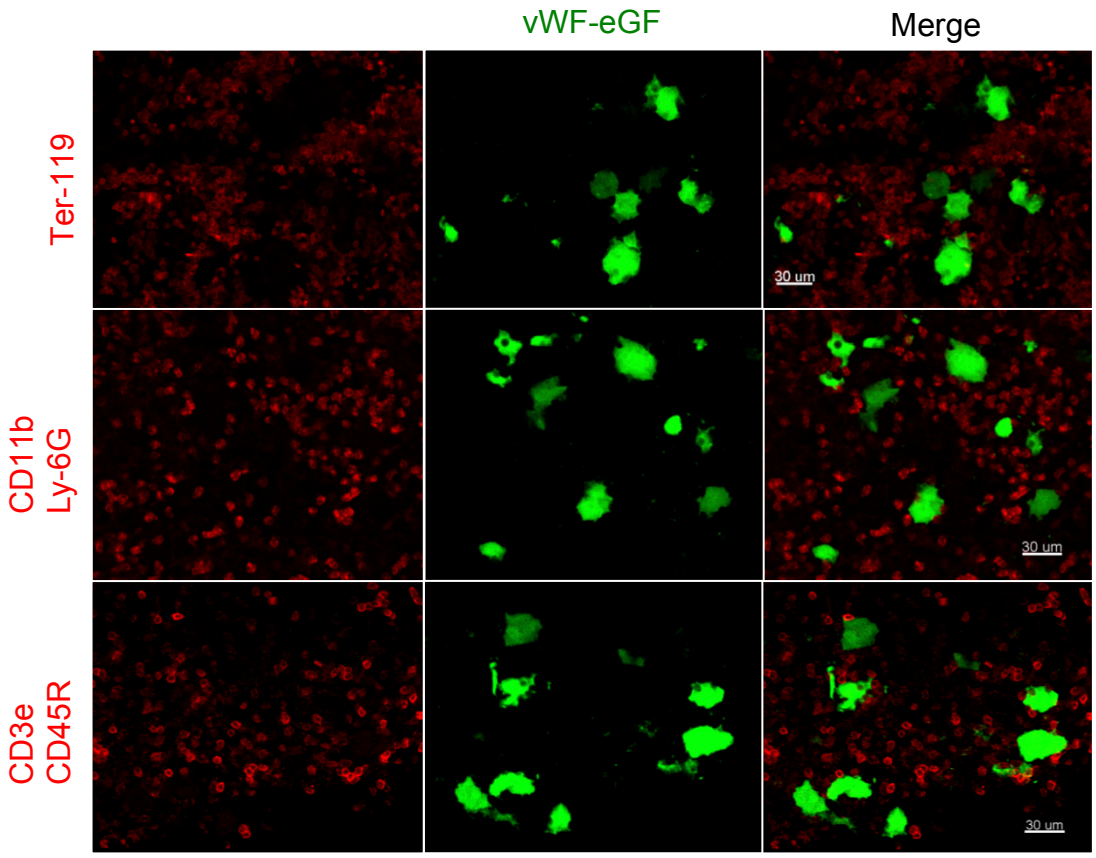


Figure 4.16 Immunostaining of erythrocytes (Ter-119), granulocytes (CD11b, Ly-6G) and lymphocytes (CD3e, CD45R) in the bone marrow of vWF-eGFP mouse. Scale bar= 30µm.

## 4.5 Short term dynamics of megakaryocytes in the calvarial bone marrow in vivo

Currently, it is widely accepted that MK has the ability to migrate, both in vivo and in vitro [33-35]. It was previously shown that MKs migrate towards the vascular niche which was mediated by stromal derived factor 1 (SDF-1) [33]. However, in our previous investigations we found that MKs are not migratory. In order to test the motility of MKs in vivo, we performed calvarium live imaging using several mouse strains CD41-YFP, PF4 Cre × Rosa26-mT/mG and vWF-eGFP, in which the MKs are detected by their distinct morphology as well as fluorescent protein expression. We found that their velocity remains very low in all three mouse

strains (Fig. 4. 17). To exam the localization of MKs in calvarial bone marrow, we quantified the distance from MKs to vessels in live imaging of different fluorescent mouse models. We found nearly all MKs are lying directly at the vessel (Fig. 4. 18). Together, these data suggest that MKs stably occupy the vascular niche and they do not migrate.

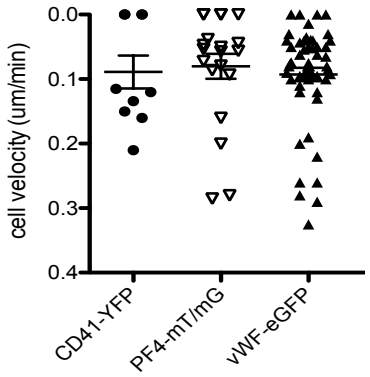


Figure 4.17 The velocity of MKs in CD41-YFP (n=10 cells from 3 mice), PF4 Cre × Rosa26-mT/mG (n=20 cells from 4 mice), vWF-eGFP mice (n=54 cells from 7 mice) at steady state, quantified in calvarium live imaging data.

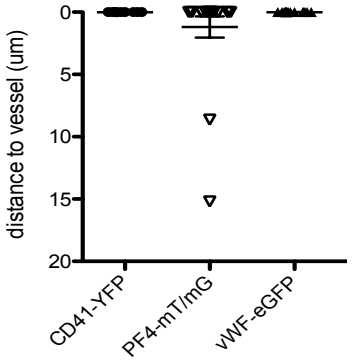


Figure 4.18 Distance of MKs to vessels in CD41-YFP (n=10 cells from 3 mice), PF4 Cre × Rosa26-mT/mG (n=20 cells from 4 mice) and vWF-eGFP mice (n=18 cells from 7 mice) at steady state, quantified in calvarium live imaging data.

## 4.6 Short term dynamics of distinct MKP populations in the calvarial bone marrow in vivo

Since MKs do not migrate, next we would like to explore the dynamics of MK progenitors. Therefore, we used vWF-eGFP mice to investigate the MKP motility within the bone marrow in vivo. Interestingly, we found that MKPs display heterogeneous motility that can be categorized further into two sub-populations. Some MKPs have very low traveling speed, while another fraction of MKPs have high motility which migrate constantly (Fig. 4. 19). We quantified the diameters and traveling speed for all the cells in the images and we observed the distribution of three cell populations (Fig. 4. 20). Based on these observations, we distinguished the populations by their size and motility, with the following standard: the MKs have a size ≥20μm and migrating speed <0.5μm/min; the non-motile MKPs have a size <20μm and migrating speed <0.5μm/min; the motile MKPs have a size <20μm and migrating speed ≥0.5μm/min. We found out that the majority of the $vWF^+$ cells in the calvarium are MKs, while the non-motile and motile MKPs are in lower numbers (Fig. 4. 21). We also found that the motile MKPs have robust movement compared to the non-motile MKPs (Fig. 4. 22), and, interestingly, they are generally much smaller than the non-motile cells (diameter ~10μm) (Fig. 4. 23). We also looked at the spatial relationships between vessels and different MKPs in calvarial imaging. As shown, both MKs and non-motile MKPs are highly close to the vessels, while a fraction of motile MKPs are distant from the vessels (Fig. 4. 24), probably due to their feature of migration. During their migration, they show displacement shift towards the vessels (Fig. 4. 25). Combined, these data for the first time demonstrated the heterogeneity of MKPs dynamics. Most MKPs are not migratory, and they in general have intimate associations with the vascular niche, while a very small fraction of MKPs are migrating actively.

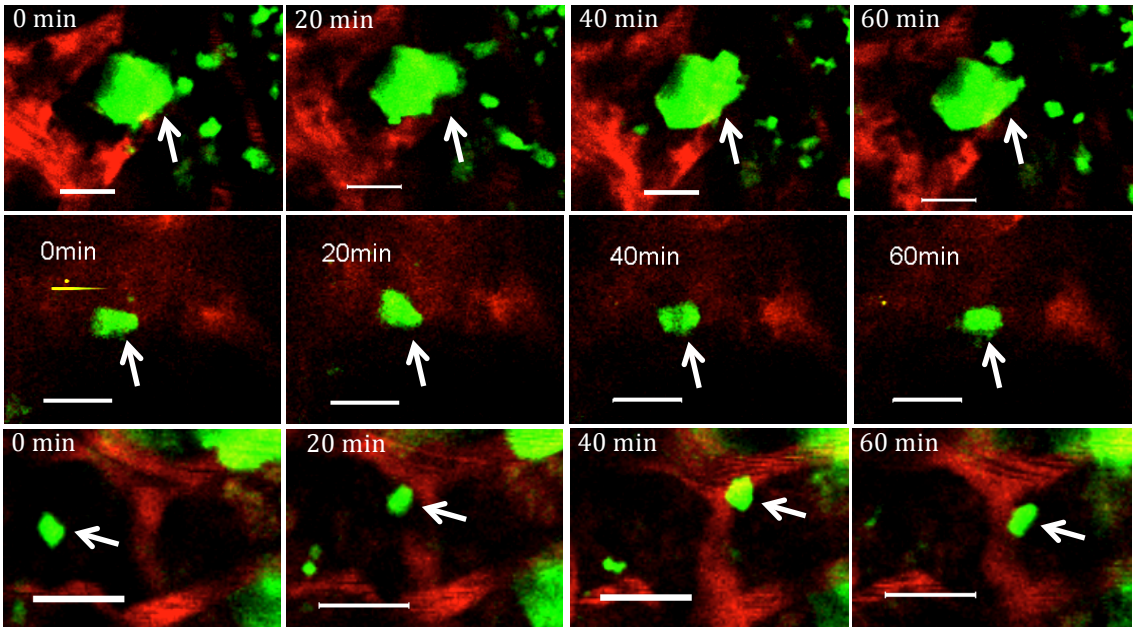


Figure 4.19 Single cell dynamics of three MK populations over time: upper, MK; middle, non-motile MKP; lower, motile MKP. Scale bar= 20μm.

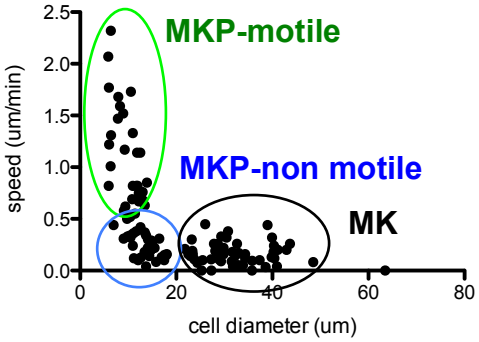


Figure 4.20 The size and traveling speed of $vWF^{+}$ cells in live imaging of vWF-eGFP mice. The cells distribute in three populations, MKP-motile, MKP-non motile and MK. A total number of 116 cells from 7 mice are included.

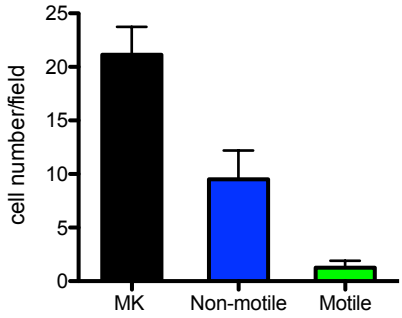


Figure 4.21 The number of MKs, non-motile MKPs and motile MKPs in one image volume (558μm ×558μm × ~30μm). Data are pooled from 4 mice. Error bar=SEM.

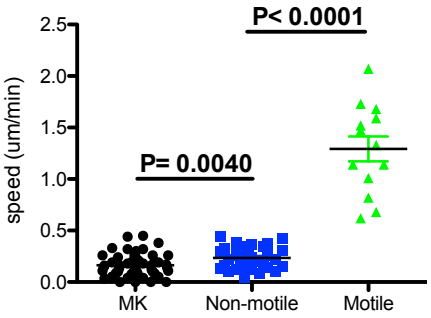


Figure 4.22 The traveling speed of MKs (n=52), non-motile MKPs (n=33) and motile MKPs (n=31). Data are pooled from 7 mice. For comparison of MKs with non-motile MKPs, unpaired t-test is used, P=0.004; for comparison of non-motile MKPs with motile MKPs, unpaired t-test with Welch's correction is used, P<0.0001. Error bar=SEM.

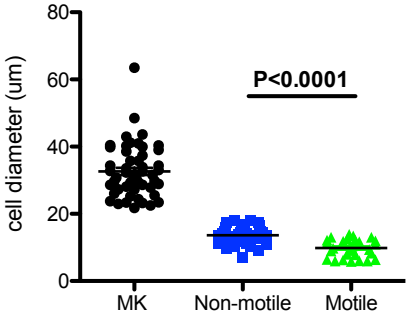


Figure 4.23 The diameters of MKs (n=52), non-motile MKPs (n=33) and motile

MKPs (n=31). Data are pooled from 7 mice. For comparison of non-motile MKPs with motile MKPs, unpaired t-test is used, P<0.0001. Error bar=SEM.

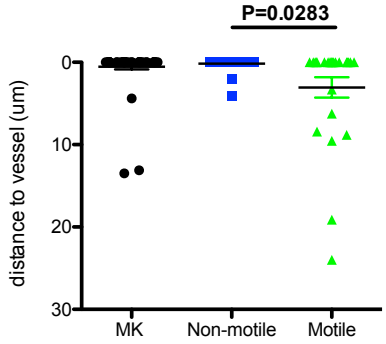


Figure. 4.24 The distance of MKs (n=58 cells), non-motile MKPs (n=36 cells) and motile MKPs (n=26 cells) to vessels in vWF-eGFP mice. Data are pooled from 7 mice. Unpaired t-test with Welch's correction; P=0.0283; error bar=SEM.

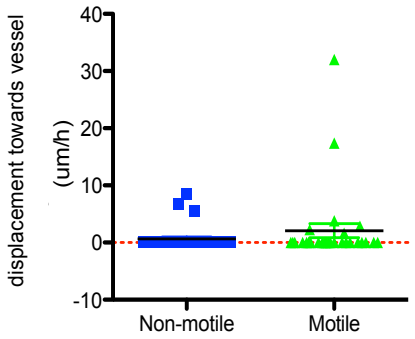


Figure. 4.25 The displacement of non-motile MKPs (n=33 cells) and motile MKPs (n=29 cells) towards vessels in vWF-eGFP mice. Data are pooled from 7 mice.

## 4.7 Short term dynamics of MK-MKP interaction in the calvarial bone marrow in vivo

During our in vivo observations we directly visualized MKPs and MKs interactions, shown in Fig. 4. 26 that a MKP coming close towards a MK. This provides us a hint that there might be intimate interactions within the MK populations.

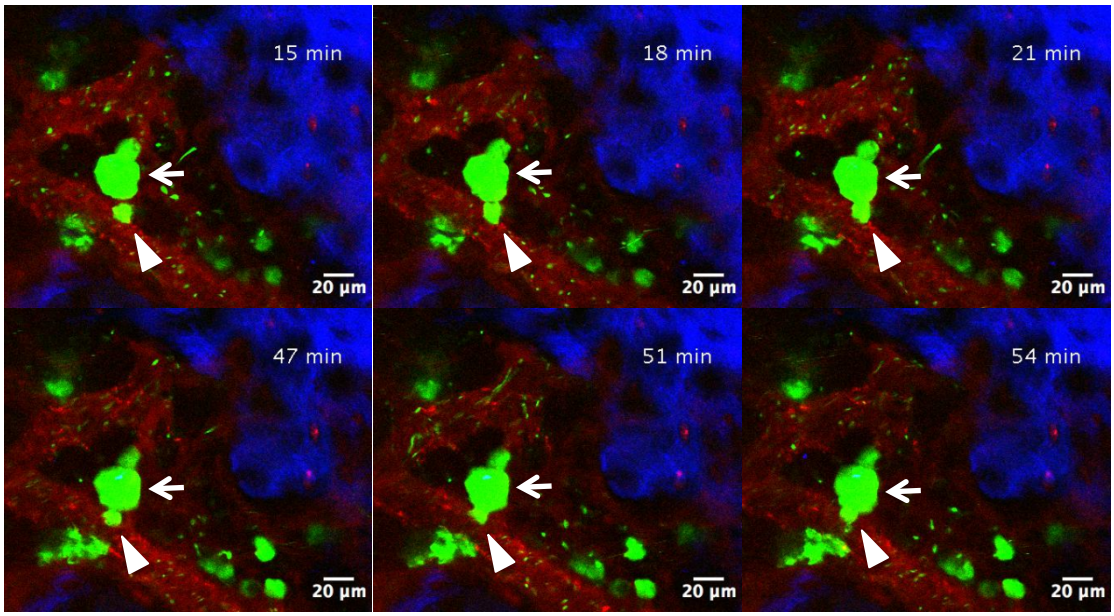


Figure 4.26 Snaptshots from a calvarial live imaging movie from a vWF-eGFP mouse. Dextran-TRITC was injected intravenously for the vascular label. SHG shows the bone structure. Arrow indicates a MK. Arrowhead indicates a migrating MKP. Scale bar= 20µm.

## 4.8 Long term dynamics of megakaryocytes in the calvarial bone marrow in vivo

Next, we performed chronic imaging to visualize the dynamics of MK populations in vWF-eGFP mice over long period of time (~2 days). After images were obtained, three-dimensional reconstruction was performed for $vWF^+$ cells (green) as well as vessel structure (red) (Fig. 4. 27). When we were tracking single cells over time, we found the vast majority of $vWF^+$ cells stay at the exact same position during the whole imaging period, as the static cells occupied 95.02 ± 1.23 % (n=5 areas from 5 mice) of the whole population (Fig. 4. 28). Then we focused on the mature MKs. We found that MKs do not shift their locations during the development, with 97.81 ± 1.7 % (n=8 areas from 5 mice) of the MKs remain at the exact same position (Fig. 4. 29). As mature MKs are forming proplatelets and giving rise to platelets, they become smaller and finally disappear with an average speed of 622.8 ± 101.2 $\mu m^3$ per hour (n=14 cells from 5 mice) (Fig. 4. 30, 31).

Together, it further confirms that MKs are static cells and their spatial localization remains quite stable.

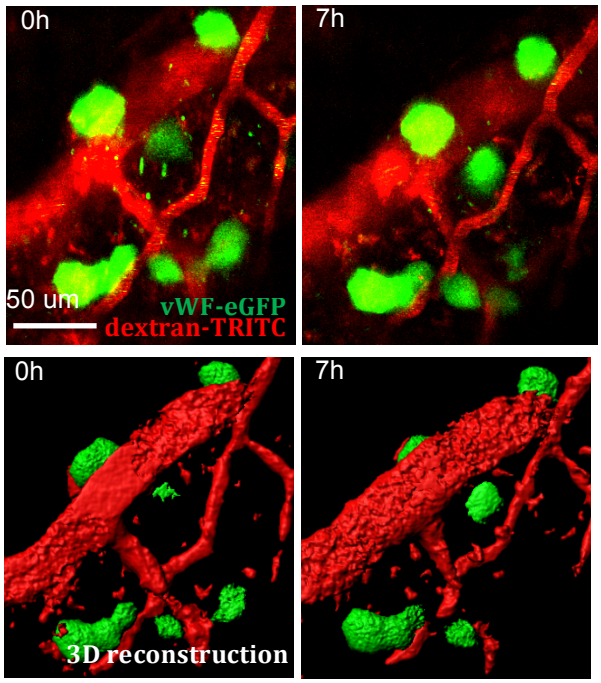


Figure 4.27 Snapshots of chronic image series (upper) and corresponding 3D reconstructed images (lower) from one bone marrow area of a vWF-eGFP mouse calvarian at time point 0h and 7h. Vessesls are labeled with dextran-TRITC. Scale bar= 50 μm.

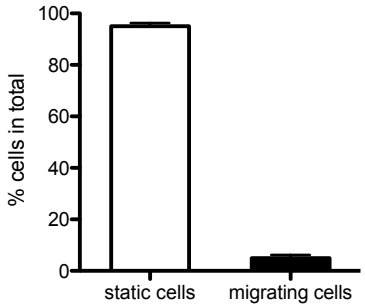


Figure 4.28 Percentage of $vWF^{+}$ cells which remain static and which change locations during the entire chronic imaging period. Data are pooled from 5 mice. Error bar=SEM.

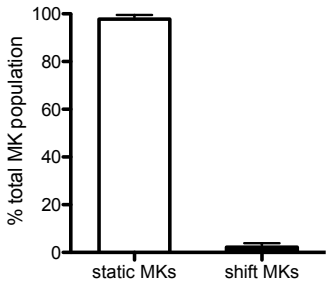


Figure 4.29 Percentage of MKs which remain static and which change locations during the entire chronic imaging period. Data are pooled from 5 mice. Error bar=SEM.

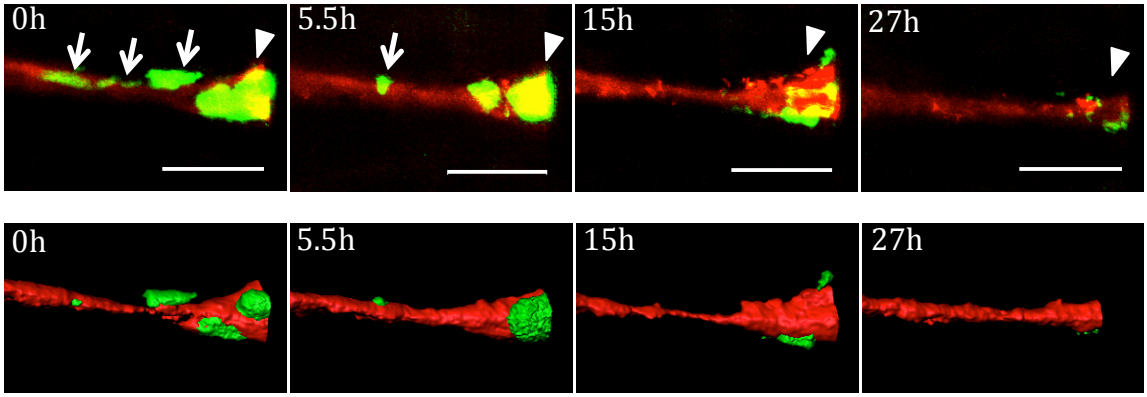


Figure 4.30 Snapshots of chronic image series (upper) and corresponding 3D reconstructed images (lower) from one bone marrow area of a vWF-eGFP mouse calvarian. Vessesls are labeled with dextran-TRITC. Arrowhead indicates a MK. Arrows indicate the proplatelet of this MK in the vessel. Scale bar= 50μm.

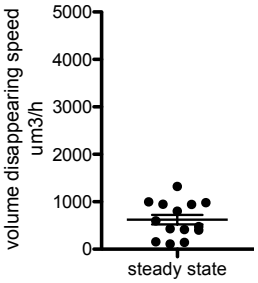


Figure 4.31 Volume disappearing speed of MKs in vWF-eGFP mice (n=14 cells from 4 mice). Error bar=SEM.

## 4.9 Long term dynamics of MK progenitors in the calvarial bone marrow in vivo

Next we explored the long term dynamics of MK progenitors using chronic imaging technique. We detected a group of $vWF^+$ small cells, which we proposed as non-motile MK progenitors, are gradually growing up in average speed of 328.9 ± 27.01 $\mu m^3$ per hour (n=53 cells from 5 mice) without spatial shift (Fig. 4. 32, 33). We also found another group of MKPs are migrating actively within the bone marrow while their size remains small without increase, which we term motile MKPs (Fig. 4. 34). When we compared these two heterogeneous MKP sub-populations, we found motile MKPs are generally smaller than non-motile MKPs (Fig. 4. 35). These observations are in consistent with our previous findings in live imaging. When we were tracking the cells in chronic imaging, we found non-motile MKPs are growing constantly over time, while motile MKPs remain the same size without maturation (Fig. 4. 36). Altogether, these results confirm our previous finding of two heterogeneous MKP sub-populations, and also reveal that MKP maturation takes place in situ.

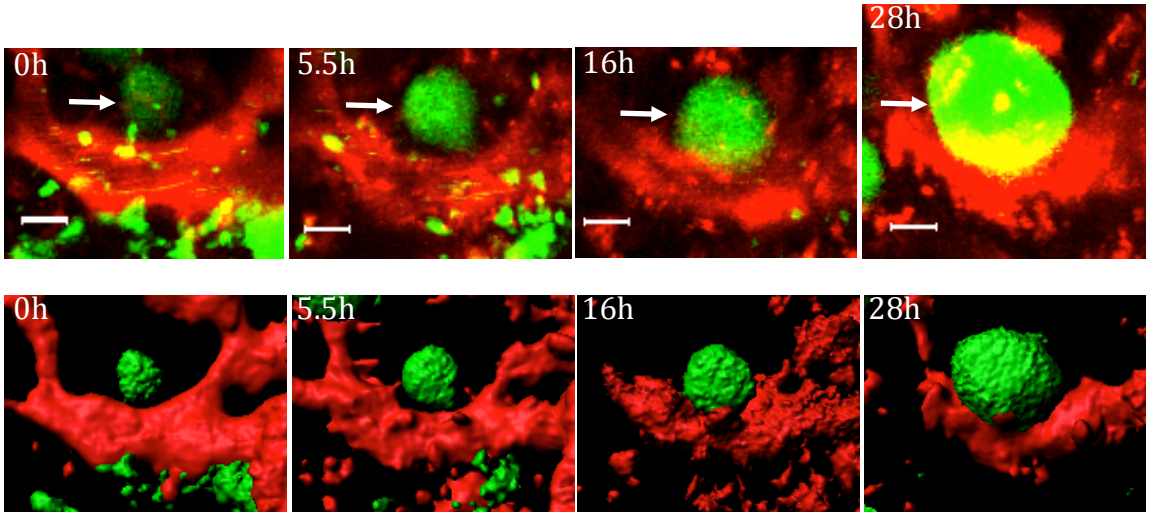


Figure 4.32 Snapshots of chronic image series (upper) and corresponding 3D reconstructed images (lower) from one bone marrow area of a vWF-eGFP mouse calvarian. Vessesls are labeled with dextran-TRITC. Arrow indicates a small

vWF$^+$ cell (MKP) is gradually growing up. Scale bar= 10μm.

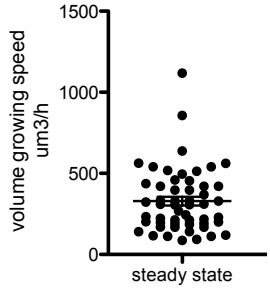


Figure 4.33 Volume growing speed of non-motile MKPs in vWF-eGFP mice (n=53 cells from 5 mice). Error bar=SEM.

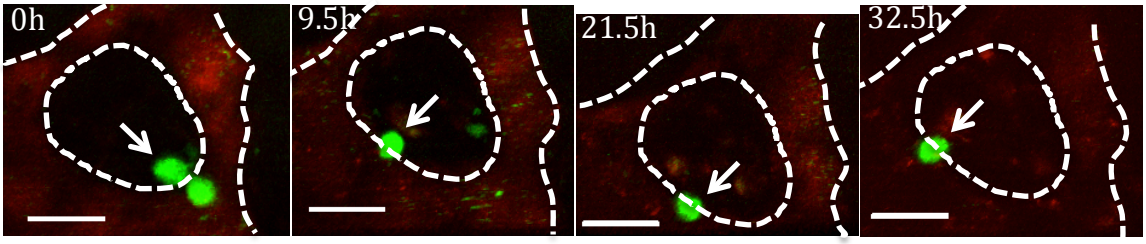


Figure 4.34 Snapshots of chronic image series from one bone marrow area of a vWF-eGFP mouse calvarian. Vessesls are labeled with dextran-TRITC and contoured. A small vWF$^+$ cell (MKP, arrow-pointed) is migrating in the bone marrow. Scale bar= 30μm.

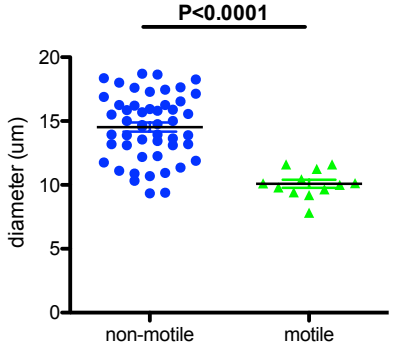


Figure 4.35 Diameters of non-motile MKPs (n=50 cells) and motile MKPs (n=12 cells). Data are pooled from 5 mice. Unpaired t-test with Welch's correction,

P<0.0001, error bar=SEM.

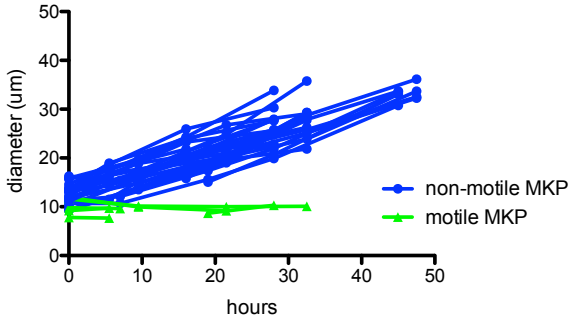


Figure 4.36 Diameters of non-motile and motile MKPs over time. For non-motile MKPs, n=27 cells from 5 mice. For motile MKPs, n=6 cells from 3 mice.

## 4.10 The definition of megakaryopoietic island

When we were tracking single cells over time, we found some big cells are disappearing (such as cell #1 shown in Fig. 4. 37), some small cells are continuously growing big (such as cell #2 shown in Fig. 4. 37), and some small cells appear and start growing (such as cell #3 and #4 shown in Fig. 4. 37). We quantified the number of $vWF^+$ cells in confined bone marrow areas and found the cell number always remains constant although there are cells appearing and disappearing (Fig. 4. 38, 39). This data strongly proposes for a functional unit of MK populations which we term as megakaryopoietic island (MK island) from now on. When we tracked the positioning of single cells in chronic image series, we found that most cells have close connections with the vessels throughout the entire development process (Fig. 4. 40). This is in consistent with our previous finding in bone marrow whole-mount staining that MK populations are predominately localized at the vascular niche. In total, 68 $vWF^+$ small cells from 5 mice were involved in the analysis. Among them we found 66 cells from 5 mice always appear at the vessels at every time point of imaging, while only one cell shift its position away from the vessel and another cell migrate towards the vessel (Fig. 4. 41). This data indicates that vessels are tightly associated with MK

islands.

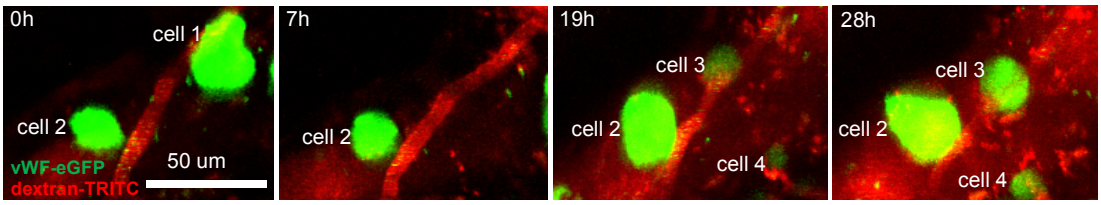


Figure 4.37 Snapshots of chronic image series from one bone marrow area of a vWF-eGFP mouse calvarian over time. Vessesls are labeled with dextran-TRITC. Cell 1 indicates a mature MK disappear after 7h. Cell 2 indicates a immature MK growing up gradually. Cell 3 and 4 indicate small MKPs appear, settle down and start growing. Scale bar= 50 μm.

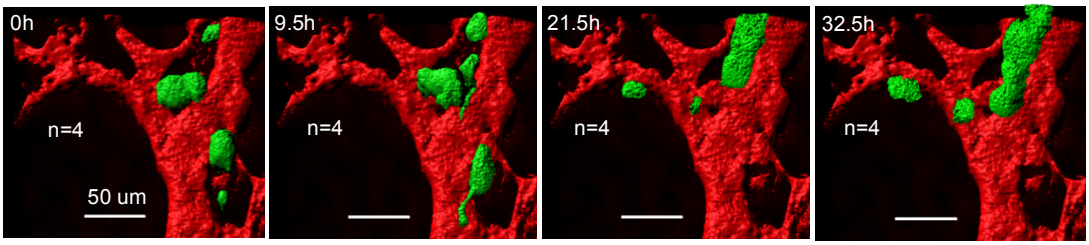


Figure 4.38 Snapshots of reconstructed chronic image series from one bone marrow area of a vWF-eGFP mouse calvarian over time. Vessesls are labeled with dextran-TRITC. Number of $vWF^{+}$ cells was measured in every image. Scale bar= 50 μm.

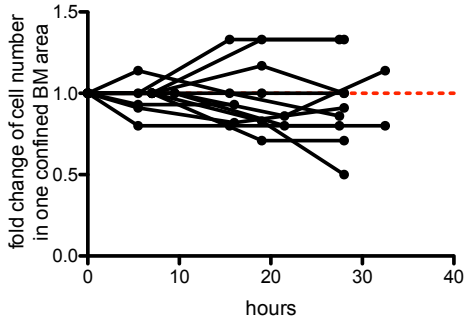


Figure 4.39 Fold change of cell number in one confined bone marrow area over time. Data are pooled from 12 areas from 5 vWF-eGFP mice.

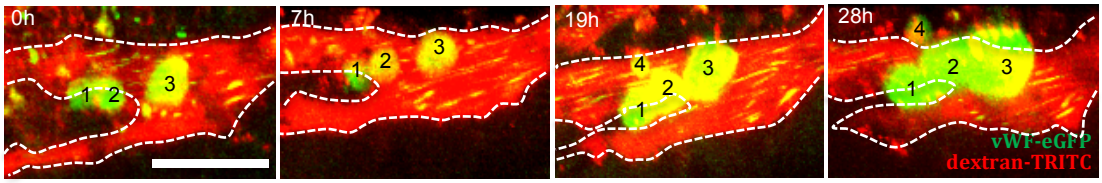


Figure 4.40 Sample snapshots of chronic image series from one bone marrow area of a vWF-eGFP mouse calvarian. Vessesls are labeled with dextran-TRITC and contoured. Cell 1, 2 and 3 indicate growing MKPs attached to a vessel. Cell 4 indicates a new MKP appear and settle down close to the MK island. Scale bar= 50μm.

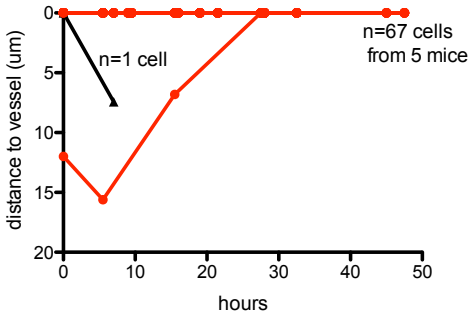


Figure 4.41 Distance of MKPs to vessels over time. Red lines indicate cells which are attached to vessels or coming to vessels. Black lines indicate cells that do not show associations with the vessels. A total number of 68 cells from 5 mice are included.

## 4.11 The spatial relationships between megakaryocytes and precursors

In order to further confirm the existence of MK islands, next we explored the spatial relationships between MKs and precursors. In whole-mount staining we found that MKPs are generally localized adjacent to MKs (Fig. 4. 42). We frequently observed direct MK-MKP contact with a considerable ratio of 25.93 ± 2.49 % (n=3) MKPs involved (Fig. 4. 43). This suggests that MKPs are generally localized adjacent to MKs. In whole-mount staining of vWF-eGFP mice, we found a rare population of $CD41^{-}$ $vWF^{+}$ small cells located adjacent to MKs (Fig. 4. 44)

which we assumed are platelet-biased stem cells. To confirm the localization of these cells, we performed whole-mount staining of bones from vWF-eGFP mice with CD41 and CD150, and we found $vWF^+$ HSCs are more likely to appear in proximity to MKs than $vWF^-$ HSCs (Fig. 4. 45-46). This suggests that platelet-biased stem cells are spatially close to the MKs. Altogether, these results prove that MK populations are in intimate spatial relationships, further indicating an anatomic basis of MK island.

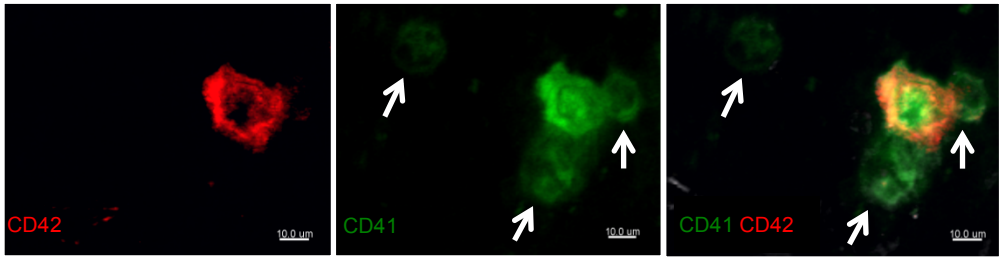


Figure 4.42 Representative whole-mount immunostaining of megakaryocytes and progenitors in murine sternum bone. CD42 labeled mature MKs. CD41 labeled early and late stage of MKs. Arrowheads indicate MKPs. Scale bar= 10μm.

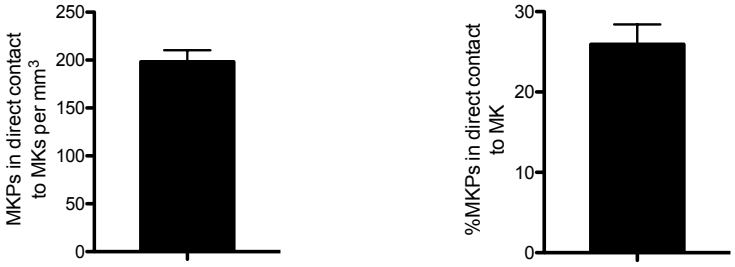


Figure 4.43 Density (left) and percentage (right) of MKPs which are directly attached to the MKs in C57Bl6 mice (n=3). Error bar=SEM.

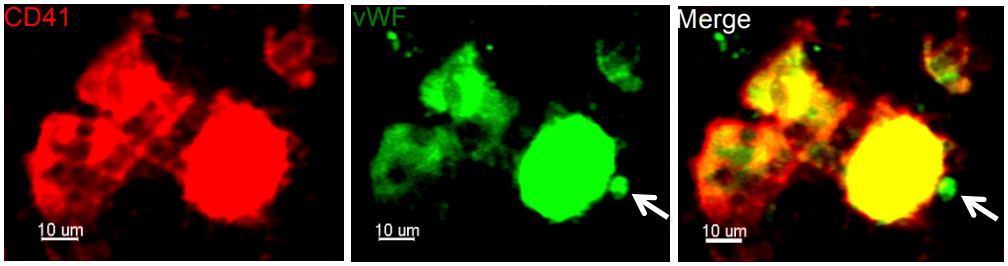

Figure 4.44 Representative whole-mount immunostaining of megakaryocytes and progenitors in vWF-eGFP mouse sternum bone. CD41 labeled MKPs and mature MKs. vWF-eGFP labeled all stages of MKs. Arrow indicates a small $CD41^-$ $vWF^+$ cell. Scale bar= 10μm.

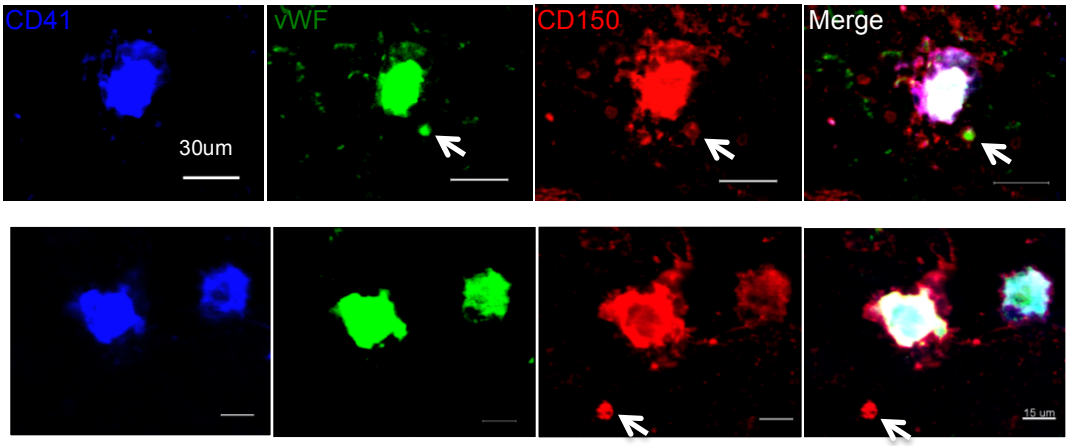


Figure 4.45 Representative whole-mount immunostaining of megakaryocytes and hematopoietic stem cells in vWF-eGFP mouse sternum bone. Arrow indicates HSCs. Upper image: MK was stained as $CD41^+$ $vWF^+$ $CD150^+$ big cell; vWF+ HSC (platelet biased HSC) was stained as $CD41^-$ $vWF^+$ $CD150^+$ small cell; Scale bar= 30μm. Lower image: $vWF^-$ HSC (other HSC) was stained as $CD41^-$ $vWF^-$ $CD150^+$ small cell; Scale bar= 15μm.

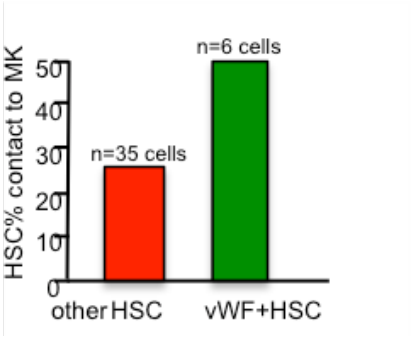


Figure. 4. 46 Percentage of $vWF^-$ HSCs (n=35 cells) and $vWF^+$ HSCs (n=6 cells) which have direct contact to MKs. Data are pooled from 3 mice.

## 4.12 The observation of MK island

In order to directly observe the formation of MK islands, we generated BM chimeras from β-actin-Cre × Rosa26-Confetti mice. After bone marrow Lin$^-$ Sca-1$^+$ c-kit$^+$ (LSK) cells were transplanted into irradiated C57Bl6 mice pretreated with Tamoxifen, Cre was activated and donor LSK cells started to express one out of four fluorescent proteins. When LSK cells homing to recipient bone marrow, they engrafted and reconstituted the injured bone marrow. Then we would be able to observe the clonal expansion of single-color progenies origin from one stem cell (Fig. 4. 47). As shown in a whole-sternum mosaic image, plenty of single-color cell colonies were detected (Fig. 4. 48). Among these lineages, a few MK islands were also detected by the huge morphology. The MKs in one island are of the same color and they are gathering close (Fig. 4. 48). The observation of MK islands reveals the clonal expansion of MK lineage and their unit-like expansion.

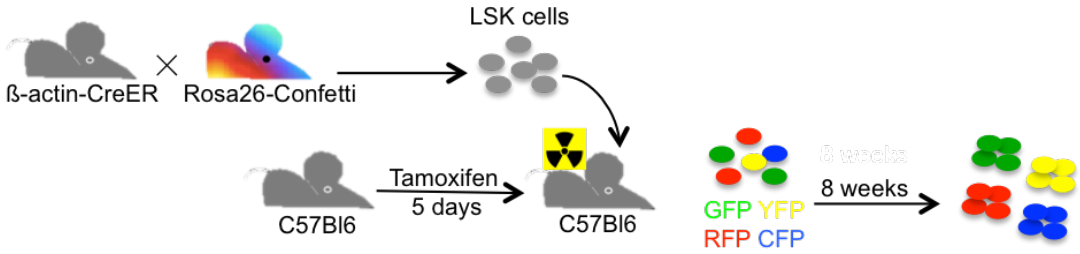


Figure 4.47 Bone marrow transplantation scheme for Confetti chimeras.

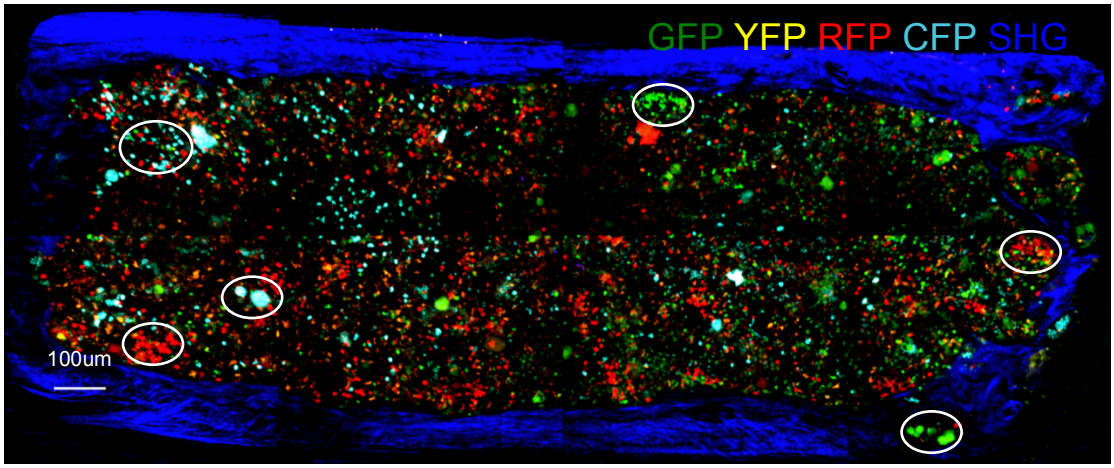

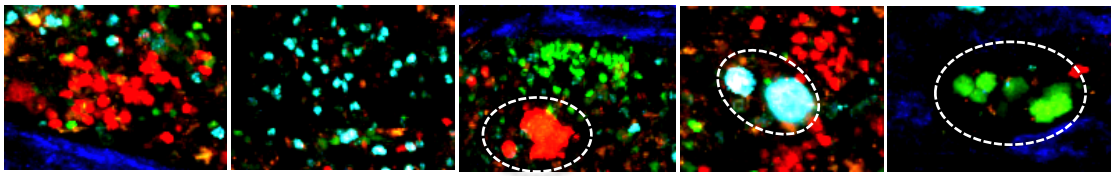

Figure 4.48 Representative whole-mount sternum mosaic image (upper) and screenshots of various lineage cell colonies (lower) from Confetti chimera 24h after platelet depletion. Confetti cells randomly express one of four fluorescent proteins GFP, YFP, RFP and CFP. SHG=second harmonic generation. Upper, circles indicate cell colonies. Lower, first two images show other lineage cell colonies; circles in last three images indicate MK islands. Scale bar= 100μm.

**Part II: Adaptions of megakaryopoiesis during hematopoietic stress**

4.13 Acute response of MK populations upon induced thrombocytopenia

Platelet depletion has been widely used as a manipulation to induce thrombocytopenia and trigger the development of MKs [110, 111]. Mice were injected GPIb (CD42) antibody intravenously to neutralize platelets, as a mimic of immuno-thrombocytopenia. The platelet number rapidly drops to <10% as soon as the depletion antibody is injected. Then we observed the acute MK response upon this stress condition. First of all, we performed calvarial live imaging of vWF-eGFP mouse 6h after platelet depletion. Our observation shows the main effect in the initial phase of platelet depletion is the stimulation of rapid platelet production, displayed by lots of MK cytoplasmic fragmentation taking place within the bone marrow (Figure 4. 49). Later on, the small pieces of MK fragments are moving and splitting into smaller pieces and finally into single platelets that transmigrate into the blood circulation (Figure 4. 50). The whole process of MK fragmentation lasts several hours. This pattern of thrombopoiesis lasts longer time compared to single proplatelet consumption, however it generates much more platelets at once. After 12h, we detected small $vWF^{+}$ cells are dividing into

daughter cells, indicating strong proliferation at this time frame (Figure 4. 51).

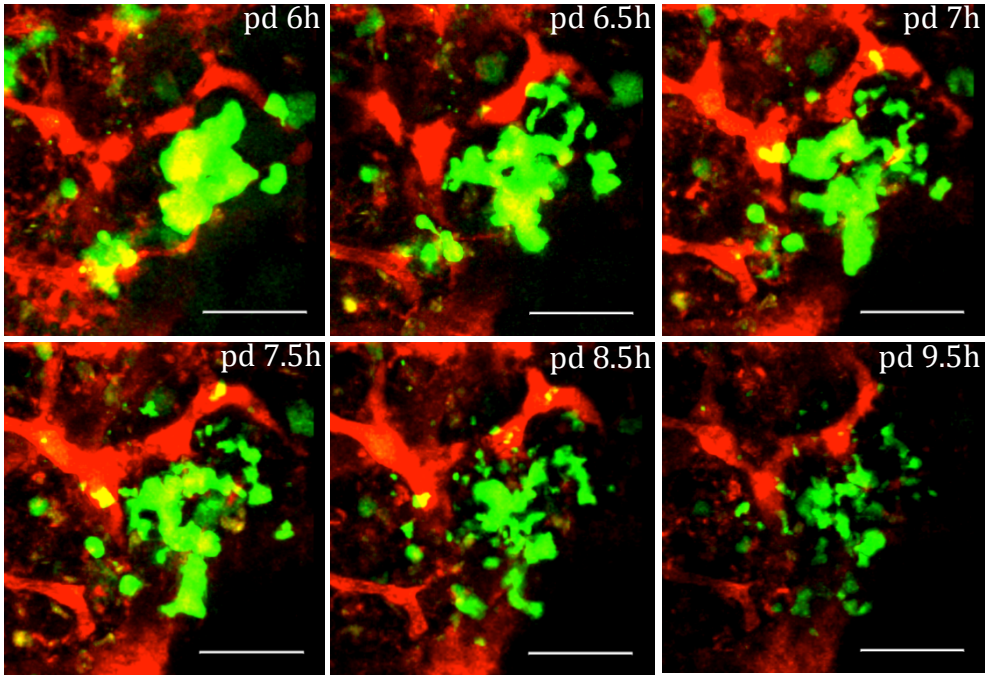


Figure 4.49 MK fragmentation within the calvarial bone marrow of a living vWF-eGFP mouse at early phase (6-10h) after platelet depletion. Green GFP cells are MK, fragments and platelets. Dextran-TRITC for vessels. Scale bar= 50 µm.

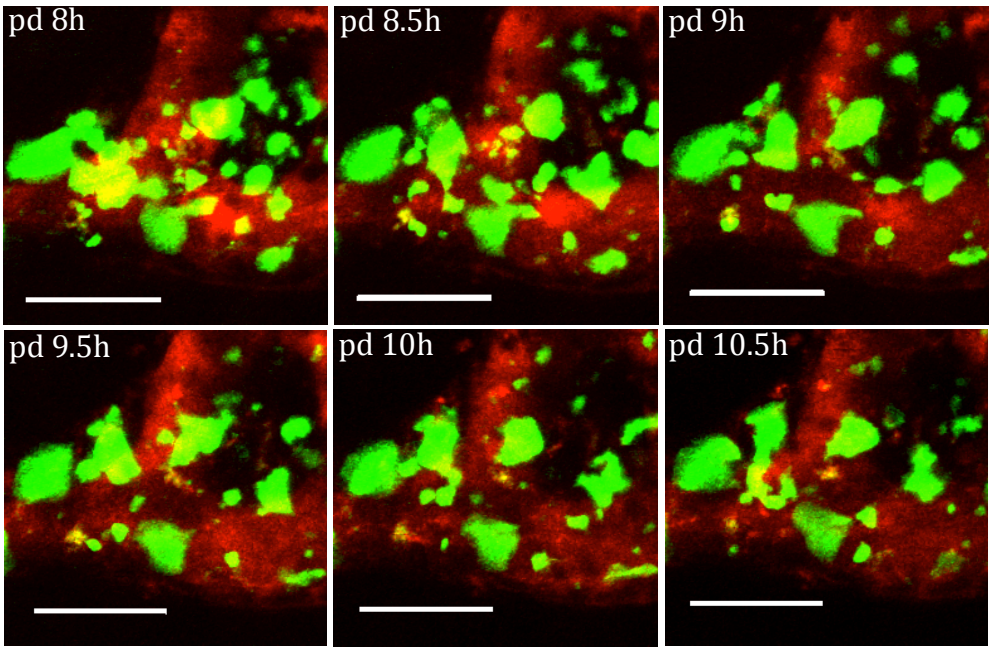

Figure 4.50 MK fragments split into platelets and enter the vessels after platelet depletion. Green GFP cells are MKs, fragments and platelets. Dextran-TRITC for vessels. Scale bar= 50μm.

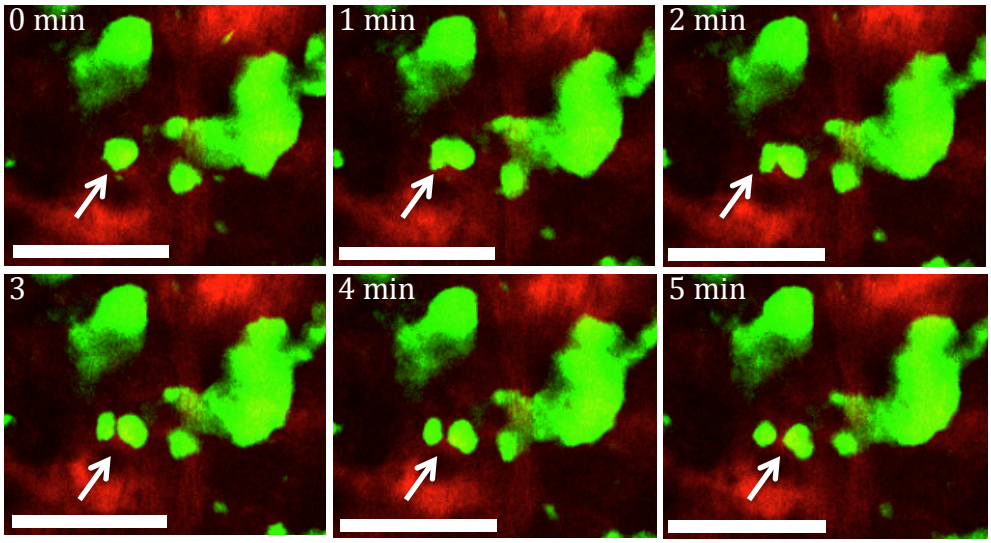


Figure 4.51 A small vWF$^{+}$ cell (MKP, arrow indicated) is dividing into two daughter cells in 5 minutes at 13h after platelet depletion. Dextran-TRITC for vessels. Scale bar= 50μm.

4.14 The quantity of MK populations in time sequence after platelet depletion

Peripheral blood was collected for measuring platelet count before and 0h, 12h, 24h, 48h, 4 days and 8 days after platelet depletion. We detected a sharp reduction of platelets as soon as the injection was applied. The platelet level remained very low within the first 2 days and then gradually rising up. After 4 days the number of platelet recovered to normal level (Figure 4. 52). We measured the number of MKs and MKPs in sternum bone marrow of platelet depleted mice with more quantitative analysis. As described previously, platelet depletion induces acute and rapid MK consumption. However, the number of MKs remains constantly without dropping (Figure 4. 53), proposing for a mechanism that can urgently replenish the loss of MKs and balance MK homeostasis. We also found a huge and rapid increase of MKPs initiated immediately after depletion (Figure 4.

53). Therefore we asked the question: how is the signal guiding proliferation and maturation quickly conveyed to the MKPs so efficiently? In order to answer this question, we looked for a time point when the effect of megakaryopoiesis is most augmented for the following studies. MKPs undergo quick expansion after depletion and reach the peak level at 24h. Tpo is known as the most powerful regulator of megakaryopoiesis in cell proliferation and maturation. We measured the level of Tpo in blood and observed an elevating Tpo level within the first 12h after depletion, and then it goes down (Fig. 4. 54). It means that platelet depletion brings the strongest proliferation signal on MK lineage cells at 12h. We performed EdU flow cytometry analysis to test the proliferation of MKPs at 12h. We gained bone marrow cells from vWF-eGFP mice, and defined MKPs as $vWF^+$ $CD41^+$ $CD42^-$ cells (Fig. 4. 55). We found a robust increase in both the fraction of proliferating MKPs as well as the intensity of the proliferation (Fig. 4. 56-57). Taken together, these data point out that 12h is the ideal time point for observing the dynamics of MKPs in the model of platelet depletion. Therefore, we adopted this time point in our further investigations.

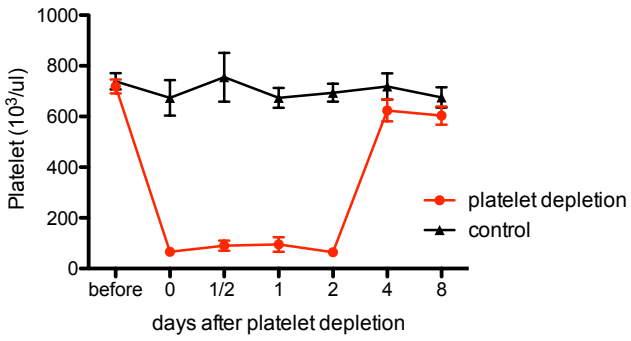


Figure 4.52 Peripheral blood platelet numbers in mice after injection of anti-CD42 antibody (platelet depletion) and isotype control antibody (control) at certain time points. n≥3 mice in each group. Error bar=SEM.

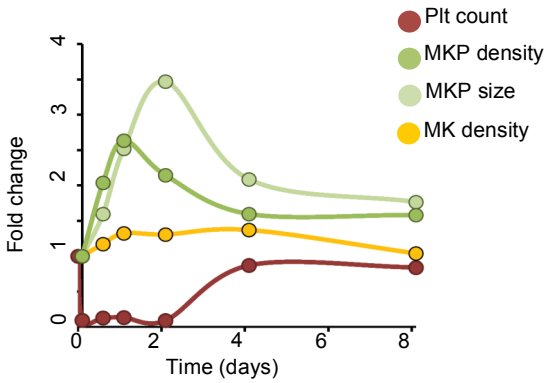


Figure 4. 53 Fold change of platelet count, MKP density (number/mm3 marrow), MKP size and MK density after platelet depletion. Platelet count was gained from peripheral blood measurement. MKs and MKPs was quantified in whole-mount sternum staining from ≥3 mice in each group.

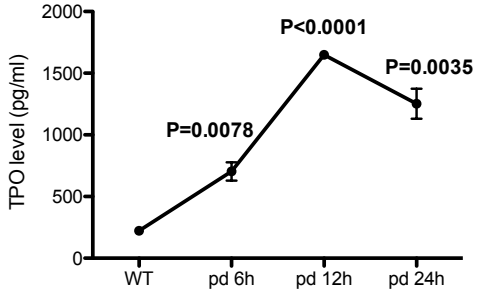


Figure 4.54 Tpo level in serum of WT mice (n=6 mice) and mice treated with platelet depletion at certain time points (n=4 mice per group). For comparison of WT to pd 6h and to pd 24h, unpaired t-test with Welch's correction are used; for comparison of WT to pd 12h, unpaired t-test is used. Error bar=SEM.

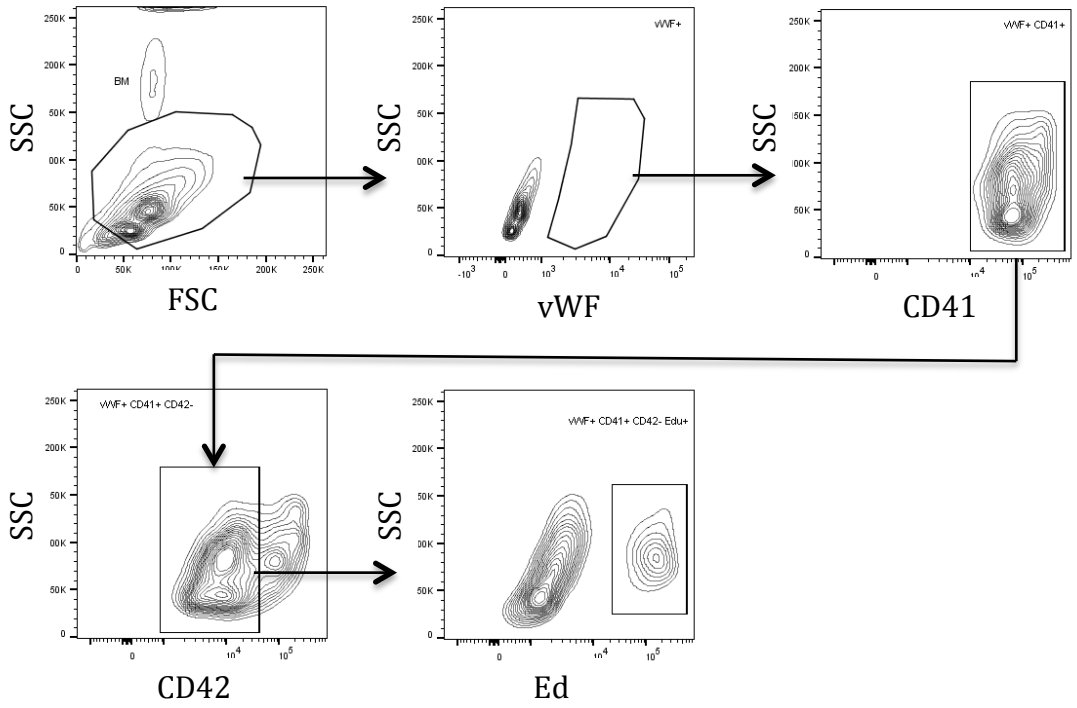


Figure 4.55 Gating strategy of flow cytometry analysis of EdU$^{+}$ vWF$^{+}$ CD41$^{+}$ CD42$^{-}$ MKPs.

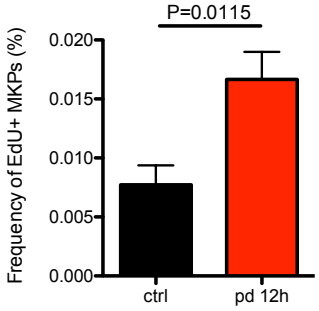


Figure 4.56 Frequency of EdU$^{+}$ MKPs in bone marrow of mice 12h after injection of anti-CD42 antibody (pd 12h, n=3 mice) and isotype control antibody (ctrl, n=3 mice). Paired t-test; P=0.0115; error bar=SEM.

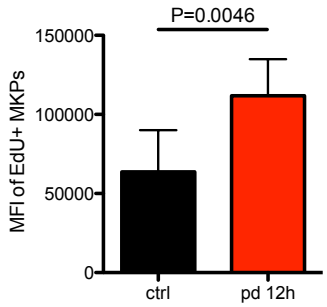


Figure 4.57 Mean fluorescent intensity of EdU on EdU$^+$ MKPs in bone marrow of mice 12h after injection of anti-CD42 antibody (pd 12h, n=3 mice) and isotype control antibody (ctrl, n=3 mice). Paired t-test; P=0.0046; error bar=SEM.

4.15 Distribution of MK populations within the bone marrow niche after platelet depletion

We induced the mice with immune thrombocytopenia (platelet depletion) to see whether there was repositioning of the MK populations after megakaryopoietic stress. We performed whole-mount staining of sternum from mice received platelet depletion. As shown in (Fig. 4. 58), after 24h the bone marrow looked more crowded and we observed more MK islands in high density. Since we previously detected a strong proliferation signal after 12h, next we checked the bone marrow from mice 12h after depletion. We found the total number of MKs in the bone marrow has a slight but not significant increase (Fig. 4. 59), while the fraction of MKs in different distance scales towards the vessels remains the same (Fig. 4. 60), indicating that MKs stably occupy the vascular niche without changing their location. Besides, we found a significant higher fraction of the MKPs appear at the vessels, and a lower fraction of the MKPs away from the vessels (Fig. 4. 61-62). This demonstrates a higher number of MKPs appear at the vessels after stress. We also found a higher fraction of MKPs that show direct contact with the MKs (Fig. 4. 63). Together, these data suggest that after hematopoietic stress MKPs proliferate in close proximity to MKs within the MK islands.

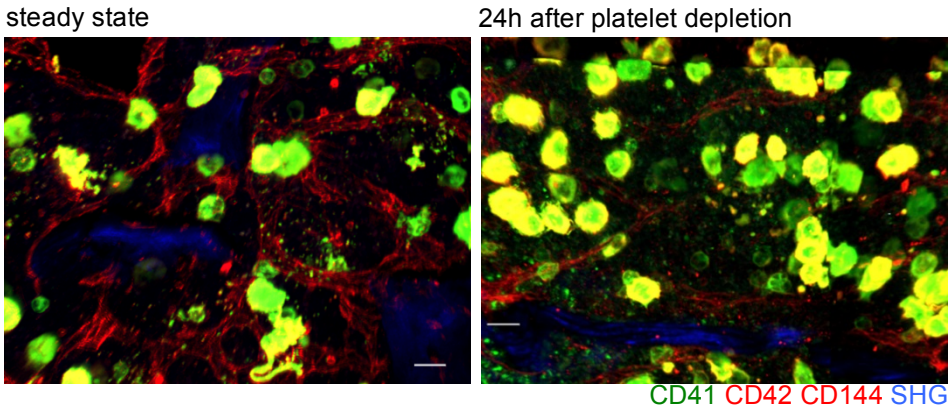


Figure 4.58 Representative whole-mount immunostaining of MKs, MKPs and vessels in sternum bone marrow of mice 24h after platelet depletion. CD41 (green) labeled early and late stage of MKs. CD42 (red) labeled mature MKs. CD144 (red) labeled endothelial cells. SHG (blue) shows bone structure. Scale bar = 20μm.

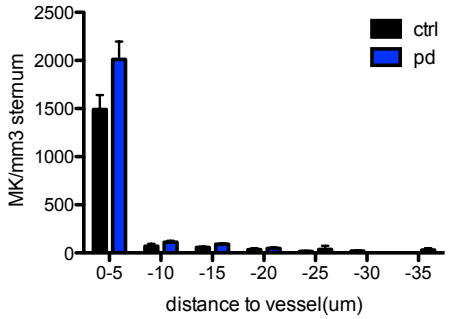


Figure 4.59 Distance between MKs and the vessels, and the number of MKs per 1mm$^3$ sternum bone marrow in platelet depleted 12h mice (blue) and control mice (black). The distances were binned into 5-μm intervals. n=4 in each group. Error bar=SEM.

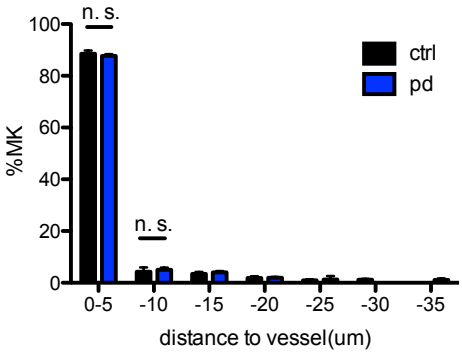

Figure 4.60 Distance between MKs and the vessels, and the percentage of MKs in platelet depleted 12h mice (blue) and control mice (black). The distances were binned into 5-μm intervals. n=4 in each group. Error bar=SEM.

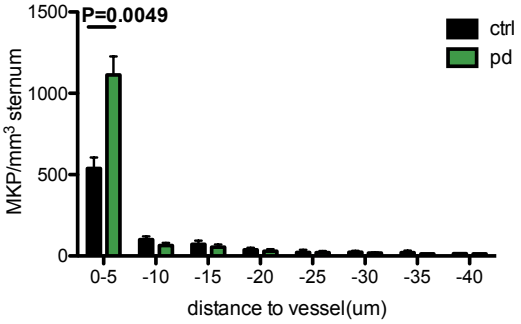


Figure 4.61 Distance between MKPs and the vessels, and the number of MKPs per 1mm$^3$ sternum bone marrow in platelet depleted 12h mice (green) and control mice (black). The distances were binned into 5-μm intervals. n=4 mice per group. Unpaired t-test; P=0.0049; error bar=SEM.

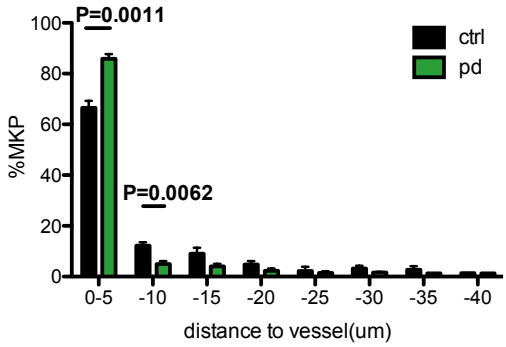


Figure 4.62 Distance between MKPs and the vessels, and the percentage of MKPs in platelet depleted 12h mice (green) and control mice (black). The distances were binned into 5-μm intervals. n=4 mice per group. Unpaired t-test; P=0.0011 (left); P=0.0062 (right); error bar=SEM.

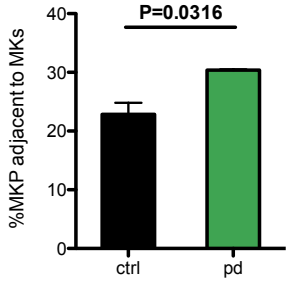


Figure 4.63 Percentage of MKPs which are directly attached to the MKs in platelet depleted 12h mice (green) and control mice (black). n=4 mice per group. Unpaired t-test with Welch's correction; P=0.0316; error bar=SEM.

4.16 Short term dynamics of MK populations in the calvarial bone marrow in vivo after platelet depletion

We treated vWF-eGFP mice with platelet depletion, and performed calvarial live imaging after 12h. We found the velocity of MKs remain a low level which is comparable with the velocity in steady state (Fig. 4. 64). We also quantified the distance from MKs to vessels and found nearly all MKs are lying directly at the vessel after platelet depletion (Fig. 4. 65). However, we observed the change of MK morphology, as shown by lower cell sphericity 12h after platelet depletion (Figure 4. 66), indicating the shape of MKs become more irregular at this time point, probably sue to the increasing formation of proplatelets and cell activation. Altogether, these data are in consistent with our previous finding that MKs are static cells which do not migrate. It further indicates that the MKs stably occupy the vascular niche and this tight association is not altered under hematopoietic stress despite increased irregularity.

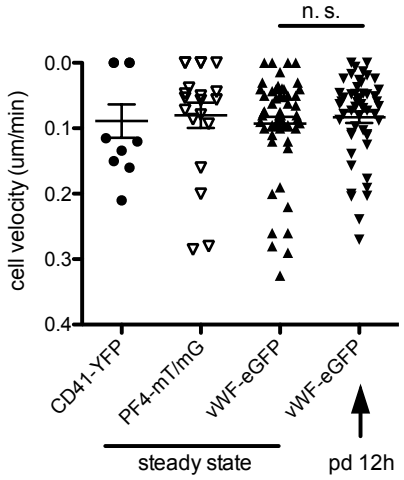


Figure 4.64 The velocity of MKs in CD41-YFP (n=10 cells from 3 mice), PF4 Cre × Rosa26-mT/mG (n=20 cells from 4 mice), vWF-eGFP mice at steady state (n=54 cells from 7 mice) as well as 12h after injection of anti-CD42 antibody (n=51 cells from 6 mice). Unpaired t-test; error bar=SEM. n. s. = no significance (P=0.47).

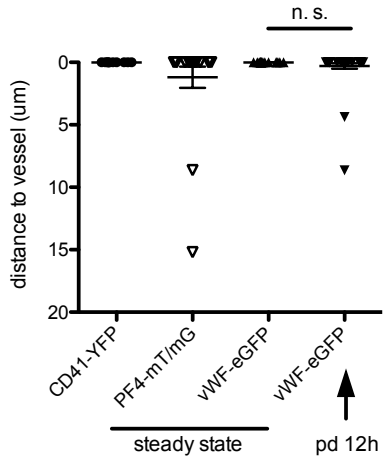


Figure 4.65 Distance of MKs to vessels in CD41-YFP (n=10 cells from 3 mice), PF4 Cre × Rosa26-mT/mG (n=20 cells from 4 mice) and vWF-eGFP mice at steady state (n=18 cells from 7 mice) as well as 12h after platelet depletion (n=44 cells from 6 mice), quantified in live imaging data. Unpaired t-test with Welch's correction; P=0.18; error bar=SEM. n. s. = no significance.

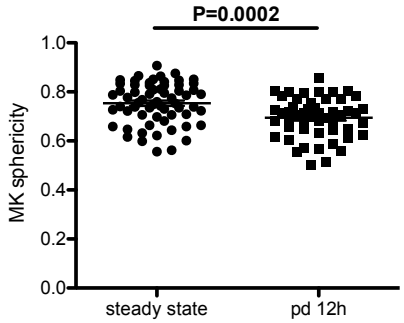


Figure 4.66 MK sphericity in vWF-eGFP mice at steady state (n=63 cells from 7 mice) and 12h after platelet depletion (n=51 cells from 6 mice). Unpaired t-test; P=0.0002; error bar=SEM.

4.17 Long term dynamics of MK populations in the calvarial bone marrow in vivo after platelet depletion

Next, we performed chronic imaging to visualize long term dynamics of MK populations in vWF-eGFP mice after platelet depletion (Fig. 4. 67). When we were tracking single cells, we found the vast majority of $vWF^+$ cells stay at the exact same position during the imaging period, as the static cells occupied 88.83 ± 4.46 % (n=4 areas from 4 mice) of the whole population (Fig. 4. 68). Then we focused on the mature MKs. We found that MKs do not change locations during the observation period, with 92.64 ± 3.38 % (n=7 areas from 4 mice) of the MKs remain at the exact same position (Fig. 4. 69). This finding resembles what we observed in steady state, and further confirms the stable assembly of MKs. Interestingly, the volume disappearing speed of MKs is 1817 ± 430.6 $\mu m^3$ per hour (n=11 cells from 4 mice), much faster than in normal conditions (Fig. 4. 70). This suggests that the signal of acute platelet loss leads to accelerated MK cytoplasmic consumption. Next we explored the long term dynamics of MK progenitors after platelet depletion. As in steady state, we detected non-motile MKPs which are growing and motile MKPs which do not grow up (Fig. 4. 71). We found a similar growing speed of non-motile MKPs compared with those in steady states (Fig. 4. 72-73). In addition, when we tracked the positioning of single cells

in chronic image series, we found that most cells have close connections with the vessels throughout the entire development process (Fig. 4. 74). This is in consistent with our previous finding in steady state. Together, these results demonstrate that platelet depletion leads to higher speed of platelet production while the spatial organization of MK islands remain stable.

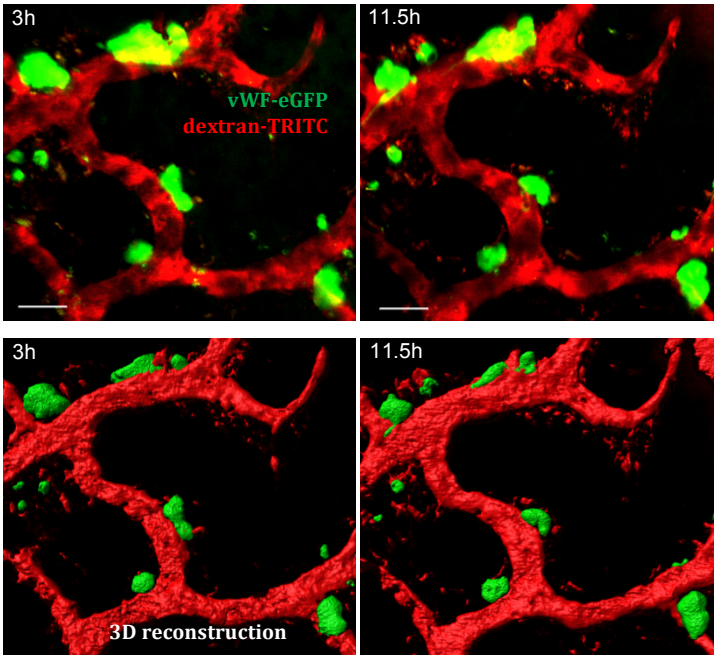


Figure 4.67 Snapshots of chronic image series (upper) and corresponding 3D reconstructed images (lower) from one bone marrow area of a vWF-eGFP mouse calvarian after platelet depletion. Vessels are labeled with dextran-TRITC. Scale bar= 30μm.

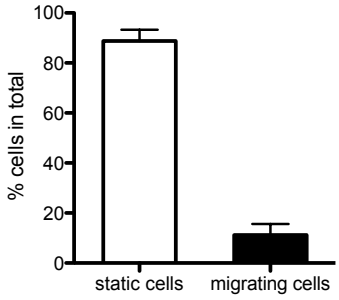


Figure 4.68 After platelet depletion, percentage of $vWF^{+}$ cells which remain static and which shift location during the entire chronic imaging period. Data are pooled

from 4 mice. Error bar=SEM.

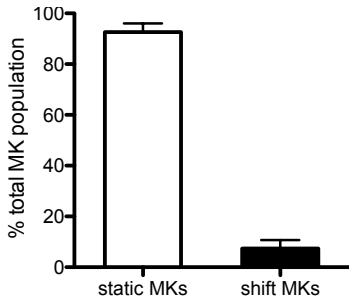


Figure 4.69 After platelet depletion, percentage of MKs which remain static and which change locations during the entire chronic imaging period. Data are pooled from 4 mice. Error bar=SEM.

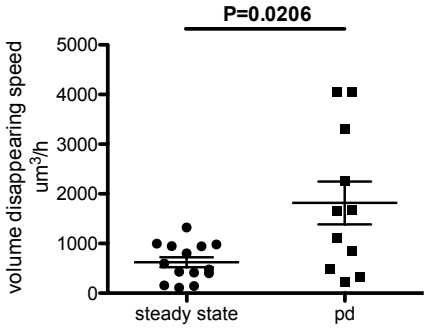


Figure 4.70 Volume disappearing speed of mature MKs in vWF-eGFP mice at steady state (n=14 cells from 4 mice) as well as under platelet depletion (n=11 cells from 4 mice). Unpaired t-test with Welch's correction; P=0.0206; error bar=SEM.

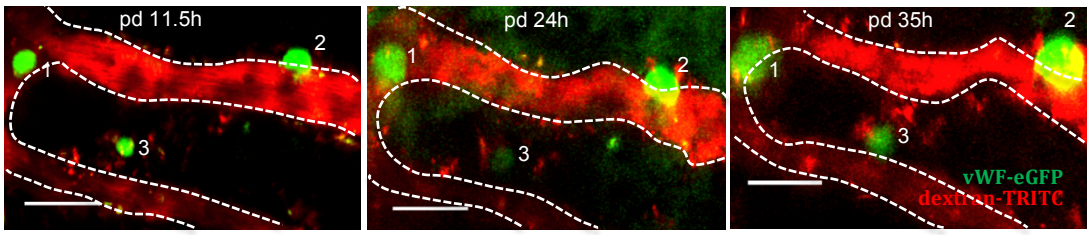


Figure 4.71 Snapshots of chronic image series from one bone marrow area of a vWF-eGFP mouse calvarian after platelet depletion. Vessels are labeled with

dextran-TRITC and contoured. Cell 1 and 2 indicate non-motile MKPs growing up. Cell 3 indicates a MKP coming towards the vessel and growing. Scale bar= 30µm.

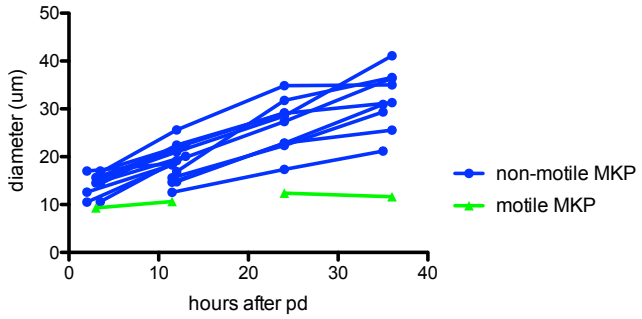


Figure 4.72 Diameter of non-motile and motile MKPs after platelet depletion. For non-motile MKPs, n=15 cells from 4 mice. For motile MKPs, n=2 cells from 2 mice.

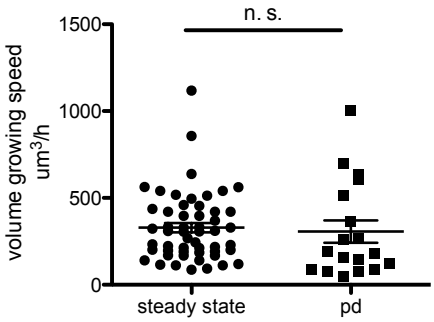


Figure 4.73 Volume growing speed of non-motile MKPs in vWF-eGFP mice at steady state (n=53 cells from 5 mice) as well as under platelet depletion (n=18 cells from 4 mice). Unpaired t-test; P=0.71; error bar=SEM. n s, no significance.

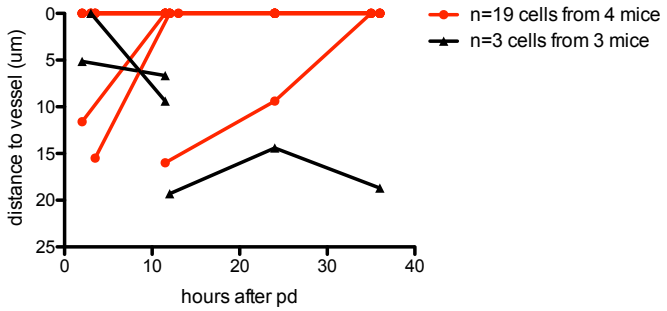


Figure 4.74 Distance of MKPs to vessels after platelet depletion. Red lines indicate cells which are attached to vessels or coming to vessels. Black lines indicate cells that do not show associations with the vessels. A total number of 22 cells from 4 mice are included.

## 4.18 Spatial adaptions of MK populations upon Thrombopoietin treatment

Previously we found an elevated Tpo level after platelet depletion. Tpo is known as the most important trigger of megakaryopoiesis in regulating the expansion of MK progenitors and the differentiation of MKPs towards MKs [91]. Next we investigated the spatial adaptions of MK populations using Tpo treatment as a mimic of hematopoietic stimulation. We injected the mice with Tpo (8ng/g body weight) i.p. daily for 3 days. Then the sternum was harvested for whole-mount staining of MK populations. After Tpo treatment, we observed increasing number of MKs and MKPs in BM that formed enhanced MK islands (Fig. 4. 75). Compared with the effect of platelet depletion, a direct Tpo treatment lead to similar number of MKPs (Fig. 4. 76) but even higher number of MKs (Fig. 4. 77). Meanwhile, there was also higher fraction of MKPs in direct contact to MKs (Fig. 4. 78). This indicates that Tpo leads to the expansion of MK lineage and more frequent MK-MKP interaction. There are two interpretations: firstly, Tpo enhances the interaction between MKs and MKPs; secondly, Tpo triggers the proliferation of MKPs and leads to increasing contact number. Combines, these data suggest that Tpo induces megakaryopoiesis which takes place in the form of MK islands. This close spatial relationship of MKPs and mature MKs within MK islands also

suggests a close communication between both cell types, which is important for maintenance of megakaryopoiesis.

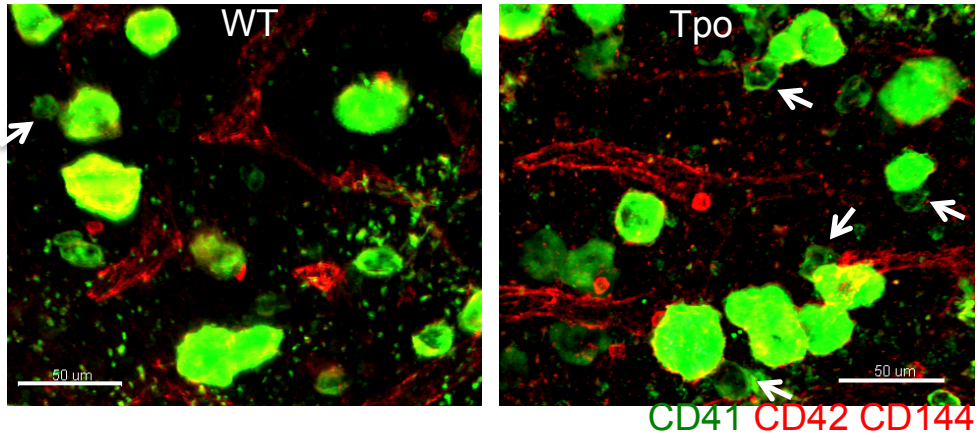


Figure 4.75 Representative whole-mount immunostaining of MKs, MKPs and vessels in sternum bone marrow of WT mouse and mouse treated with Tpo. CD41 (green) labeled early and late stage of MKs. CD42 (red) labeled mature MKs. CD144 (red) labeled endothelial cells. Arrows indicate MKPs which directly attach to MKs. Scale bar =50μm.

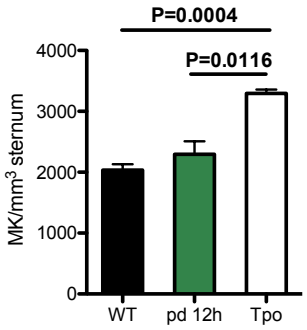


Figure 4.76 Number of MKs per $mm^3$ sternum marrow in WT mice (n=3 mice), 12h after platelet depletion (n=4 mice), and mice received 3 days Tpo injection (n=3 mice). Unpaired t-test is used. Error bar=SEM.

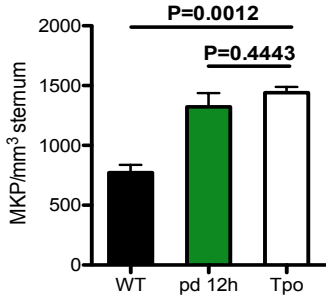


Figure 4.77 Number of MKPs per $mm^3$ sternum marrow in WT mice (n=3 mice), 12h after platelet depletion (n=4 mice), and mice received 3 days Tpo injection (n=3 mice). Unpaired t-test is used. Error bar=SEM.

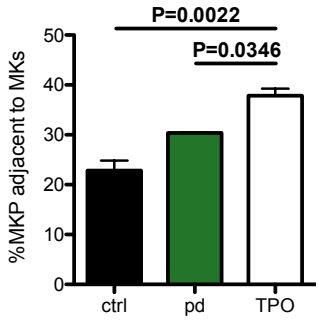


Figure 4.78 Percentage of MKPs which are in direct contact with MKs in control mice received platelet isotype control antibody injection (n=4 mice), 12h after platelet depletion (n=4 mice), and mice received 3 days Tpo injection (n=3 mice). For comparison of ctrl with TPO, unpaired t-test is used; for comparison of pd with TPO, unpaired t-test with Welch's correction is used. Error bar=SEM.

**Part III: Megakaryopoiesis after megakaryocytes depletion**

4.19 PF4 Cre × Rosa26-iDTR mouse as MK depletion model

Previous studies revealed a close connection between MKs and their precursors during megakaryopoiesis. To address in detail the role of MKs in regulating their progenitors and maintaining MK islands, we developed a mouse model of MK depletion, the PF4 Cre × Rosa26-iDTR mouse. After injection of diphtheria toxin

for 7 consecutive days, the Cre-targeted PF4$^{+}$ cells (primarily megakaryocytes and platelets) are substantially depleted [112]. For control group, Cre$^{-}$ mice were received parallel DT treatment. Peripheral blood measurement showed a continuous platelet loss to nearly 5% in MK depletion group, while the platelet level in Cre- mice received DT remain normal (Fig. 4. 79). We measured serum Tpo level and observed increasing Tpo in MK depletion group (Fig. 4. 80), indicating that the absence of MKs brings strong proliferation signal. Since it has been reported recently that platelet factor 4 is expressed not only on MK lineage but also a fraction of other myeloid cells including monocytes, macrophages and dendritic cells **[11]**, we checked if the depletion of PF4 cells also leads to other lineage cell deficiency. We measured non-MK lineage cells in the blood and found a similar level of erythrocytes, granulocytes, monocytes and lymphocytes compared to control mice (Fig. 4. 81). This indicates that our PF4 Cre × Rosa26-iDTR mouse model specifically depleted platelet without affecting the level of other lineage cells.

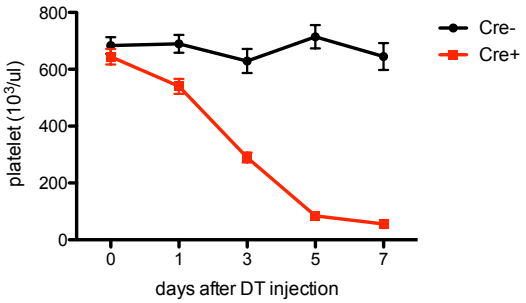


Figure 4.79 Peripheral platelet count in depletion (red) and control (black) groups during DT injection. n=7 mice per group. Error bar=SEM.

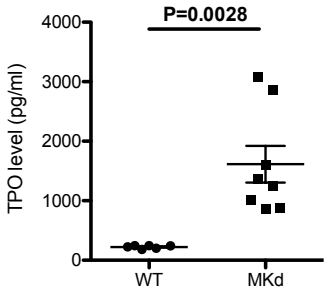


Figure 4.80 Tpo level in serum of WT mice (n=6 mice) and mice with MK depletion (n=8 mice). Unpaired t-test with Welch's correction is used; P=0.0028; Error bar=SEM.

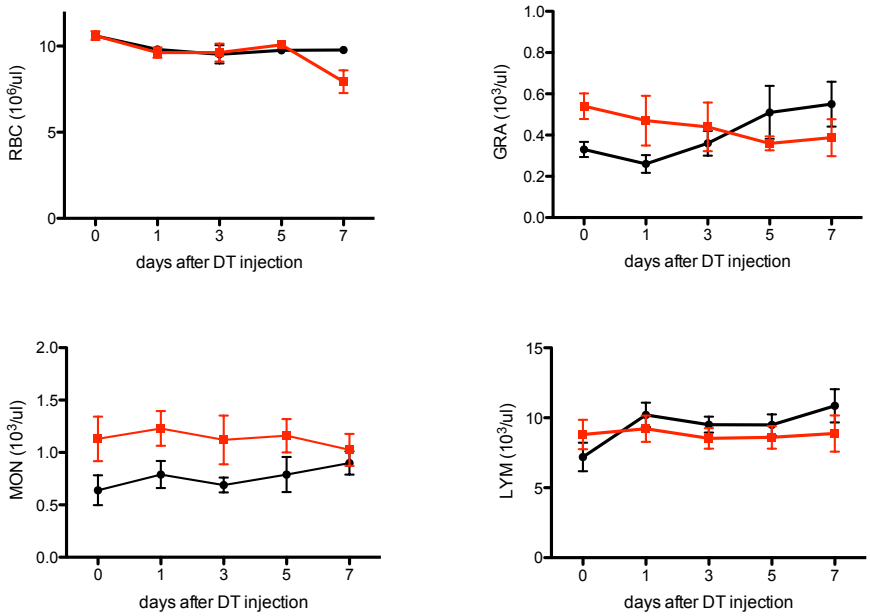


Figure 4.81 Peripheral lineage cell count in depletion (red) and control (black) groups during DT injection. n=7 mice per group. Error bar=SEM.

## 4.20 Distribution of MK progenitors in MK-depleted sternum bone marrow

After 7 days DT treatment, we harvested sternum and performed whole-mount staining (Fig. 4. 82). The number of MKs per $mm^3$ sternum marrow severely decreased (Fig. 4. 83), which indicates an efficient depletion of MKs. Instead, the number of MKPs greatly increased from 656 ± 80 (n=7) to 2308 ± 49 (n=7) per

$mm^3$ sternum, indicating strong megakaryopoiesis (Fig. 4. 83). This is in consistent with our previous finding of increased Tpo level, and was further confirmed by in vitro CFU-MK assay shown as the BM cells produced more MK colonies (Fig. 4. 84). Next, we measured the distribution of MKPs to vessels under this stress condition. There was increasing number of MKPs appear close to the vessels (Fig. 4. 85), similar as we saw in platelet depletion. However, the fraction of these MKPs showed that they do not preferably accumulate at the vessels (Fig. 4. 86). These data suggest that the absence of MKs leads to enhanced megakaryopoiesis, however without an increased association with the vessels.

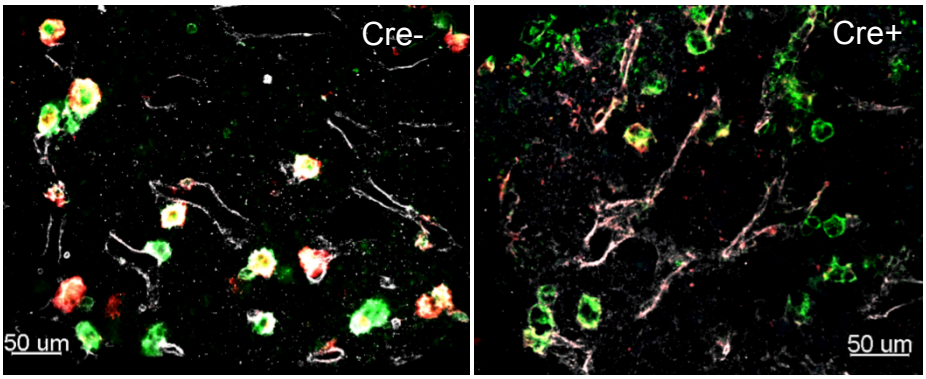


Figure 4.82 Representative whole-mount immunostaining of MKs, MKPs and vessels in sternum bone marrow of PF4 Cre × Rosa26-iDTR ($Cre^+$) and control mouse ($Cre^-$). CD41 (green) labeled early and late stage of MKs. CD42 (red) labeled mature MKs. CD144 (white) labeled endothelial cells. Scale bar= 50μm.

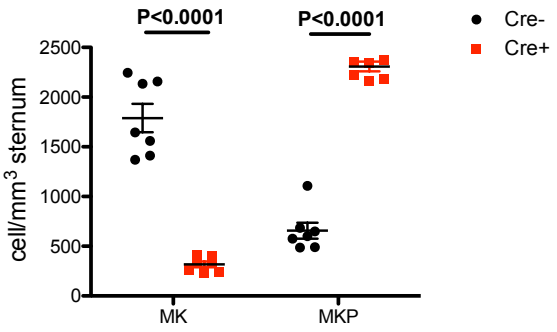


Figure 4.83 Number of MKs and MKPs per $mm^3$ sternum marrow in PF4 Cre × Rosa26-iDTR ($Cre^+$) and control mouse ($Cre^-$). n=7 mice per group. For

comparison of MK, unpaired t-test with Welch's correction is used, P<0.0001; for comparison of MKP, unpaired t-test is used, P<0.0001. Error bar=SEM.

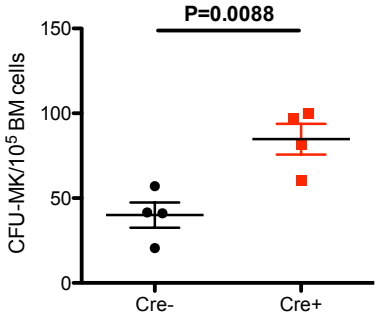


Figure 4.84 Number of CFU-MK colonies per $10^5$ seeded bone marrow cells in PF4 Cre × Rosa26-iDTR ($Cre^+$) and control mouse ($Cre^-$). n=4 mice per group. Unpaired t-test; P=0.0088; error bar=SEM.

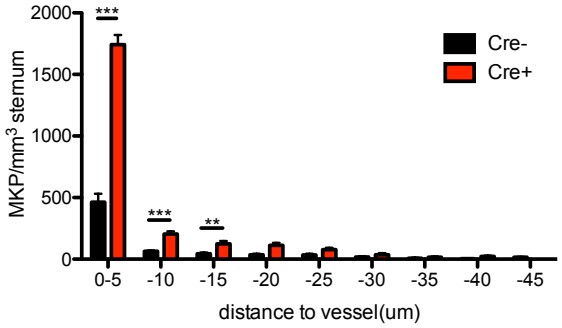


Figure 4.85 Distance between MKPs and the vessels, and the number of MKPs per $1mm^3$ sternum marrow in PF4 Cre × Rosa26-iDTR ($Cre^+$) and control mouse ($Cre^-$). The distances were binned into 5-μm intervals. n=7 mice per group. Unpaired t-test; P<0.0001; error bar=SEM.

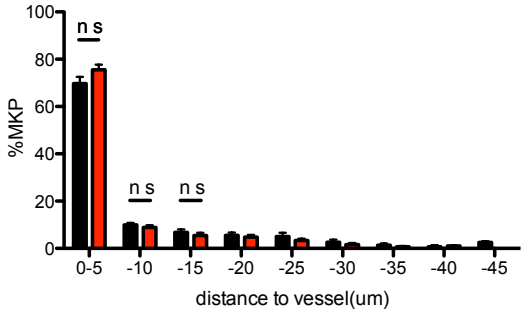


Figure 4.86 Distance between MKPs and the vessels, and the percentage of MKPs in PF4 Cre × Rosa26-iDTR ($Cre^+$) and control mouse ($Cre^-$). The distances were binned into 5-μm intervals. n=7 mice per group. Unpaired t-test; error bar=SEM. n. s. = no significance.

4.21 Short term dynamics of MK precursors in the MK-depleted calvarial bone marrow in vivo

In order to visualize in vivo the dynamics of MKPs under the condition of MK depletion, we generated PF4 Cre × Rosa26-iDTR × vWF-eGFP mouse which has depleted MKs and platelets, and GFP labeled MKPs and stem cells. After DT treatment for 3 days, we performed calvarian in vivo imaging using Two-photon microscopy. Our results show that there are increasing number of $vWF^+$ small cells which are actively migrating (Fig. 4. 87). Moreover, the velocity of these motile cells after MK depletion are higher than their counterparts at steady state (Fig. 4. 88), and Interestingly, the size of the motile cells after MK depletion is also bigger (Fig. 4. 89). Together, these data indicate that the depletion of MKs leads to higher motility of their precursors.

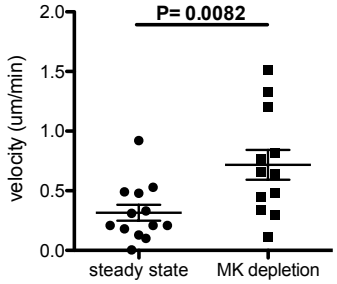

Figure 4.87 The migrating velocity of vWF$^+$ small cells in vWF-eGFP mice at steady state (n=13 cells from 5 mice) and in PF4 Cre × Rosa26-iDTR × vWF-eGFP mice received 3 days DT treatment (n=12 cells from 4 mice). Unpaired t-test; P= 0.0082; Error bar=SEM.

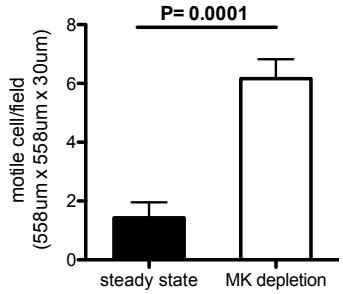


Figure 4.88 The number of migrating vWF$^+$ small cells per microscope field in vWF-eGFP mice at steady state (data from 5 mice) and in PF4 Cre × Rosa26-iDTR × vWF-eGFP mice received 3 days DT treatment (data from 4 mice). Unpaired t-test; P= 0.0001; Error bar=SEM.

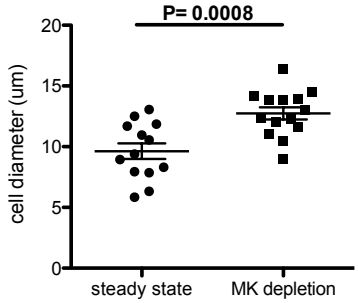


Figure 4.89 The diameter of migrating vWF$^+$ small cells in vWF-eGFP mice at steady state (n=13 cells from 5 mice) and in PF4 Cre × Rosa26-iDTR × vWF-eGFP mice received 3 days DT treatment (n=14 cells from 4 mice). Unpaired t-test; P= 0.0008; Error bar=SEM.

## 4.22 Long term dynamics of MK precursors in the MK-depleted calvarial bone marrow in vivo

Next we performed chronic imaging using PF4 Cre × Rosa26-iDTR × vWF-eGFP mice to investigate the long term dynamics of MKPs in the absence of MKs. According to our preliminary observation, 7 days DT treatment leads to severe bleeding and potential death. Therefore we decided to perform operation and the following imaging after 3 days DT treatment. During imaging period we continued DT injection daily. When we were trying to tracking single cells, we found it difficult since the cells shift locations more frequently than in steady state or after platelet depletion (Fig. 4. 90). There were fewer cells that remain static (Fig. 4. 91). This suggests a disruption of MK islands when MKs are depleted. Then we focused on the non-motile MKPs. Surprisingly, we found the cells stop growing any more (Fig. 4. 92-93). The volume growing speed of small cells was significantly lower than in normal condition (Fig. 4.94), meanwhile the volume disappearing speed of big cells also decreased compared to normal condition (Fig. 4. 95). Together, chronic imaging of MK depletion model shows an abnormal megakaryopoiesis with increased MKP number but disrupted localization and decreased maturation, and further indicates that MKs serve as crucial niche cells in supporting MK precursors, forming MK islands and regulating normal megakaryopoiesis.

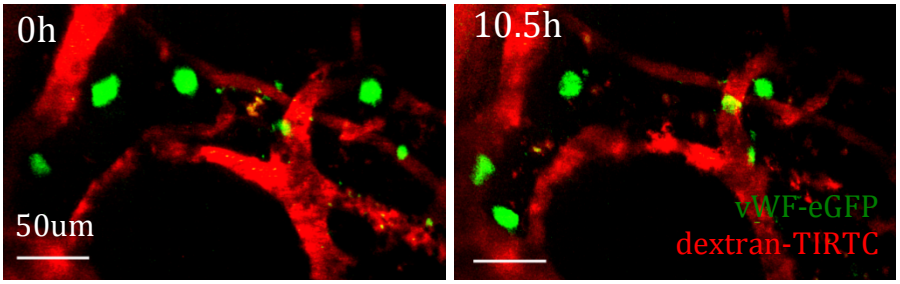


Figure 4.90 Snapshots of chronic image series from one bone marrow area of a PF4 Cre × Rosa26-iDTR × vWF-eGFP mouse received 3 days DT injection. Vessels are labeled with dextran-TRITC. Scale bar =50 μm.

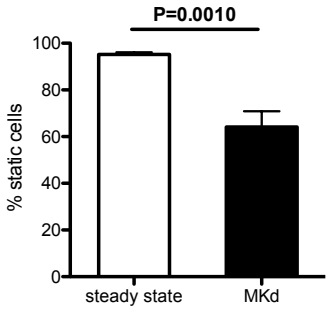


Figure 4.91 Percentage of static cells (which remain static during the observation period) in normal vWF-eGFP mice (n=5) and PF4 Cre × Rosa26-iDTR × vWF-eGFP mice received 3 days DT injection (n=4). Unpaired t-test; P=0.001; error bar=SEM.

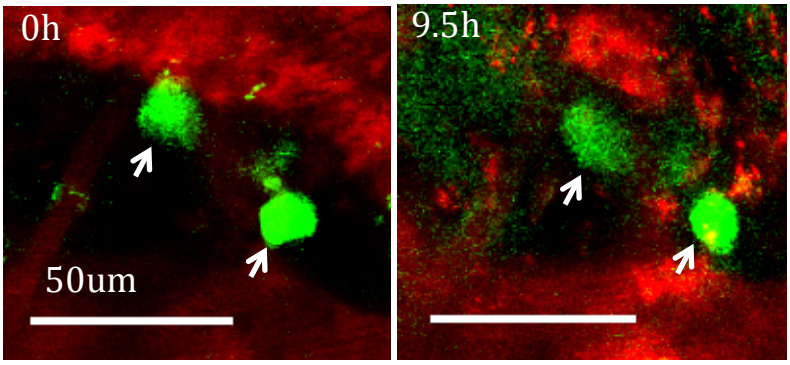


Figure 4.92 Snapshots of chronic image series from one bone marrow area of a PF4 Cre × Rosa26-iDTR × vWF-eGFP mouse received 3 days DT injection. Vessels are labeled with dextran-TRITC. Arrows indicate non-motile MKPs at time point 0h (left) and after 9.5h (right). Scale bar =50 μm.

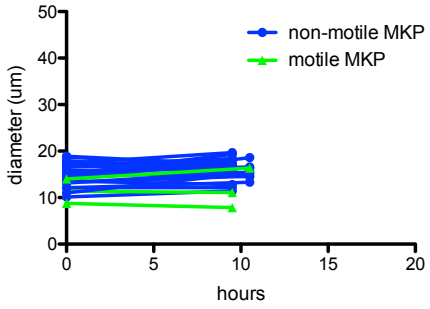


Figure 4.93 Diameters of non-motile and motile MKPs over time in PF4 Cre × Rosa26-iDTR × vWF-eGFP mice received 3 days DT injection. For non-motile

MKPs, n=19 cells from 4 mice. For motile MKPs, n=3 cells from 3 mice.

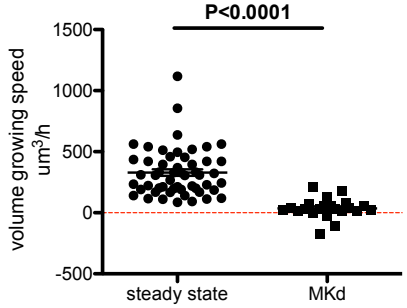


Figure 4.94 Volume growing speed of non-motile MKPs in vWF-eGFP mice at steady state (n=53 cells from 5 mice) as well as MK depletion (n=18 cells from 4 mice). Unpaired t-test; P<0.0001; error bar=SEM.

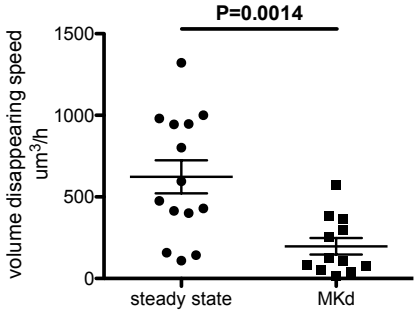


Figure 4.95 Volume disappearing speed of big vWF$^{+}$ cells (≥20 µm) in vWF-eGFP mice at steady state (n=14 cells from 4 mice) as well as MK depletion (n=12 cells from 4 mice). Unpaired t-test with Welch's correction; P=0.0014; error bar=SEM.

# 5 DISCUSSION

## 5. 1 Discussion of methodology

### 5. 1. 1 Identification of MK populations

One fundamental concern prior to this study was the definition for MK populations. This is also one of the most challenging difficulties in the field of megakaryocyte biology. During MK development, certain markers can be used to identify MKs at different stages of maturation.

First, we discuss the markers for in vitro or ex vivo definition. Platelet-biased HSCs, which have the potential to differentiate into MKs, were previously identified as $Lin^-$ $Sca\text{-}1^+$ $c\text{-}kit^+$ $CD150^+$ $CD48^-$ $vWF^+$ cells by FACs [50]. CD41 is an early stage marker of megakaryocytic lineage and other myeloid progenitors [45, 51]. Although it has been shown that CD41 marks primitive hematopoiesis and is expressed on embryonic HSCs [120], it is widely accepted that adult stem cells lack the CD41 antigen. However, it was recently reported that CD41 is actually expressed on a fraction of adult HSCs and increases with age [121]. Considering the $CD41^+$ fraction of HSCs is extremely low as shown in 8 weeks old mice [121], an age that we always use in our study, we considered that platelet-biased HSCs are still CD41 negative. Therefore in our whole-mount staining we labeled platelet-biased HSCs as $CD150^+$ $CD41^-$ $vWF^+$ cells. To identify MK progenitors and mature MKs, we used CD41 combined with CD42 in our whole-mount staining. We defined MKPs as $CD41^+$ $CD42^-$ cells, and mature MKs as double $CD41^+$ $CD42^+$ cells [45, 122]. The co-staining of CD41 and CD42 using bones from vWF-eGFP mice shows a high correlation of vWF with these markers, which confirms that CD41 and CD42 are good markers to identify MK populations. In literatures, the vast majority of current MKP researches were in vitro experiments based on the gating strategy of $Lin^-$ $Sca\text{-}1^-$ $c\text{-}kit^+$ $CD150^+$ $CD41^+$ cells as MKPs in flow cytometry or sorting [51, 123]. It was reported that CD41 also marks

erythroitic progenitors [45], indicating that our MKP staining might not be 100% pure MK lineage. CD42 is known to be a later stage marker of MK differentiation and lack the expression on early stage progenitors. However, there was one study showing that $CD41^+$ $CD42^+$ LSK cells are unipotent MK progenitors between the stage of stem cells and mature MKs [124], indicating that CD42 might also not be specific for mature MKs, and our MK staining might have stained progenitors. Despite these controversial reports, CD41 and CD42 are still the markers most widely accepted and frequently used to identify MK populations in immunostaining. Apart from the surface markers, there are other criteria for distinguishing MKPs from MKs. MKs are distinct for their huge morphology, some with protrusions. MKPs are generally smaller and more roundish in shape. In addition, MKs express much higher level of CD41 compared to MKPs, shown in images as stronger fluorescence intensity [45]. All these information help define MKs and MKPs in our whole-mount staining.

Next, we discuss the tools for in vivo detection of MK populations. It is pivotal to be able to identify these cells in the context of the bone marrow microenvironment in vivo, in order to understand their dynamics. Compared to in vitro or ex vivo staining, it is more difficult to label a pure population in vivo, due to limited dyes and fluorescence channels. There were studies injecting fluorescent-labeled antibodies of MK markers into the mice and showing a nice labeling of MKs [125]. This method is easy and efficient for labeling cells exposed in blood. However, the MKPs are within the bone marrow cavity and we have to consider whether the circulating antibodies will diffuse into the bone marrow and how long this process will take to stain MKPs [126]. Currently the in vivo labeling of MKs and MKPs largely depends on genetic mouse models. In this thesis, we used a novel mouse model: vWF-eGFP mouse. It has been found that vWF-derived eGFP is expressed on all stages of MK populations including HSCs, progenitors, MKs and platelets [50]. In vivo test shows a strong fluorescence signal of these cells with consistent fluorescence intensity. MKs are detected as huge cells with general irregular morphology. In order to further distinguish MKPs from MKs, we

quantified the cell diameter of single $CD41^+$ cells as well as double $CD41^+$ $CD42^+$ cells in sternum histology. Results showed that single $CD41^+$ cells which we assume are MKPs are usually smaller than 20 μm in size, while double $CD41^+$ $CD42^+$ cells that should be mature MKs are generally bigger than 20 μm. These values are in consistent with previous finding [123]. In this sense we were able to distinguish different MK populations and further study them in vivo. Other mouse models with fluorescent MKs include CD41-YFP mouse and PF4 Cre × Rosa26-mT/mG mouse [108, 109]. CD41-YFP mouse was first created as a mouse model with YFP-labeled MKs and platelets, and a small fraction of HSCs and progenitors at low YFP level [108]. According to previous in vivo studies from our lab, however, the efficiency of the labeling is quite low, with only a minority of MKs are YFP labeled due to unknown reasons. PF4 Cre × Rosa26-mT/mG mouse contains membrane-localized EGFP (mG) on MKs and platelets, and membrane-localized tdTomato (mT) on rest of the tissues [109]. Compared to CD41-YFP mouse, it has higher proportion of fluorescent MKs. Recently this model has been used to study platelet biogenesis in the lung [123]. However, since PF4 is a putative marker for mature MKs, this mouse model is not able to mark the MKPs we are aimed at to investigate. Besides, PF4 was reported to express also on a fraction of other cells including monocytes, macrophages and dendritic cells [127], suggesting it might be unspecific for MKs. Considering these problems, the vWF-eGFP mouse is currently the best mouse model for megakaryopoiesis studies.

### 5. 1. 2 Discussion of imaging techniques

The imaging techniques include whole-mount staining and in vivo imaging, both of which have advantages and disadvantages. The preparation of the whole-mount staining is simple and can be applied on any bones, most frequently femur and sternum. It allows the visualization of the bone marrow to a depth of ~70 μm. The mosaic function of the whole-mount staining displays 3D image for a whole sternum fragment. Then we perform quantitative analysis of the spatial

localization of the cells within this whole area of the sternum bone marrow. Therefore we generate data in more precise way. However, there are also several technical problems. First of all, we performed whole-mount BM imaging with Two-photon microscopy, in order to avoid the problem of rapid photo-bleaching in confocal microscopy. But it also brings new problems that the signal from the nearby channels partly overlap and cannot be clearly separated, for example the red channel (labeled CD144, Alexa Fluor 594) and near infra-red channel (labeled CD42, Alexa Fluor 647). Therefore a staining strategy should be carefully planned in order not to disturb the staining results. In addition, the whole-mount images nicely show the cell distribution in three-dimension but do not show any information of cell dynamics that is pivotal for the whole project. Besides, the image processing and quantitative analysis of the whole-mount images is time-consuming.

Two-photon microscopy intravital imaging serves as a good complement to whole-mount imaging. It directly displays the cell dynamics and therefore is a convincing approach for in vivo studies. However, there are also several drawbacks. A good preparation of calvarian imaging model is difficult and often requires well training. A lot of things should be paid attention in order to ensure the quality of the images, including good care of the animal, a proper preparation of the imaging window, imaging settings as well as the data processing. Besides, the calvarian is currently the only non-invasive way to image an intact BM, which greatly limits the available BM area. One challenge we came across is how to distinguish cells and MK fragments in vWF-eGFP mice calvarian imaging. During thrombopoiesis MKs form cytoplasmic fragments that are released into the BM. These fragments are in various size and morphology, some of which are highly similar to small migrating cells. In order to further distinguish small $vWF^+$ cells (MKPs) from these MK fragments, one solution is to inject dyes that stain the nuclear of the cells, for example Hoechst. However, the test of Hoechst showed that the signal severely leaks to the GFP channel. As a compromise to this problem, we carefully tracked the dynamics of the $vWF^+$ small “objects”, and

strictly excluded those adjacent to fragmented MKs, and finally distinguished small objects which are roundish and no branch-like shape as MKPs. The chronic imaging as another solution could clearly show the growth of MKPs and therefore excludes the possibility of a wrong definition for MKPs.

## 5. 2 Discussion of results

### 5. 2. 1 Cell dynamics of MKs and MKPs in vivo

An important aspect of megakaryopoiesis we explored is cell migration. Multiple in vivo studies have shown vivid dynamics of hematopoietic cell migration within the bone marrow. These cells, including hematopoietic stem cells, lymphocytes, neutrophils, are migrating in diverse patterns according to cell types as well as stress conditions [106, 128-130]. Nevertheless, it still remains unclear how MKs and MKPs dynamically behave and function within intact BM.

By performing calvarian live imaging in three mouse strains in which the MKs express fluorescent proteins, we found that MKs are static cells which don't migrate. This observation contradicts with many previous studies which showed that MKs migrate toward the vascular niche in the presence of SDF-1 and FGF-4 [30, 31]. In those studies, the perspective of MK migration was depending on two interpretations. First, it was shown that SDF-1 receptor CXCR4 is expressed on MKs [131]. As SDF-1 serves as a chemokine for hematopoietic cells, the high gradient of SDF-1 present at the perivascular niche could attract the migration of MKs through SDF-1-CXCR4 signaling [33]. It was also proved in vitro that MKs migrate or transmigrate in response to SDF-1. Second, previous studies showed that HSCs and MKs localized at the osteoblastic niche [56, 57, 79], which provides a possibility for the repositioning of MKs from the endosteum towards sinusoid. Actually, most of those studies were either using ex vivo histology with two-dimensional sections or in vitro assays [30, 33, 35]. Considering the complexity of the real bone marrow, histological sections often generate false

spatial impressions, while in vitro assays simplify bone marrow components and their effect on target cells. In our study we tried to avoid these problems and yield more reliable results. By using whole-mount staining we were able to analyze within three-dimensional volume of a whole piece of sternum bone marrow with a depth of ~70 μm. Compared with previous two-dimensional sections, it generates less mistakes and more accuracy in deciphering cell spatial localization. Indeed, we found that MKs are predominately resided at the vascular niche instead of any other niches in bone marrow. Potentially this indicates no necessaries for a migration to reach the endothelium. On the other hand, our calvarian imaging of living mice confirmed that MKs are slightly changing morphology in situ rather than migrating. They are static cells which don't show any spatial shift even under stress conditions.

In addition, we explored the migration of MKPs within the BM by tracking cells in living vWF-eGFP mice. We distinguished MKPs as vWF+ small cells, and we unprecedentedly visualized the dynamics of two subtypes of MKPs. One group of vWF+ small cells are migrating actively and do not show any cytoplasmic growth over time, which we term "motile MKPs". The other group of vWF+ small cells are relatively static with very low speed, while they are growing constantly over time, which we term "non-motile MKPs". Theoretically these two MKPs could be completely independent groups, or could lie in hierarchy sequence. Based on the hints from our study, we tended to accept the latter one. Although it is yet beyond current methodology to isolate these two groups of cells in vitro and test their stages and functions, we already discovered that the motile MKPs are a tiny population with small cell size comparable with stem cells, and are migrating actively in bone marrow without differentiation. These evidences tempted us to assume they are very early stage progenitors or stem cells. The non-motile MKPs, as we showed, are much smaller in size than mature MKs but bigger than motile ones. They appear highly at the extravascular region attaching to the sinusoid, and gradually increase cell volume in situ without any spatial shift during this entire process. We propose that they are in hierarchy derived from motile MKPs.

Once the differentiation is initiated, they stop migration and settle down in proximity to vessels and start to differentiate into mature MKs in situ. To confirm this hypothesis in future work, it would be very interesting to find feasible method to isolate the cells reliably and perform functional assays.

### 5. 2. 2 The definition of megakaryopoietic islands

The term “island” was for the first time used on hematopoietic cells by Bessis in 1958, to describe the developing erythroblasts [132]. Later on, it was characterized in detail that the anatomic structure of an erythroblastic island consists of a central macrophage and the surrounding erythroblasts, and the macrophage forms cytoplasmic protrusions that bind the erythrocytes into clusters [133-135]. In human marrow, the number of erythroblasts in one island varies between 5 to more than 30 cells [136]. There were several postulations concerning the functional relevance of the central macrophages, as a key component of the erythroblastic islands [137, 138]. On one hand, the embraced macrophages might serve as iron pool that helps form erythrocytes. On the other hand, during the maturation of erythrocytes the extruded nuclei might be phagocytized by macrophages [137, 138]. These thoughts are the early sprout for the perspective that the erythroblastic island may provide a “niche” for the development of erythrocytes.

In our investigation of the confetti chimera’s bone marrow, we observed a lot of hematopoietic cell colonies, including the MK colonies, which we distinguished by their huge morphology. This indicates that megakaryocyte can form colonies as other hematopoietic cells, the erythrocytes for example. Furthermore, we observed that the MK precursors are in close proximity to MKs, and the spatial localization of the MK populations remain stable during megakaryopoiesis and thrombopoiesis. This provides the anatomic basis of an “island”. In addition, we observed that the sinusoid is tightly associated with the entire process of MKP growth. Based on these observations, we defined the functional unit of MK

populations and sinusoid as a “megakaryopoietic island”. Similar to the erythroblastic island we discussed above, here the MK island also provides a functional “niche” for the MK lineage that not only ensures platelet production but also maintains MK numbers. When we depleted MKs, the island structure is dispersed and MKP growth is severely disturbed. This points to the assumption that MK is an important component within the MK island. However, it does not rule out the possibility that the sinusoid also play a role in regulating the function of MK islands. The bone marrow microenvironment is comprised of multiple niche cells and they are anatomically adjacent. Currently it still remains unclear whether distinct niches function individually or combined and complemented [139]. We found that the MK islands are lying highly adjacent to the sinusoids. Therefore both niches might co-regulate megakaryopoiesis. It was shown that the blockage of endothelial receptors VCAM-1 and VLF-4 inhibits BM hematopoietic progenitors migration towards the sinusoid as well as the maturation of the MKs [30]. However, this paper did not investigate the impact of vessel blockage to the MK-MKP interactions. In our study, we did not observe a difference of the vessel structure in steady state compared to those after platelet depletion and MK depletion. In order to find out whether the vessel might provide another important contribution to the MK islands, the function of the vessels should be tested and the blocking experiment should be carried out.

Although MKs do not preferably distribute in areas other than the vessels, it still remains difficult to define a clear boundary for individual MK island due to the dense network of the BM vessels as well as the certain amount of MK populations. In this thesis, there is also no standard for an exact cellularity within one MK island. According to our whole-mount as well as the in vivo images, the number of MK lineage cells in one island varies between 2 to 10 in steady state, and increases during hematopoietic stress. In our chronic imaging, we sometimes observed that small $vWF^{+}$ cells appear into the imaging area, settle down to the MK island and start growing big. These new cells might come from neighboring islands. This suggests that distinct MK islands might exchange cells at stem cell

or early progenitor level. As future work, it would be interesting to find out if different MK islands communicate with each other in cellular or molecular level.

### 5. 2. 3 The novel functions of MK and MK island

Previously it has been shown that MKs exert versatile roles as niche cells and support other cell types in bone marrow, apart from the function of platelet production [79, 82-84]. In steady state, MKs regulate the quiescence of HSCs [83]. When under stress conditions, MKs promote the regeneration of HSCs and myeloid progenitor cluster formation [82, 84]. In addition, it was reported that MKs influence the proliferation and differentiation of osteoblasts [79]. All these information highlight MKs as niche cells and as important regulators of BM homeostasis. However, it has never been shown that a mature blood cell can serve directly as niche cell and regulate its own lineage. In this thesis, we further discovered an essential role of MKs in regulating their own lineage precursors, which is taking place within megakaryopoietic islands. We detected that MK populations are gathering into islands in which MK precursors are close or directly attached to MKs. In steady state we observed that MKs provide a niche where platelet-biased stem cells and MK progenitors are localized. The MKPs start proliferating next to MKs under hematopoietic stress. When MKs are depleted, the MK islands are disrupted and MKP maturation is severely disturbed by measuring the localization as well as the cell volume. This indicates that MKs sustain MK islands and control the growth of MKPs. This information reveal the character of “niche cell” and support our initial hypothesis that MKs function as niche cells to regulate their own precursors.

The findings of this thesis also have important implications on the maintenance of MK homeostasis, which balance not only platelet production but also the function of other cell types controlled by MKs. Therefore, when large numbers of platelets are consumed urgently and MKs quickly break up into platelets to supply the need, there should be a mechanism to fill up the loss of MKs and sustain bone marrow

homeostasis. Since MKs regulate the development of their own precursors by close communication, they are assumed to convey expansion signal quickly into the adjacent MKPs and trigger MK replenishment under stress conditions.

### 5. 2. 4 The potential molecular interactions between MKs and MKPs

The communication between two cell types is mediated by cell-cell interaction, which is believed to be important for the development as well as the functions of the target cells [56]. Cell-cell interaction is achieved mainly through either cell-cell firm adhesion or soluble factors secretion. In this thesis, we disclosed a tight cellular connection between MKs and MKPs in high-resolution whole-mount images. We postulated that MKPs receive the regulating signal either by direct MK-MKP adhesion through adhesion molecules or by soluble factors secreted from MKs to MKPs.

In the first form, the cells are binding to each other via adhesion molecules expressed on the cell surface, and then the signal is conveyed to intercellular signaling pathways and initiate cell activity. The adhesion molecules can be categorized into four major types: selectin, integrin, immunoglobulin superfamily as well as cadherin [140]. MKs express various adhesion molecules including glycoproteins, VCAM-1, ICAM-1 and vWF [47, 141]. VLF-4/VCAM-1 and CD226 were shown to mediate the adhesion of MKs to human umbilical vein endothelial cells [29, 142]. Connexin is a gap junction protein that is responsible for direct intercellular communication between two cell types [143]. Through this direct contact the cytoplasm of the cells exchange small signaling molecules that are essential for the physiological functions of the cells [140, 143, 144]. It was reported that MKs express connexin 43 which build the connection to osteoblasts and regulate their proliferation and differentiation [145]. Kindlin-3 is a protein abundant in MKs and platelets, and is responsible for the integrin activation and platelet aggregation during thrombus formation [146, 147]. To test whether direct integrin-mediated adhesion plays an important role, one choice is to use PF4 Cre

× Kindlin-3$^{fl/fl}$ mouse in which the kindlin-3 expression on MKs is depleted and which leads to defective adhesion with other cells.

On the other hand, the cell-cell interaction can be mediated by soluble factors which is secreted from one cell, bind to the receptors of the target cell and activate the intracellular signaling. MK cytoplasm accumulates and secretes abundant soluble factors including inflammatory cytokines and chemokines. There were two publications showing that MKs secrete high level of CXCL4 and TGF-β1 that regulate the quiescence of HSCs [82, 83]. It was also reported that MKs express CXCL12 which is an important chemokine for hematopoietic cell migration [148]. CXCR4, the receptor of CXCL12, is expressed on MK progenitors and was shown to mediate the MKP migration [149]. Therefore, it might also be possible that MKs attract and retain MKPs by the secretion of CXCL12. Currently it remains unclear how MKs communicate with their precursors and what molecules are involved in this process. As future work, we will explore the molecular candidates discussed above.

### 5. 2. 5 Clinical implications of this study

One of the main causes of thrombocytopenia is the decreased production of platelets in BM [150]. Numerous factors can injure stem cells and lead to dysplasia or defective hematopoiesis, including leukemia, viral infection, irradiation and some chemotherapy drugs [151]. In these situations, the platelet biogenesis is disturbed and the platelet number in circulation is decreased. Severe thrombocytopenia might cause intracranial hemorrhage, which is fatal [152]. Currently the treatments for thrombocytopenia include medicines, blood or platelet transfusion and splenectomy [153, 154]. However none of them cure the disease from the basis. In order to find out an efficient treatment, it is urgently needed to understand in detail how megakaryopoiesis and thrombopoiesis take place in BM. In this thesis, we discovered that the close gathering of MK populations (MK islands) is important for sustaining normal megakaryopoiesis.

Therefore, for patients with thrombocytopenia or decreased MK number, a careful examination of the spatial distribution of MKs and MKPs in BM should be focused on. Future work on exploring the molecular mechanisms will reveal how these regulations are controlled, which might provide a therapeutic target for treating certain hematological diseases.

## 5. 3 Summary

Despite numerous studies on megakaryocytes and platelet formation, it still remains unknown how megakaryocytes are developed from hematopoietic stem cells and progenitors in vivo. In this thesis, we show that megakaryopoiesis takes place in functional units of MKs and their precursors at BM sinusoids which we termed “megakaryopoietic island”. Importantly, MKs play an important role in regulating both the positioning and cytoplasmic growth of MK progenitors thereby maintaining MK islands.

In the first part, we investigated the localization and dynamics of MK populations in steady state. From whole-mount staining of MKs, MKPs and platelet-biased stem cells, we found that the MK populations are in close proximity to each other. This provides an anatomic basis for the structure of MK islands. From calvarian live imaging of these cells, we found that the development of MK populations are statically taking place in situ, without any spatial redistribution. Although there are cells growing and disappearing, the density of MK populations remain constant within one MK island.

In the second part, we investigated megakaryopoiesis under hematopoietic stress. We triggered the mice with platelet depletion as a mimic of thrombocytopenia to exaggerate megakaryopoiesis. We found that the initial response of MKs towards this stress is the high fragmentation and rapid production of large amount of platelets. This is followed by enhanced MKP proliferation within MK islands later on. The number of MKs remain stable during this stress condition. The intimate

anatomic relationship between MKs and MKPs provides the possibility that a coordinated signal quickly conveyed from MKs to their precursors, which fill up the need of platelets as well as replenish MK pool under emergency conditions. The treatment of thrombopoietin as another trigger of megakaryopoiesis also increases the density of MK islands. These results shed light on the MK island as the central cellular unit of the regulation of megakaryopoiesis.

In the last part, we investigated in detail the role of MKs in regulating their precursors by using PF4 Cre × Rosa26-iDTR mouse as the MK depletion model. After Mk depletion, we observed increased MKP expansion. However, the MKPs are dispersed within the BM and cease growing. These results indicate that the disruption of MKs and MK islands leads to abnormal MKP expansion without proper localization and maturation, and further highlight the important role of MKs and MK islands in regulating its own lineage.

In summary, the work of this thesis for the first time reveals that megakaryopoiesis dynamically takes place as megakaryopoietic islands within the bone marrow, and provides visual evidence that megakaryocytes regulate their own precursors in order to balance platelet production and maintain homeostasis. The findings of this thesis unprecedentedly show how megakaryopoiesis vividly takes place in vivo over long time. It refreshes our knowledge that a mature blood can function as niche cell to regulate the development of its own lineage. It contributes to a better understanding of the two major functions of MK island, platelet production and MK turnover, and how these two functions are coordinated in order to sustain this lineage under certain hematopoietic stress. These findings also open a new scope for future clinical diagnose and treatment of patients with thrombocytopenia or decreased MK number.

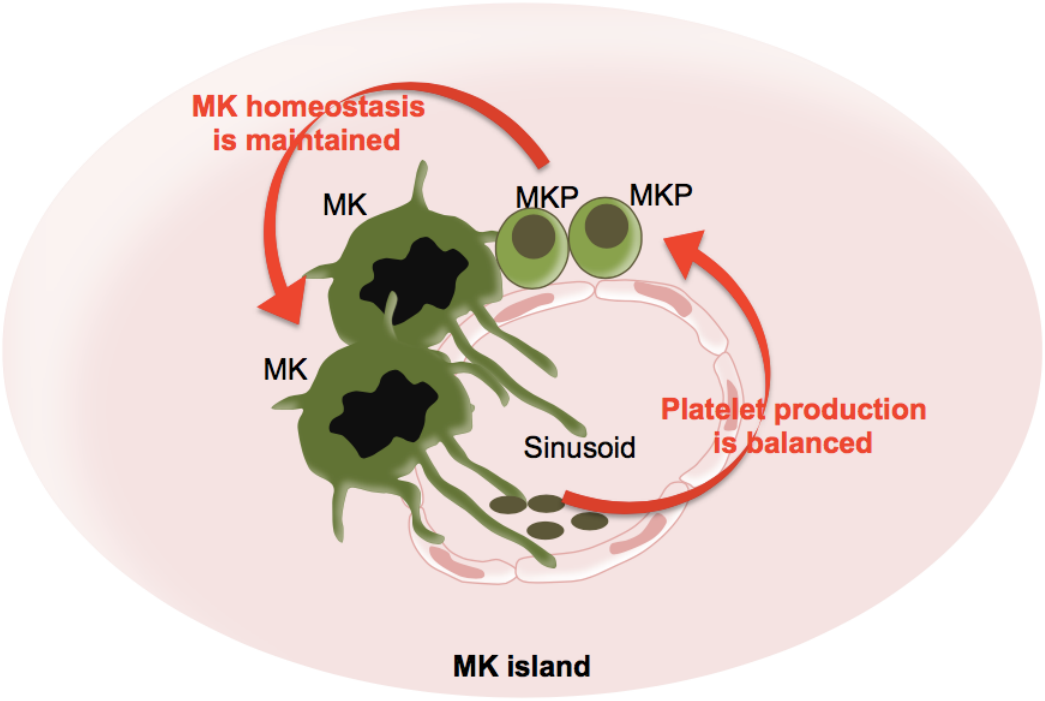


Figure 5. 1 Two major functions of MKs are coordinated within MK island.

# 6 REFERENCES


1. Furie B, Furie BC. Thrombus formation in vivo. J Clin Invest, 2005. 115(12): 3355-62.
2. Gawaz M, Langer H, May AE. Platelets in inflammation and atherogenesis. J Clin Invest, 2005. 115(12): 3378-84.
3. Zaslavsky A, Baek KH, Lynch RC, Short S, Grillo J, Folkman J, Italiano JE, Jr, Ryeom S. Platelet-derived thrombospondin-1 is a critical negative regulator and potential biomarker of angiogenesis. Blood, 2010. 115(22): 4605–13.
4. Gay LJ, Felding-Habermann B. Contribution of platelets to tumour metastasis. Nature Reviews Cancer, 2011. 11, 123-134.
5. Engelmann B, Massberg S. Thrombosis as an intravascular effector of innate immunity. Nat Rev Immunol, 2013. 13(1): 34-45.
6. Wright JH. The origin and nature of the blood plates. Boston Med Surg J, 1906. 23: 643–645.
7. Wright JH. The histogenesis of blood platelets. J Morphol, 1910. 21: 263–278.
8. Odell T, Jackson CJ, Reiter R. Generation cycle of rat megakaryocytes. Exp Cell Res, 1968. 53, 321.
9. Ebbe S, Stohlman F Jr. Megakaryocytopoiesis in the rat. Blood, 1965. 26, 20–34.
10. Ebbe, S. Biology of megakaryocytes. Prog Hemost Thromb, 1976. 3, 211–229.
11. Therman, E., Sarto, G., & Stubblefiels, P. Endomito- sis: A reappraisal. Hum Genet, 1983. 63, 13–18.
12. Machlus KR, Italiano JE Jr. The incredible journey: From megakaryocyte development to platelet formation. J Cell Biol, 2013. 201(6): 785-96.
13. Yamada, F. The fine structure of the megakaryocyte in the mouse spleen. Acta Anat, 1957. 29, 267–290.
14. Italiano JE Jr, Lecine P, Shivdasani RA, Hartwig JH. Blood platelets are

assembled principally at the ends of proplatelet processes produced by differentiated megakaryocytes. J Cell Biol, 1999. 147(6): 1299-312.

15. Junt T, Schulze H, Chen Z, Massberg S, Goerge T, Krueger A, Wagner DD, Graf T, Italiano JE Jr, Shivdasani RA, von Andrian UH. Dynamic visualization of thrombopoiesis within bone marrow. Science, 2007. 317(5845): 1767-70.
16. Zhang L, Orban M, Lorenz M, Barocke V, Braun D, Urtz N, Schulz C, von Brühl ML, Tirniceriu A, Gaertner F, Proia RL, Graf T, Bolz SS, Montanez E, Prinz M, Müller A, von Baumgarten L, Billich A, Sixt M, Fässler R, von Andrian UH, Junt T, Massberg S. A novel role of sphingosine 1-phosphate receptor S1pr1 in mouse thrombopoiesis. J Exp Med, 2012. 209(12): 2165-81.
17. Nishimura S, Nagasaki M, Kunishima S, Sawaguchi A, Sakata A, Sakaguchi H, Ohmori T, Manabe I, Italiano JE Jr, Ryu T, Takayama N, Komuro I, Kadowaki T, Eto K, Nagai R. IL-1α induces thrombopoiesis through megakaryocyte rupture in response to acute platelet needs. J Cell Biol, 2015. 209(3): 453-66.
18. Nakeff A, Maat B. Separation of megakaryocytes from mouse bone marrow by velocity sedimentation. Blood, 1974. 43(4): 591-5.
19. Morrison SJ, Scadden DT. The bone marrow niche for haematopoietic stem cells. Nature, 2014. 505(7483): 327–334.
20. Mendelson A, Frenette PS. Hematopoietic stem cell niche maintenance during homeostasis and regeneration. Nat Med, 2014. 20(8): 833–846.
21. Schofield R. The relationship between the spleen colony-forming cell and the haemopoietic stem cell. Blood Cells, 1978. 4(1-2): 7-25.
22. Visnjic D, Kalajzic Z, Rowe DW, Katavic V, Lorenzo J, Aguila HL. Hematopoiesis is severely altered in mice with an induced osteoblast deficiency. Blood, 2004.103(9): 3258-64.
23. Ding L, Saunders TL, Enikolopov G, Morrison SJ. Endothelial and perivascular cells maintain haematopoietic stem cells. Nature, 2012. 481(7382): 457–462.

24. Winkler IG, Barbier V, Nowlan B, Jacobsen RN, Forristal CE, Patton JT, Magnani JL, Lévesque JP. Vascular niche E-selectin regulates hematopoietic stem cell dormancy, self renewal and chemoresistance. Nat Med, 2012. 18(11): 1651-7.
25. Omatsu Y, Sugiyama T, Kohara H, Kondoh G, Fujii N, Kohno K, Nagasawa T. The essential functions of adipo-osteogenic progenitors as the hematopoietic stem and progenitor cell niche. Immunity, 2010. 33(3): 387-99.
26. Katayama Y, Battista M, Kao WM, Hidalgo A, Peired AJ, Thomas SA, Frenette PS. Signals from the sympathetic nervous system regulate hematopoietic stem cell egress from bone marrow. Cell, 2006. 124(2): 407-21.
27. Lucas D, Scheiermann C, Chow A, Kunisaki Y, Bruns I, Barrick C, Tessarollo L, Frenette PS. Chemotherapy-induced bone marrow nerve injury impairs hematopoietic regeneration. Nat Med, 2013. 19(6): 695-703.
28. Tavassoli M, Aoki M. Localization of megakaryocytes in the bone marrow. Blood Cells, 1989.15(1): 3-14.
29. Avraham H, Cowley S, Chi SY, Jiang S, Groopman JE. Characterization of adhesive interactions between human endothelial cells and megakaryocytes. J Clin Invest, 1993. 91(6): 2378-84.
30. Avecilla ST, Hattori K, Heissig B, Tejada R, Liao F, Shido K, Jin DK, Dias S, Zhang F, Hartman TE, Hackett NR, Crystal RG, Witte L, Hicklin DJ, Bohlen P, Eaton D, Lyden D, de Sauvage F, Rafii S. Chemokine-mediated interaction of hematopoietic progenitors with the bone marrow vascular niche is required for thrombopoiesis. Nat Med, 2004. 10(1): 64-71.
31. Pitchford SC, Lodie T, Rankin SM. VEGFR1 stimulates a CXCR4-dependent translocation of megakaryocytes to the vascular niche, enhancing platelet production in mice. Blood, 2012. 120(14): 2787-95.
32. Eldor A, Fuks Z, Levine RF, Vlodavsky I. Measurement of platelet and megakaryocyte interaction with the subendothelial extracellular matrix. Methods Enzymol, 1989. 169: 76-91.

33. Niswander LM, Fegan KH, Kingsley PD, McGrath KE, Palis J. SDF-1 dynamically mediates megakaryocyte niche occupancy and thrombopoiesis at steady state and following radiation injury. Blood, 2014. 124(2): 277-86.
34. Hamada T, Möhle R, Hesselgesser J, Hoxie J, Nachman RL, Moore MA, Rafii S. Transendothelial Migration of Megakaryocytes in Response to Stromal Cell-derived Factor 1 (SDF-1) Enhances Platelet Formation. J Exp Med, 1998. 188(3): 539–548.
35. Mazharian A, Thomas SG, Dhanjal TS, Buckley CD, Watson SP. Critical role of Src-Syk-PLC{gamma}2 signaling in megakaryocyte migration and thrombopoiesis. Blood, 2010. 116(5): 793-800.
36. Golde D. The stem cell. Sci Am, 1991. 265, 86–93. 2.
37. Ogawa, M. Differentiation and proliferation of hematopoietic stem cells. Blood, 1993. 81, 2844–2853.
38. Morrison SJ, Wandycz AM, Hemmati HD, Wright DE, Weissman IL. Identification of a lineage of multipotent hematopoietic progenitors. Development, 1997. 124(10): 1929-39.
39. Akashi K, Traver D, Miyamoto T, Weissman IL. A clonogenic common myeloid progenitor that gives rise to all myeloid lineages. Nature, 2000. 404(6774): 193-7.
40. Kondo M, Weissman IL, Akashi K. Identification of clonogenic common lymphoid progenitors in mouse bone marrow. Cell, 1997. 91(5): 661-72.
41. Debili N, Coulombel L, & Croisille L. Characterization of a bipotent erythro-megakaryocytic progenitor in human bone marrow. Blood, 1996. 88, 1284–1296.
42. McDonald TP, Sullivan PS. Megakaryocytic and erythrocytic cell lines share a common precursor cell. Exp Hematol, 1993. 21, 1316–1320.
43. Nakeff A, Daniels–McQueen S. In vitro colony assay for a new class of megakaryocyte precursor: Colony- forming unit megakaryocyte (CFU-M). Proc Soc Exp Biol Med, 1976. 151, 587–590.

44. Long M, Williams N, &Ebbe S. Immaturemegakaryocytes in the mouse: Physical characteristics, cell cycle status, and in vitro responsiveness to thrombopoietic stimulatory factor. Blood, 1982. 59, 569–575.
45. Debili N, Robin C, Schiavon V, Letestu R, Pflumio F, Mitjavila-Garcia MT, Coulombel L, Vainchenker W. Different expression of CD41 on human lymphoid and myeloid progenitors from adults and neonates. Blood, 2001. 97(7): 2023-30.
46. Klimchenko O, Mori M, Distefano A, Langlois T, Larbret F, Lecluse Y, Feraud O, Vainchenker W, Norol F, Debili N. A common bipotent progenitor generates the erythroid and megakaryocyte lineages in embryonic stem cell-derived primitive hematopoiesis. Blood, 2009. 114(8): 1506-17.
47. Lagrue-Lak-Hal AH, Debili N, Kingbury G, Lecut C, Le Couedic JP, Villeval JL, Jandrot-Perrus M, Vainchenker W. Expression and function of the collagen receptor GPVI during megakaryocyte maturation. J Biol Chem, 2001. 276(18): 15316-25.
48. Clay D, Rubinstein E, Mishal Z, Anjo A, Prenant M, Jasmin C, Boucheix C, Le Bousse-Kerdilès MC. CD9 and megakaryocyte differentiation. Blood, 2001. 97(7): 1982-9.
49. Nakorn TN, Miyamoto T, Weissman IL. Characterization of mouse clonogenic megakaryocyte progenitors. Proc Natl Acad Sci U S A, 2003. 100(1): 205-10.
50. Sanjuan-Pla A, Macaulay IC, Jensen CT, Woll PS, Luis TC, Mead A, Moore S, Carella C, Matsuoka S, Bouriez Jones T, Chowdhury O, Stenson L, Lutteropp M, Green JC, Facchini R, Boukarabila H, Grover A, Gambardella A, Thongjuea S, Carrelha J, Tarrant P, Atkinson D, Clark SA, Nerlov C, Jacobsen SE. Platelet-biased stem cells reside at the apex of the haematopoietic stem-cell hierarchy. Nature, 2013. 502(7470): 232-6.
51. Haas S, Hansson J, Klimmeck D, Loeffler D, Velten L, Uckelmann H, Wurzer S, Prendergast ÁM, Schnell A, Hexel K, Santarella-Mellwig R, Blaszkiewicz S, Kuck A, Geiger H, Milsom MD, Steinmetz LM, Schroeder T, Trumpp A, Krijgsveld J, Essers MA. Inflammation-Induced Emergency

Megakaryopoiesis Driven by Hematopoietic Stem Cell-like Megakaryocyte Progenitors. Cell Stem Cell, 2015. 17(4): 422-34.

52. Notta F, Zandi S, Takayama N, Dobson S, Gan OI, Wilson G, Kaufmann KB1, McLeod J, Laurenti E, Dunant CF, McPherson JD, Stein LD, Dror Y, Dick JE. Distinct routes of lineage development reshape the human blood hierarchy across ontogeny. Science, 2016. 351(6269): aab2116.
53. Shin JY, Hu W, Naramura M, Park CY. High c-Kit expression identifies hematopoietic stem cells with impaired self-renewal and megakaryocytic bias. J Exp Med, 2014. 211(2): 217-31.
54. Chang Y, Bluteau D, Debili N, Vainchenker W. From hematopoietic stem cells to platelets. J Thromb Haemost, 2007. 5 Suppl 1: 318-27.
55. Zhang J, Niu C, Ye L, Huang H, He X, Tong WG, Ross J, Haug J, Johnson T, Feng JQ, Harris S, Wiedemann LM, Mishina Y, Li L. Identification of the haematopoietic stem cell niche and control of the niche size. Nature, 2003. 425(6960): 836-41.
56. Calvi LM, Adams GB, Weibrecht KW, Weber JM, Olson DP, Knight MC, Martin RP, Schipani E, Divieti P, Bringhurst FR, Milner LA, Kronenberg HM, Scadden DT. Osteoblastic cells regulate the haematopoietic stem cell niche. Nature, 2003. 425(6960): 841-6.
57. Nilsson SK, Johnston HM, Coverdale JA. Spatial localization of transplanted hemopoietic stem cells: inferences for the localization of stem cell niches. Blood, 2001. 97(8): 2293-9.
58. Kiel MJ, Yilmaz OH, Iwashita T, Yilmaz OH, Terhorst C, Morrison SJ. SLAM family receptors distinguish hematopoietic stem and progenitor cells and reveal endothelial niches for stem cells. Cell, 2005. 121(7): 1109-21.
59. Greenbaum A, Hsu YM, Day RB, Schuettpelz LG, Christopher MJ, Borgerding JN, Nagasawa T, Link DC. CXCL12 in early mesenchymal progenitors is required for haematopoietic stem-cell maintenance. Nature, 2013. 495(7440): 227-30.

60. Ding L, Morrison SJ. Haematopoietic stem cells and early lymphoid progenitors occupy distinct bone marrow niches. Nature, 2013. 495(7440): 231-5.
61. Kunisaki Y, Bruns I, Scheiermann C, Ahmed J, Pinho S, Zhang D, Mizoguchi T, Wei Q, Lucas D, Ito K, Mar JC, Bergman A, Frenette PS. Arteriolar niches maintain haematopoietic stem cell quiescence. Nature, 2013. 502(7473): 637-43.
62. Pallotta I, Lovett M, Rice W, Kaplan DL, Balduini A. Bone marrow osteoblastic niche: a new model to study physiological regulation of megakaryopoiesis. PLoS One, 2009. 4(12): e8359.
63. Massimo Marenzana, Timothy R. Arnett. The Key Role of the Blood Supply to Bone. Bone Res, 2013. 1(3): 203–215.
64. Tavassoli M. Structure and function of sinusoidal endothelium of bone marrow. Prog Clin Biol Res, 1981. 59B: 249-56.
65. Williams DE, Eisenman J, Baird S, Rauch C, Ness KV, March CJ, Park LS,Martin U, Mochizuki DY, Boswell HS, Burgess GS, Cosman D, Lyman SD: Identification of a ligand for the c-kit proto-oncogene. Cell, 1990. 63: 163.
66. Zsebo KM, Williams DA, Geissler EN, Broudy VC, Martin FH, Atkins HL, Hsu R-Y, Birkett NC, Okino KH, Murdock DC, Jacobsen FW, Langley KE, Smith KA, Takeishi T, Cattanach BM, Galli SJ, Suggs SV: Stem cell factor is encoded at the S1locus of the mouse and is the ligand for c-kit tyrosine kinase receptor. Cell, 1990. 63: 213.
67. Huang E, Nocka K, Beier DR, Chu T-Y, Buck J, Lahm H-W, Wellner D, Leder P, Besmer P: The hematopoietic growth factor KL is encoded by the SI locus and is the ligand of the c-kit receptor, the gene product of the W locus. Cell, 1990. 63: 225.
68. Ogawa M, Nishikawa S, Yoshinaga K, Hayashi S, Kunisada T, Nakao J, Kina T, Sudo T, Kodama H, Nishikawa S. Expression and function of c-Kit in fetal hemopoietic progenitor cells: transition from the early c-Kit-independent

to the late c-Kit-dependent wave of hemopoiesis in the murine embryo. Development, 1993. 117(3): 1089-98.

69. Tsuji K, Zsebo KM, Ogawa M. Enhancement of murine blast cell colony formation in culture by recombinant rat stem cell factor, ligand for c-kit. Blood, 1991. 78(5): 1223-9.
70. Ogawa M, Matsuzaki Y, Nishikawa S, Hayashi S, Kunisada T, Sudo T, Kina T, Nakauchi H, Nishikawa S. Expression and function of c-kit in hemopoietic progenitor cells. J Exp Med, 1991. 174(1): 63-71.
71. Avraham H, Vannier E, Cowley S, Jiang SX, Chi S, Dinarello CA, Zsebo KM, Groopman JE. Effects of the stem cell factor, c-kit ligand, on human megakaryocytic cells. Blood, 1992. 79(2): 365-71.
72. Avraham H, Scadden DT, Chi S, Broudy VC, Zsebo KM, Groopman JE. Interaction of human bone marrow fibroblasts with megakaryocytes: role of the c-kit ligand. Blood, 1992. 80(7): 1679-84.
73. Jiang S, Levine JD, Fu Y, Deng B, London R, Groopman JE, Avraham H. Cytokine production by primary bone marrow megakaryocytes. Blood, 1994. 84(12): 4151-6.
74. Wickenhauser C, Lorenzen J, Thiele J, Hillienhof A, Jungheim K, Schmitz B, Hansmann ML, Fischer R. Secretion of cytokines (interleukins-1 alpha, -3, and -6 and granulocyte-macrophage colony-stimulating factor) by normal human bone marrow megakaryocytes. Blood, 1995. 85(3): 685-91.
75. Psaila B, Lyden D, Roberts I. Megakaryocytes, Malignancy and Bone Marrow Vascular Niches. J Thromb Haemost, 2012. 10(2): 177–188.
76. Wendy A. Ciovacco, Ying-Hua Cheng, Mark C. Horowitz, Melissa A. Kacena. Immature and Mature Megakaryocytes Enhance Osteoblast Proliferation and Inhibit Osteoclast Formation. J Cell Biochem, 2010. 109(4): 774–781.
77. Lemieux JM, Horowitz MC, Kacena MA. Involvement of integrins alpha(3)beta(1) and alpha(5)beta(1) and glycoprotein IIb in megakaryocyte-induced osteoblast proliferation. J Cell Biochem, 2010. 109(5): 927-32.

78. Dominici M, Rasini V, Bussolari R, Chen X, Hofmann TJ, Spano C, Bernabei D, Veronesi E, Bertoni F, Paolucci P, Conte P, Horwitz EM. Restoration and reversible expansion of the osteoblastic hematopoietic stem cell niche after marrow radioablation. Blood, 2009. 114(11): 2333-43.
79. Olson TS, Caselli A, Otsuru S, Hofmann TJ, Williams R, Paolucci P, Dominici M, Horwitz EM. Megakaryocytes promote murine osteoblastic HSC niche expansion and stem cell engraftment after radioablative conditioning. Blood, 2013. 121(26): 5238-49.
80. Möhle R, Green D, Moore MA, Nachman RL, Rafii S. Constitutive production and thrombin-induced release of vascular endothelial growth factor by human megakaryocytes and platelets. Proc Natl Acad Sci U S A, 1997. 94(2): 663-8.
81. Kopp HG, Hooper AT, Broekman MJ, Avecilla ST, Petit I, Luo M, Milde T, Ramos CA, Zhang F, Kopp T, Bornstein P, Jin DK, Marcus AJ, Rafii S. Thrombospondins deployed by thrombopoietic cells determine angiogenic switch and extent of revascularization. J Clin Invest, 2006. 116(12): 3277-91.
82. Zhao M, Perry JM, Marshall H, Venkatraman A, Qian P, He XC, Ahamed J, Li L. Megakaryocytes maintain homeostatic quiescence and promote post-injury regeneration of hematopoietic stem cells. Nat Med, 2014. 20(11): 1321-6.
83. Bruns I, Lucas D, Pinho S, Ahmed J, Lambert MP, Kunisaki Y, Scheiermann C, Schiff L, Poncz M, Bergman A, Frenette PS. Megakaryocytes regulate hematopoietic stem cell quiescence through CXCL4 secretion. Nat Med, 2014. 20(11): 1315-20.
84. Hérault A, Binnewies M, Leong S, Calero-Nieto FJ, Zhang SY, Kang YA, Wang X, Pietras EM, Chu SH, Barry-Holson K, Armstrong S, Göttgens B2, Passegué E. Myeloid progenitor cluster formation drives emergency and leukaemic myelopoiesis. Nature, 2017. 544(7648): 53-58.
85. Kaushansky K, Lok S, Holly RD, Broudy VC, Lin N, Bailey MC, Forstrom JW, Buddle MM, Oort PJ, Hagen FS, Roth GJ, Papayannopoulou T, Foster DC.

Promotion of megakaryocyte progenitor expansion and differentiation by the c-Mpl ligand thrombopoietin. Nature, 1994. 369(6481): 568-71.

86. Gurney AL, Carver-Moore K, de Sauvage FJ, Moore MW. Thrombocytopenia in c-mpl-deficient mice. Science, 1994. 265(5177): 1445-7.
87. de Graaf CA, Metcalf D. Thrombopoietin and hematopoietic stem cells. Cell Cycle, 2011. 10(10): 1582-9.
88. Debili N, Wendling F, Cosman D, Titeux M, Florindo C, Dusanter-Fourt I, Schooley K, Methia N, Charon M, Nador R. The Mpl receptor is expressed in the megakaryocytic lineage from late progenitors to platelets. Blood, 1995. 85(2): 391-401.
89. Fishley B, Alexander WS. Thrombopoietin signalling in physiology and disease. Growth Factors, 2004. 22(3): 151-5.
90. Geddis AE, Linden HM, Kaushansky K. Thrombopoietin: a pan-hematopoietic cytokine. Cytokine Growth Factor Rev, 2002. 13(1): 61-73.
91. Debili N, Wendling F, Katz A, Guichard J, Breton-Gorius J, Hunt P, Vainchenker W. The Mpl-ligand or thrombopoietin or megakaryocyte growth and differentiative factor has both direct proliferative and differentiative activities on human megakaryocyte progenitors. Blood, 1995. 86(7): 2516-25.
92. Lok S, Kaushansky K, Holly RD, Kuijper JL, Lofton-Day CE, Oort PJ, Grant FJ, Heipel MD, Burkhead SK, Kramer JM, et al. Cloning and expression of murine thrombopoietin cDNA and stimulation of platelet production in vivo. Nature, 1994. 369(6481): 565-8.
93. Zucker-Franklin D, Kaushansky K. Effect of thrombopoietin on the development of megakaryocytes and platelets: an ultrastructural analysis. Blood, 1996. 88(5): 1632-8.
94. Broudy VC, Lin NL, Kaushansky K. Thrombopoietin (c-mpl ligand) acts synergistically with erythropoietin, stem cell factor, and interleukin-11 to

enhance murine megakaryocyte colony growth and increases megakaryocyte ploidy in vitro. Blood, 1995. 85(7): 1719-26.

95. Qian S, Fu F, Li W, Chen Q, de Sauvage FJ. Primary role of the liver in thrombopoietin production shown by tissue-specific knockout. Blood, 1998. 92(6): 2189-91.
96. Grozovsky R, Begonja AJ, Liu K, Visner G, Hartwig JH, Falet H, Hoffmeister KM. The Ashwell-Morell receptor regulates hepatic thrombopoietin production via JAK2-STAT3 signaling. Nat Med, 2015. 21(1): 47-54.
97. Nagahisa H, Nagata Y, Ohnuki T, Osada M, Nagasawa T, Abe T, Todokoro K. Bone marrow stromal cells produce thrombopoietin and stimulate megakaryocyte growth and maturation but suppress proplatelet formation. Blood, 1996. 87(4): 1309-16.
98. Emmons RV, Reid DM, Cohen RL, Meng G, Young NS, Dunbar CE, Shulman NR. Human thrombopoietin levels are high when thrombocytopenia is due to megakaryocyte deficiency and low when due to increased platelet destruction. Blood, 1996. 87(10): 4068-71.
99. Müller-Newen G, Stope MB, Kraus T, Ziegler P. Development of platelets during steady state and inflammation. J Leukoc Biol, 2017. 101(5): 1109-1117.
100. Ito T, Ishida Y, Kashiwagi R, Kuriya S. Recombinant human c-Mpl ligand is not a direct stimulator of proplatelet formation in mature human megakaryocytes. Br J Haematol, 1996. 94(2): 387-90.
101. Denk W, Strickler JH, Webb WW. Two-photon laser scanning fluorescence microscopy. Science, 1990. 248(4951): 73-6.
102. Helmchen F, Denk W. Deep tissue two-photon microscopy. Nat Methods, 2005. 2(12): 932-40.
103. Lassailly F, Foster K, Lopez-Onieva L, Currie E, Bonnet D. Multimodal imaging reveals structural and functional heterogeneity in different bone marrow compartments: functional implications on hematopoietic stem cells. Blood, 2013. 122(10): 1730-40.

104. Mazo IB, Gutierrez-Ramos JC, Frenette PS, Hynes RO, Wagner DD, von Andrian UH. Hematopoietic progenitor cell rolling in bone marrow microvessels: parallel contributions by endothelial selectins and vascular cell adhesion molecule 1. J Exp Med, 1998. 188(3): 465-74.
105. Holtmaat A, Bonhoeffer T, Chow DK, Chuckowree J, De Paola V, Hofer SB, Hübener M, Keck T, Knott G, Lee WC, Mostany R, Mrsic-Flogel TD, Nedivi E, Portera-Cailliau C, Svoboda K, Trachtenberg JT, Wilbrecht L. Long-term, high-resolution imaging in the mouse neocortex through a chronic cranial window. Nat Protoc, 2009. 4(8): 1128-44.
106. Hawkins ED, Duarte D, Akinduro O, Khorshed RA, Passaro D, Nowicka M, Straszkowski L, Scott MK, Rothery S, Ruivo N, Foster K, Waibel M, Johnstone RW, Harrison SJ, Westerman DA, Quach H, Gribben J, Robinson MD, Purton LE, Bonnet D, Lo Celso C. T-cell acute leukaemia exhibits dynamic interactions with bone marrow microenvironments. Nature, 2016. 538(7626): 518-522.
107. Le VH, Lee S, Lee S, Wang T, Hyuk Jang W, Yoon Y, Kwon S, Kim H, Lee SW, Hean Kim K. In vivo longitudinal visualization of bone marrow engraftment process in mouse calvaria using two-photon microscopy. Sci Rep, 2017. 7: 44097.
108. Zhang J, Varas F, Stadtfeld M, Heck S, Faust N, Graf T. CD41-YFP mice allow in vivo labeling of megakaryocytic cells and reveal a subset of platelets hyperreactive to thrombin stimulation. Exp Hematol, 2007. 35(3): 490-499.
109. Muzumdar MD, Tasic B, Miyamichi K, Li L, Luo L. A global double-fluorescent Cre reporter mouse. Genesis, 2007. 45(9): 593-605.
110. Bergmeier W, Rackebrandt K, Schroder W, Zirngibl H, Nieswandt B. Structural and functional characterization of the mouse von Willebrand factor receptor GPIb-IX with novel monoclonal antibodies. Blood, 2000. 95: 886-93.
111. Nieswandt B, Bergmeier W, Rackebrandt K, Gessner JE, and Zirngibl H. Identification of critical antigen-specific mechanisms in the development of immune thrombocytopenic purpura in mice. Blood, 2000. 96: 2520-27.

112. Buch T, Heppner FL, Tertilt C, Heinen TJ, Kremer M, Wunderlich FT, Jung S, Waisman A. A Cre-inducible diphtheria toxin receptor mediates cell lineage ablation after toxin administration. Nat Methods, 2005. 2(6): 419-26.
113. Livet J, Weissman TA, Kang H, Draft RW, Lu J, Bennis RA, Sanes JR, Lichtman JW. Transgenic strategies for combinatorial expression of fluorescent proteins in the nervous system. Nature, 2007. 450(7166): 56-62.
114. Emmenlauer M, Ronneberger O, Ponti A, Schwarb P, Griffa A, Filippi A, Nitschke R, Driever W, Burkhardt H. XuvTools: free, fast and reliable stitching of large 3D datasets. J Microsc, 2009. 233(1): 42-60.
115. Schulze H. Culture of murine megakaryocytes and platelets from fetal liver and bone marrow. Methods Mol Biol, 2012. 788: 193-203.
116. Mead TJ, Lefebvre V. Proliferation assays (BrdU and EdU) on skeletal tissue sections. Methods Mol Biol, 2014. 1130: 233-43.
117. Ambekar R, Chittenden M, Jasiuk I, Toussaint KC Jr. Quantitative second-harmonic generation microscopy for imaging porcine cortical bone: comparison to SEM and its potential to investigate age-related changes. Bone, 2012. 50(3): 643-50.
118. Ruggeri ZM. Von Willebrand factor, platelets and endothelial cell interactions. J Thromb Haemost, 2003. 1(7): 1335-42.
119. Yuan L, Chan GC, Beeler D, Janes L, Spokes KC, Dharaneeswaran H, Mojiri A, Adams WJ, Sciuto T, Garcia-Cardeña G, Molema G6, Kang PM, Jahroudi N, Marsden PA, Dvorak A, Regan ER, Aird WC. A role of stochastic phenotype switching in generating mosaic endothelial cell heterogeneity. Nat Commun, 2016. 7: 10160.
120. Robin C, Ottersbach K, Boisset JC, Oziemlak A, Dzierzak E. CD41 is developmentally regulated and differentially expressed on mouse hematopoietic stem cells. Blood, 2011. 117(19): 5088-91.
121. Gekas C, Graf T. CD41 expression marks myeloid-biased adult hematopoietic stem cells and increases with age. Blood, 2013. 121(22): 4463-72.

122. Bluteau D, Lordier L, Di Stefano A, Chang Y, Raslova H, Debili N, Vainchenker W. Regulation of megakaryocyte maturation and platelet formation. J Thromb Haemost. 2009. 7 Suppl 1:227-34.
123. Lefrançais E, Ortiz-Muñoz G, Caudrillier A, Mallavia B, Liu F, Sayah DM, Thornton EE, Headley MB, David T, Coughlin SR, Krummel MF, Leavitt AD, Passegué E, Looney MR. The lung is a site of platelet biogenesis and a reservoir for haematopoietic progenitors. Nature, 2017. 544(7648): 105-109.
124. Nishikii H, Kanazawa Y, Umemoto T, Goltsev Y, Matsuzaki Y, Matsushita K, Yamato M, Nolan GP, Negrin R, Chiba S. Unipotent Megakaryopoietic Pathway Bridging Hematopoietic Stem Cells and Mature Megakaryocytes. Stem Cells, 2015. 33(7): 2196-207.
125. Dütting S, Gaits-Iacovoni F, Stegner D, Popp M, Antkowiak A, van Eeuwijk JMM, Nurden P, Stritt S, Heib T, Aurbach K, Angay O, Cherpokova D, Heinz N, Baig AA, Gorelashvili MG, Gerner F, Heinze KG, Ware J, Krohne G, Ruggeri ZM, Nurden AT, Schulze H, Modlich U, Pleines I, Brakebusch C, Nieswandt B. A Cdc42/RhoA regulatory circuit downstream of glycoprotein Ib guides transendothelial platelet biogenesis. Nat Commun, 2017. 8: 15838.
126. McArdle S, Mikulski Z, Ley K. Live cell imaging to understand monocyte, macrophage, and dendritic cell function in atherosclerosis. J Exp Med, 2016. 213(7): 1117-31.
127. Pertuy F, Aguilar A, Strassel C, Eckly A, Freund JN, Duluc I, Gachet C, Lanza F, Léon C. Broader expression of the mouse platelet factor 4-cre transgene beyond the megakaryocyte lineage. J Thromb Haemost, 2015. 13(1): 115-25.
128. Lo Celso C, Fleming HE, Wu JW, Zhao CX, Miake-Lye S, Fujisaki J, Côté D, Rowe DW, Lin CP, Scadden DT. Live-animal tracking of individual haematopoietic stem/progenitor cells in their niche. Nature, 2009. 457(7225): 92.
129. Devi S, Wang Y, Chew WK, Lima R, A-González N, Mattar CN, Chong SZ, Schlitzer A, Bakocevic N, Chew S, Keeble JL, Goh CC, Li JL, Evrard M,

Malleret B, Larbi A, Renia L, Haniffa M, Tan SM, Chan JK, Balabanian K, Nagasawa T, Bachelerie F, Hidalgo A, Ginhoux F, Kubes P, Ng LG. Neutrophil mobilization via plerixafor-mediated CXCR4 inhibition arises from lung demargination and blockade of neutrophil homing to the bone marrow. J Exp Med, 2013. 210(11): 2321–2336.

130. Rashidi NM, Scott MK, Scherf N, Krinner A, Kalchschmidt JS, Gounaris K, Selkirk ME, Roeder I, Lo Celso C. In vivo time-lapse imaging shows diverse niche engagement by quiescent and naturally activated hematopoietic stem cells. Blood, 2014. 124(1): 79–83.
131. Kowalska MA, Ratajczak J, Hoxie J, Brass LF, Gewirtz A, Poncz M, Ratajczak MZ. Megakaryocyte precursors, megakaryocytes and platelets express the HIV co-receptor CXCR4 on their surface: determination of response to stromal-derived factor-1 by megakaryocytes and platelets. Br J Haematol, 1999. 104(2): 220-9.
132. Bessis M. Erythroblastic island, functional unity of bone marrow. Rev Hematol, 1958. 13(1):8-11.
133. Bessis M, Breton-Gorius J. The erythroblastic islet and the rhopheocytosis of ferritin in inflammation. Nouv Rev Fr Hematol, 1961. 1: 569–582.
134. Keyhani E, Bessis M. Electron microscope study of the erythroblastic island using the cryo-scouring method. Nouv Rev Fr Hematol, 1969. 9: 803–816.
135. Policard A, Bessis M. Micropinocytosis and rhopheocytosis. Nature, 1962.194: 110–111.
136. Lee SH, Crocker PR, Westaby S, Key N, Mason DY, Gordon S, Weatherall DJ. Isolation and immunocytochemical characterization of human bone marrow stromal macrophages in hemopoietic clusters. J Exp Med, 1988. 168: 1193–1198.
137. Chasis JA, Mohandas N. Erythroblastic islands: niches for erythropoiesis. Blood, 2008. 112(3): 470-478.
138. Manwani D, Bieker JJ. The Erythroblastic Island. Current topics in developmental biology, 2008. 82: 23-53.

139. Wilson A, Trumpp A. Bone-marrow haematopoietic-stem-cell niches. Nat Rev Immunol, 2006. 6(2): 93-106.
140. Cooper GM. The Cell, 2nd edition. Sunderland (MA): Sinauer Associates; 2000.
141. Hagiwara T, Nagasawa T, Nagahisa H, Takizawa M, Osada M, Abe T. Expression of adhesion molecules on cytoplasmic processes of human megakaryocytes. Exp Hematol, 1996. 24(6): 690-5.
142. Kojima H, Kanada H, Shimizu S, Kasama E, Shibuya K, Nakauchi H, Nagasawa T, Shibuya A. CD226 mediates platelet and megakaryocytic cell adhesion to vascular endothelial cells. J Biol Chem, 2003. 278(38): 36748-53.
143. Kumar NM, Gilula NB. The gap junction communication channel. Cell, 1996. 84(3): 381-8.
144. Chen S, Lewallen M, Xie T. Adhesion in the stem cell niche: biological roles and regulation. Development, 2013. 140(2): 255–265.
145. Ciovacco WA, Goldberg CG, Taylor AF, Lemieux JM, Horowitz MC, Donahue HJ, Kacena MA. The role of gap junctions in megakaryocyte-mediated osteoblast proliferation and differentiation. Bone, 2009. 44(1): 80-6.
146. Ussar S, Wang HV, Linder S, Fässler R, Moser M. The Kindlins: subcellular localization and expression during murine development. Exp Cell Res, 2006. 312(16): 3142-51.
147. Moser M, Nieswandt B, Ussar S, Pozgajova M, Fässler R. Kindlin-3 is essential for integrin activation and platelet aggregation. Nat Med, 2008. 14(3): 325-30.
148. Massberg S, Konrad I, Schürzinger K, Lorenz M, Schneider S, Zohlnhoefer D, Hoppe K, Schiemann M, Kennerknecht E, Sauer S, Schulz C, Kerstan S, Rudelius M, Seidl S, Sorge F, Langer H, Peluso M, Goyal P, Vestweber D, Emambokus NR, Busch DH, Frampton J, Gawaz M. Platelets secrete stromal cell-derived factor 1alpha and recruit bone marrow-derived progenitor cells to arterial thrombi in vivo. J Exp Med, 2006. 203(5): 1221-33.

149. Wang JF, Liu ZY, Groopman JE. The alpha-chemokine receptor CXCR4 is expressed on the megakaryocytic lineage from progenitor to platelets and modulates migration and adhesion. Blood, 1998. 92(3): 756-64.
150. Bromberg ME. Immune thrombocytopenic purpura--the changing therapeutic landscape. N Engl J Med, 2006. 355(16): 1643-5.
151. Conley CL, Evans RS, Harrington WJ, Schwartz SO. Panels in Therapy. X. Treatment of Acute ITP. Blood, 1956. 11(4): 384-90.
152. Psaila B, Petrovic A, Page LK, Menell J, Schonholz M, Bussel JB. Intracranial hemorrhage (ICH) in children with immune thrombocytopenia (ITP): study of 40 cases. Blood, 2009. 114(23): 4777–4783.
153. Cheng Y, Wong RS, Soo YO, Chui CH, Lau FY, Chan NP, Wong WS, Cheng G. Initial treatment of immune thrombocytopenic purpura with high-dose dexamethasone. N Engl J Med, 2003. 349(9): 831-6.
154. Lum LG, Tubergen DG, Corash L, Blaese RM. Splenectomy in the management of the thrombocytopenia of the Wiskott-Aldrich syndrome. N Engl J Med, 1980. 302(16): 892-6.

# 7 APPENDIX

## Abbreviations

| | |
|---|---|
| min | minute |
| ml | milliliter |
| mm | millimeter |
| mM | millimolar |
| nm | nanometer |
| n | number |
| µg | microgram |
| µl | microliter |
| µm | micrometer |
| 2P-IVM | Two-photon Intravital Microscopy |
| 3D | 3 dimension |
| BM | bone marrow |
| BSA | bovine serum albumin |
| CAR cell | CXCL12-abundent reticular cell |
| CD | Cluster of differentiation |
| CFP | cyan fluorescent protein |
| CFU | colony-forming unit |
| CFU-MK | colony-forming unit-megakaryocyte |
| CLP | common lymphoid progenitor |
| CMP | common myeloid progenitor |
| DMEM | Dulbecco's Modified Eagle Medium |
| DMS | Demarcation membrane system |
| DMSO | Dimethyl sulfoxide |
| DT | Diphtheria toxin |
| EDTA | Ethylenediaminetetraacetic acid |
| EdU | 5-ethynyl-2’-deoxyuridine |

| | |
|---|---|
| EGFP | Enhanced green fluorescent protein |
| FACS | Fluorescence-activated cell sorting |
| FCS | fetal calf serum |
| FGF-4 | Fibroblast growth factor-4 |
| FITC | Fluorescein isothiocyanate |
| FL | Fetal liver |
| fl | floxed gene |
| G-CSF | Granulocyte-colony stimulating factor |
| GFP | green fluorescent protein |
| GMP | granulocytes/macrophage progenitor |
| GP | Glycoprotein |
| HSC | Hematopoietic stem cell |
| ICAM-1 | Intercellular adhesion molecule 1 |
| IL | Interleukin |
| LFA-1 | lymphocyte function-associated antigen 1 |
| LSK | $Lin^{-}$ $Sca\text{-}1^{+}$ $c\text{-}Kit^{+}$ |
| MEP | Megakaryocytic-erythrocytic progenitor |
| MK | Megakaryocyte |
| MK island | Megakaryopoietic island |
| MKP | Megakaryocyte progenitor |
| MPP | Multipotent progenitor |
| MSC | Mesenchymal stem cell |
| NaCl | Natrium chloride |
| NGS | Normal goat serum |
| NIR | near infrared |
| OPO | optical parametric oscillator |
| PBS | Phosphate buffer saline |
| PDGF | Platelet-derived growth factor |
| PE | Phycoerythrin |
| PF4 | Platelet factor 4 |
| PFA | Paraformaldehyde |

| | |
|---|---|
| PI | Propidium Iodide |
| PMT | Photo Multiplier Tube |
| RFP | Red Fluorescent Protein |
| rm | Recombinant mouse |
| RT | room temperature |
| SEM | standard error of the mean |
| S1P | Sphingosine 1-phosphate |
| SCF | Stem cell factor |
| SDF-1 | Stromal cell-derived factor-1 |
| SHG | Second Harmonic Generation |
| SLAM | Signaling lymphocyte activation molecule |
| TGF-β1 | Transforming growth factor-β1 |
| Tpo | Thrombopoietin |
| TRITC | Tetramethylrhodamine |
| vWF | von Willebrand Factor |
| VCAM-1 | Vascular-cell adhesion molecule 1 |
| VEGF | Vascular endothelial growth factor |
| VLA-4 | Very late antigen 4 |
| VLF | Very late factor |
| WT | Wild type |
| YFP | yellow fluorescent protein |

**Acknowledgement**

First of all, I would like to thank my supervisor Prof. Dr. med Steffen Massberg for giving me the opportunity to work on this fantastic project. Without this opportunity, I would not be able to learn so much during 4 years PhD study. I sincerely thank him for his excellent supervision, encouragement and endless support of my work.

Then, I would like to thank my thesis advisory committee, Prof. Dr. Robert Oostendorp, Prof. Dr. rer. nat. Markus Moser and Prof. Dr. med Christian Schulz, for the inspiring discussions and insightful comments as well as suggestions. I thank them for helping me understand and improve this research from different aspects.

I also would like to thank Dr. med Florian Gärtner, my direct supervisor, for leading me to the research field of megakaryocyte and platelet. He taught me to use two-photon microscopy from the beginning. He offered me support as well as the freedom to explore this project as much as possible, so that I learned to think independently. He kindly provided me encouragement and suggestions when I came across a dilemma. I sincerely thank him for all of these.

I would like to thank my lovely colleagues, especially Irene Schubert, Susanne Sauer, Michael Lorenz, Anna Titova and Hellen Ishikawa, for all the help they have given to me during my PhD study. It was a great pleasure to work with them. I would also like to thank all my Chinese friends in lab. We went through the hard times together but we never gave up. I feel very lucky to have them here.

I would like to thank IRTG 914 program for offering professional trainings, and thank Dr. Verena Kochan for patiently answering all my questions regarding the structure and procedure of the PhD program.

Especially I would like to thank China Scholarship Council (CSC) for providing me 4 years financial support, so that I can pursue and finish my PhD in Germany successfully. I cherish this opportunity and make the most use of it.

Finally, I would like to express my deep gratitude to my family, for their endless love and devotion. It would not be possible to finish my study without them.

**Affidavit**

Fu, Wenwen

Surname, first name

Heiglhofstrasse 55

Street

81377, Munich

Zip code, town

Germany

Country

I hereby declare, that the submitted thesis entitled

**Megakaryopoietic islands in the bone marrow balance platelet production and maintain megakaryocyte homeostasis**

is my own work. I have only used the sources indicated and have not made unauthorized use of services of a third party. Where the work of others has been quoted or reproduced, the source is always given.

I further declare that the submitted thesis or parts thereof have not been presented as part of an examination degree to any other university.

Place, Date

Signature doctoral candidate

**Confirmation of congruency between printed and electronic version of the doctoral thesis**

Fu, Wenwen

Surname, first name

Heiglhofstrasse 55

Street

81377, Munich

Zip code, town

Germany

Country

I hereby declare, that the electronic version of the submitted thesis, entitled

**Megakaryopoietic islands in the bone marrow balance platelet production and maintain megakaryocyte homeostasis**

is congruent with the printed version both in content and format.

Munich, 27.11.2017

Place, Date

Wenwen Fu

Signature doctoral candidate